Relaxations in Complex Polymer Systems

by

Ravi P. Sharma

A dissertation submitted in partial fulfillment
of the requirements for the degree of
Doctor of Philosophy
(Materials Science and Engineering)
in the University of Michigan
2018

Doctoral Committee:

Professor Peter F. Green, Chair
Professor Ronald G. Larson
Professor Richard E. Robertson
Associate Professor Anish Tuteja

rpsharma@umich.edu
ORCID: 0000-0001-6779-2709

Acknowledgements

This thesis is a culmination of more than four years of work, over the course of which I have been fortunate to be surrounded by people who have motivated and helped me in numerous ways. It is a pleasure to get an opportunity to express my gratitude to some of them.

First and foremost I would like to thank my advisor, Professor Peter F. Green. The first project I dove into as a graduate student was perhaps my most difficult one, and I am grateful for Professor Green's willingness to provide scientific insight when I was lost, physical intuition when nothing made sense, and motivation when success looked bleak. With his help, we turned something that I may very well have given up on into work that will have a meaningful impact in the field. These experiences helped me in my latter graduate student years, and I am sure will have a long-lasting impression on me in the future.

I would also like to thank the other members of my dissertation committee, Professors Richard Robertson, Anish Tuteja, and Ronald Larson, for their support, comments, and suggestions throughout my degree. Additional thanks to Professors Robertson and Tuteja for their excellent instruction in graduate coursework on polymers.

A large part of my success rests upon the shoulders of former and current member(s) of the Green research group. Needless to say, all members of the Green group have contributed both directly and indirectly to my work, through training on laboratory equipment and techniques, to fruitful discussions about research, to day-to-day interactions; for this, I owe many

thanks to Dr. Emmanouil Glynos, Dr. Aaron Tan, Dr. Bradley Frieberg, Dr. Hengxi Yang, Dr. Bingyuan Huang, Dr. Peter Chung, Dr. Junnan Zhao, Dr. Jojo Amonoo, Dr. Anton Li, Dr. Ban Dong, Dr. Kyle Johnson, and last but certainly not least, Jill Wenderott.

Many thanks to the friends I have made at the University of Michigan, many of whom shared the struggle of pursuing a graduate degree with me. Whether it was late nights cramming for finals, hours venting when my experiments were going awry, or Saturday afternoons at the Big House (Go Blue!), they provided much needed diversions and a reminder that life goes on outside of the laboratory. With them, my experience was far more enjoyable and fulfilling, and I consider myself quite lucky to have found a family so far from home.

Finally, I would like to express my utmost appreciation for the unfaltering support from my family: my mother and father, Kamala and Jay, and my sister, Priya. My parents have given me everything I have ever asked for and allowed me to pursue any goals I chose, while of course asking for nothing in return. For this, any success I have and will achieve, including this dissertation, I share with them.

Table of Contents

List of Figures

List of Appendices

Abstract

Many applications that employ polymeric materials rely on mixtures (polymer/polymer, polymer/nanoparticle, polymer/filler). A key challenge of using these materials is understanding interrelations between the physical properties and the local and macroscale morphologies. The most common systems are mixtures of two homopolymers, A and B, which can exhibit properties that are more desirable than those of the pure components. Unlike miscible small molecule systems, miscible A/B polymer/polymer blends, while macroscopically homogeneous, can be spatially compositionally heterogeneous at the molecular level, which can cause deviations in physical properties. Applications in the areas of organic electronics, membranes, and nanoscale coatings can also require these materials to function under various conditions of geometric confinement, such as thin films. This introduces an additional complication because the proximity to an external interface (free surface or substrate) influences the local composition and morphology, leading to film thickness-dependent behavior. To this end, this dissertation explores three problems involving the role of morphology on dynamic processes in polymeric systems of different local intermolecular environments.

First, we investigate the role of local spatial compositional heterogeneity on the dynamics of the A component in bulk, miscible A/B polymer/polymer blends. The dynamics of the faster, lower glass transition temperature component A, at temperatures sufficiently high above the blend glass transition, manifest the behavior of chains relaxing in a compositionally homogeneous environment. For temperatures lower than the blend glass transition, the A

component chains relax in two distinctly different local compositional environments, manifesting the influence of spatial compositional heterogeneity.

Having investigated the role of spatial compositional fluctuations on the relaxations of the A component in A/B polymer/polymer blends, the additional effect of geometric thickness confinement at the nanoscale – confining the A/B mixture between two substrates – was studied. In thin film blends, the concentration of the A component may differ from the macroscopic average composition at different depths into the film, largely due to its preferential interactions with the confining substrates. In this case, the compositional changes driven by the interfacial interactions become dominant when the films are sufficiently thin. A key finding is that, whereas thickness confinement effects modify the dynamics of pure homopolymer chains for thicknesses up to a few nanometers, the effects on these A/B blends extend over hundreds of nanometers.

The third problem is based on the recognition that in most applications, polymer thin films can be required to contact other polymers or different "hard" materials. The vast majority of studies that investigate physical properties examine either free or supported films. Here we investigate the dynamics of a homopolymer A confined between a hard substrate C and a soft, immiscible polymer film B. A surprising finding is that the presence of the soft polymer B has the effect of increasing the relaxation rates of polymer A significantly, and over unusually large length-scales, not observed in polymers confined between two hard substrates C. These findings implicate the sensitivity of polymer dynamics to the modulus of the confining environment.

The works described in this dissertation provide a comprehensive view of how physical properties of polymers can change significantly in different environments – compositional changes, changes in mechanical moduli of the surrounding environment, and geometric

constraints. Insights gained from these studies can be used to understand and control the physical properties of polymer-based materials for future applications.

Chapter 1: Introduction

1.1 Polymer Physics: History and Open Questions

Natural macromolecular materials have been in use before the evolution of *Homo sapiens* – our Neanderthal ancestors used skins and weavings for clothing, fibers and sticks for weapons, and sap for glues and sealants.[1] Even manmade macromolecules date back to before the birth of the modern human; earliest documentation traces as far back as 180,000 years ago, when *Homo erectus* utilized controlled heating to turn birch bark pitch into an adhesive.[2] Historical evidence shows that development and use of these materials in a wide range of applications continued for centuries, through early Middle Eastern societies,[3] ancient Egypt,[4] and the Roman empire.[5] By the onset of the industrial revolution, the first instances of manmade polymers began to appear – an early example includes H. Victor Regnault accidently exposing gaseous vinyl chloride to sunlight, producing polyvinyl chloride in 1838.[6] The following year, Eduard Simon converted styrene into a solid resin using heat, producing polystyrene (although at the time thought to be styrene oxide).[7] Yet even as new macromolecular materials propagated through society, chemists held on to the belief that molecules were always small, and molecular weights could not exceed a few thousand units.[8] This line of thinking was maintained as late as the early twentieth century. It wasn't until Hermann Staudinger's seminal work[9] on the so called "macromolecular hypothesis" in 1920 that the existence of macromolecules began to gain traction. At first his views were largely conjecture, but in 1922 Staudinger provided the first experimental proof of large

molecules by observing similar behavior between unvulcanized and hydrogenated rubber, despite the former having many electron-rich double bonds and the later having none, showing the effect of covalent bonding.[10] By the mid-1930s a number of exceptional synthetic chemists had joined ranks with him,[11] and this began the rapid growth of synthesis theory and production means.

In conjunction with the development of macromolecular synthesis methods, the foundation of polymer physics was gradually established over the following 30 years, pioneered by work such as that by Kuhn on macromolecular sizes,[12] Flory and Huggins on thermodynamics,[13] and Rouse and Zimm on models of polymer dynamics.[14,15] Subsequently, the 1960s and 1970s saw the development of the main principles of modern polymer physics, including the Edwards model of the polymer chain and tube,[16] the reptation theory of chain diffusion by de Gennes,[17] and the Doi-Edwards theory of flow in polymer melts.[18]

Despite these important findings and hypotheses, the field of polymer physics remains in its infancy in terms of understanding. For example, compared to inorganics, polymeric materials are composed of more complicated interactions due to the abundance of chemical structures, and have significantly more complex morphologies due to the lack of long-range ordering. Because of this, molecular simulations are often inconclusive or unfeasible, and experimental characterization techniques remain either mostly macroscopic (differential scanning calorimetry, dynamic mechanical analysis, etc.) or suffer from low intensity due to disorder (x-ray diffraction, neutron scattering, etc.). Even the fundamentals within polymer physics remain up for debate – concepts such as the glass transition temperature (T_g) and the dynamic relaxations of polymer chains and their corresponding temperature dependences, which were introduced from an analysis of macroscopic properties, are not clear at the local or nanoscale. As such, the link

between observed macroscopic properties and microscopic observations has yet to be fully established.

One of the most important topics in materials science as a field is the structure-property relationship. Such an understanding allows one to predict the properties of a polymer system from its structure, as well as infer the structure of a system from measured macroscopic properties. By controlling and understanding these properties, today's molecular design principles have enabled polymeric materials to be used in a wide array of applications. For example, viscoelasticity plays a role in polymer processing related applications such as 3D printing[19] or tire manufacturing and performance.[20] Charge carrier mobility in polymers plays a role in the performance of organic solar cells[21] and flexible electronics.[22] Small molecule and ion transport mechanisms play a role in gas separation and purification,[23] as well as controlled drug release.[24] What all of these specific properties have in common is that they require an understanding of polymer dynamics and chain relaxation processes. As such, polymer dynamics represents an important stepping-stone in polymer physics.

At the highest level, a study of polymer relaxations is a study of molecular motions over various length-scales, from the segmental motions of the monomers that compose the macromolecule chains and govern the glass transition, to the translational motions of the entirety of the chains that facilitates viscous flow. Because polymer deformation and flow behavior is strongly time-dependent, getting characteristic times over which these motions occur provides great insight into material properties, such as the ones discussed previously, as well as an understanding of how the material will behave in application.

The relaxation rates and associated behavior of many different homopolymers have been studied extensively over the past forty or so years.[25] It is now well understood that the local

environment in which a polymer chain relaxes plays a significant and important role on the relaxation dynamics.[26–28] However, this picture is not complete and there are still unanswered scientific questions in this area associated with understanding and controlling various intermolecular interactions that affect polymer chain relaxation processes; the works in this dissertation will focus on understanding how and to what length-scales such local environments affect the dynamics of polymer chains. The environments examined are due to: (i) the heterogeneous composition in localized environments in polymer mixtures (Chapter 2), (ii) the proximity to different types of interfaces in polymer nanomaterials (Chapter 3), and (iii) the interfacially enriched wetting layers in nanoconfined polymer blends (Chapter 4). These results demonstrate the significance of local intermolecular interactions and effects on polymer dynamics and the importance of understanding them.

1.2 Dynamics and Kinetics of Glass-Forming Polymers

An important characteristic of glass-forming liquids is the non-linear increase of the viscosity with decreasing temperature (T); this is understood as the liquid falling out of equilibrium and solidifying in the absence of long-range order as T approaches T_g.[29,30] For polymers, the segmental relaxation time of the monomers, τ_{seg}, is approximately 100 seconds at $T = T_g$;[31] in network glasses and small molecules liquids, T_g is also identified with a structural relaxation time τ_{struc} of ~100 seconds, with viscosity $\eta \approx 10^{13}$ Poise.[30] Both of these relaxation times correspond to the inverse cooling rate for a typical differential scanning calorimetric (DSC) measurement of the glass transition.[32] This relationship between the segmental relaxations and T_g stems from the damped diffusion of conformational changes that occurs when a polymer segment relaxes. For a given chain, a change in conformation will change the chain's bond

lengths and angles, and will increase the probability that a neighboring polymer segment also undergoes a conformational transition. In polymeric systems composed of multiple chains, these linked and cooperative chain motions is what causes the glass transition.[29]

The non-linear dependence of η, τ_{seg}, and τ_{struc} may be understood from the phenomenological theory of Adam and Gibbs,[33] who suggested that the dynamics of liquids are characterized by so-called cooperatively rearranging regions (CRRs). They postulated that the size of the CRR – speculated by Donth[34–36] to be on the order of tens of nanometers – grows with decreasing *T*, driven by an increasing packing density and manifesting an increasing degree of relaxation cooperativity. The activation barriers associated with this behavior were assumed to be purely entropic, and likewise the relaxation times τ_{seg} and τ_{struc} of a glass-forming material could be predicted to grow exponentially with the size of the CRRs, due to their cooperative natures.

The temperature dependences of τ, or of η, not far above T_g, are well described by the Vogel-Fulcher-Tammann (VFT) equation:[37]

$$\log \tau = \log \tau_0 - \frac{B}{T - T_\infty} \tag{1.1}$$

where τ_0 is a reference relaxation time, T_∞ is the Vogel temperature related to T_g, and B is a parameter associated with thermally activated processes. The VFT equation may be derived from the Adam Gibbs theory, subject to certain assumptions.[33] It can also be derived from the classical free volume model

$$\tau = \tau_0 e^{\frac{V_0}{V_f}} \tag{1.2}$$

where V_f is the free volume and V_0 is the so-called occupied volume.[38] Furthermore, the constants T_∞ and B are related empirically to the well-known Williams-Landel-Ferry (WLF) equation[39] constants C_1 and C_2, such that

$$C_1 = \frac{B}{T_g - T_\infty} \tag{1.3}$$

and

$$C_2 = T_g - T_\infty \tag{1.4}$$

First discovered purely empirically, the generalized entropy theory (GET)[40,41] now provides a molecular picture behind these relationships – the constants are related to the chain stiffness and the cohesive van der Waals interactions between molecules.

The temperature dependencies of τ_{seg} and τ_{struc} may also be characterized in terms of the so-called fragility index m.[31] This index is a measure of how rapidly a material falls out of equilibrium in the vicinity of T_g, and is defined as

$$m(T_g) = \frac{\partial \ln \tau}{\partial \frac{T}{T_g}}\Big|_{T_g} \tag{1.5}$$

The theory predicts that, for the same homologous series of polymers,

$$m = T_g \frac{C_1}{C_2} \tag{1.6}$$

relating back to the constants of the empirical VFT and WLF equations shown previously. It further predicts many connections between fragility and polymer characteristics, including chain stiffness, intermolecular strengths, molecular weight, free volume, and cohesive interactions.[42] This in turn is related to the material's physical properties.[43]

Advances over the last two decades have linked the phenomenon of fragility in glass-forming materials to dynamic heterogeneity, or locally heterogeneous dynamics.[44,45] Long and coworkers[46] have used dynamic heterogeneity models to describe the dynamics and their consequences on the physical properties of glass-forming liquids. The basis of their work is on the existence of spatially transient domains due to density fluctuations, which are in turn responsible for heterogeneity in the dynamics. Despite migration between domains and the

observation that dynamics within domains are highly correlated, there is a region-based time-scale distribution – some areas are rapid comparative to the average, whereas other domains are slow. This accounts for the distribution of relaxation times, often characterized in terms of a Kohlrausch-Williams-Watts (KWW) relaxation parameter β.[47,48]

Recent simulations provide support for this picture and a connection back to Adam and Gibbs, although there is debate over the molecular basis and justification. Starr and Douglas[49] revealed the existence of highly correlated motions of particles as strings, the dimensions of which are associated with the CRRs. Models based on the propagation of free volume such as the locally correlated lattice (LCL) model developed by Lipson and White[50,51] implicate the temperature dependence of free volume to the cooperative nature of the glass transition. Freed's GET model[40,41] describes glass-formation in polymer systems based solely on monomer structure, interactions, stiffness, and local correlations, and finds that this adequately fits with experimental observations.

Despite the debate over the theoretical picture, it remains a fact that dynamic heterogeneity and the localized environment and morphology surrounding polymer chains has a significant effect on relaxation times, the glass transition, and fragility, which in turn has important implications on the physical properties of these materials. This dissertation focuses on answering some of these open questions concerning the effect of different local intermolecular environments on polymer chain relaxation processes: (i) different molecular compositional environments associated with the presence of other polymers in mixtures (polymer blends), (ii) the close proximity of external "walls" in nanometric thin films (polymers under nanoconfinement), and (iii) the compositionally different regions near external interfaces in polymer/polymer blend thin films (polymer blends under nanoconfinment).

1.3 Polymer Blends

It is well known that polymer blends are generally immiscible; the most common result of mixing two polymers is complete phase separation because, unlike in liquids or small molecule systems, the entropy of mixing in binary polymer/polymer blends is small.[52] However, there exists pairs of polymers that are able to form miscible blends across certain temperature and composition ranges, due to similarities in chemical structure and/or attractive interactions between chains. Complete miscibility in a polymer blend signifies that both components are thermodynamically mixed to a nanoscopic level,[53] and occurs when the change in Gibbs free energy is less than zero[52]

$$\Delta G_m = \Delta H_m - T\Delta S_m < 0 \tag{1.7}$$

and the second derivative of the Gibbs free energy at the specific concentration is nonzero[52]

$$\frac{\delta^2 \Delta G_m}{\delta^2 \phi^2}|_{T,P} > 0 \tag{1.8}$$

The Flory-Huggins theory[13] has proven to be a versatile and convenient theoretical framework for describing the thermodynamic properties of a polymer mixture. Formed as an extension of the regular solution theory for simple liquids, it makes two basic but important assumptions: (i) no change in volume upon mixing (incompressible model) and (ii) completely random mixing. In this model, the entropy of mixing is defined as

$$\Delta S_m = -R[\frac{\phi_1}{n_1}\ln \phi_1 + \frac{\phi_2}{n_2}\ln \phi_2] \tag{1.9}$$

where φ is the volume fraction of each component, *n* is the number of polymer segments, and *R* is the gas constant. Simply put, this term amounts to the number of rearrangements available for the system, known as the combinatorial entropy. For the enthalpy of mixing, the expression is solely determined from short-range, isotropic, pairwise interactions among nearest neighbor

segments. By the mean-field assumption, the local concentration is always given by the average concentration, and thus

$$\Delta H_m = RT\chi\phi_1\phi_2 \tag{1.10}$$

X, known as the interaction parameter, is a dimensionless value describing the exchange energy per monomer, normalized by the thermal energy. Combining these two expressions with the governing equation of miscibility produces the Flory-Huggins equation for a binary system

$$\Delta G_m = RT[\frac{\phi_1}{n_1}\ln\phi_1 + \frac{\phi_2}{n_2}\ln\phi_2 + \chi\phi_1\phi_2] \tag{1.11}$$

As mentioned previously, there are multiple assumptions that must be employed in order to arrive at the simplified Flory-Huggins expression for the free energy of mixing, such as incompressibility and completely random mixing. However, we know that in practicality these do not apply. Miscible polymer blends, while macroscopically homogeneous, can exhibit local inhomogeneities on the scale of nanometers.[53–58] Fundamentally, each component of a blend relaxes or diffuses in an effective compositional environment φ_{eff} that is enriched with chains of identical composition compared to the average blend composition φ_{ave}. This spatial compositional heterogeneity is known as a self-concentration (SC) effect associated with the connectivity of monomers along the chain.[59] In an A/B polymer/polymer blend, a monomer A has a higher than random probability of being next to another monomer A due to the connectivity of monomer As along the polymer A chain. Thus the monomers of each component experience a local environment rich in itself versus the macroscopic concentration. The model of Lodge and McLeish[59] postulates that the length-scale of relevance for this effect is the Kuhn length l_k. The volume that enclosed the monomers is

$$V_k = C_\infty l_k^3 \tag{1.12}$$

where C_∞ is the characteristic ratio. Within this volume, the excess of monomer of type A is defined as

$$\phi_{eff-A} = \phi_{self-A} + (1 - \phi_{self-A})\phi_{ave-A} \tag{1.13}$$

The self-concentration due to chain connectivity $\varphi_{\text{self-A}}$ is

$$\phi_{self-A} = \frac{C_{\infty,A} \cdot M_A}{N_{av} \cdot k_A \cdot \rho_A \cdot V_A} \tag{1.14}$$

where N_{av} is Avogadro's constant, M is the molecular weight of the monomer, ρ is the polymer density, and k is the number of backbone bonds per repeat unit, all of component A. A similar relation would describe that of component B.

Self-concentration is an intrinsic quantity. However, this parameter has been shown to vary in some systems, suggesting that other factors would contribute to the local composition.[60] We now know that concentration fluctuations[56,61–63] play an additional role. Local concentration fluctuations, which are always occurring in blends due to a low entropy of mixing, is a temperature-dependent phenomenon. As described by the Adam-Gibbs molecular kinetic theory,[33] the local cooperatively rearranging regions over which a polymer relaxation is influenced by other polymer chains is increased in size with decreasing temperature. Donth[34] later showed that the size of the CRRs represented a measure of the length-scales of the compositional fluctuations. Because these fluctuations are thermally driven, lowering the blend temperature increases the time-scales over which they dynamically dissipate.[56] Likewise, this has an effect on the temperature dependence of spatial compositional heterogeneity in terms of its influence on relaxation processes.

It is apparent that there is a great deal of physics that is neglected when solely relying on an idealized theory such as Flory-Huggins; this in turn has important implications on the measurement of dynamics in miscible blends. As a result of self-concentration, miscible blends

have been shown to exhibit two distinct glass transition temperatures.[59,64–66] This is also the reason for the failure of time-temperature superposition in certain miscible blends.[67] This behavior is even more pronounced in dynamically asymmetric blends, or blends in which the component T_gs differ by a large amount.[68]

It is also evident from studies of a number of miscible A/B polymer/polymer blends, using different techniques such as broadband dielectric spectroscopy, rheology, neutron scattering, and magnetic resonance, that the temperature dependencies of the segmental and translational relaxations, τ_{seg} and τ_{trans}, of the A and B components are different.[57,68–76] The dynamics of each chain is dictated by a friction factor ζ, determined in part by intra-chain bond rotations and local intermolecular interactions. It has also been shown that ζ differs for different polymers dependent on chemical makeup. For pure homopolymers, the relationship between ζ and τ is fairly well understood; for segmental relaxations, τ_{seg} is proportional to ζ. For a chain moving in an unentangled melt, the Rouse relaxation time is proportional to $M^2\zeta$, where M is the molecular weight of the chain.[77] For long and highly entangled chains ($M >> M_e$ where M_e is the molecular weight between entanglements), the translational relaxation time τ_{trans} is given by reptation theory[78]

$$\tau_{rep} \propto \frac{\zeta}{T}\frac{1}{M_e^2}M^3 \tag{1.15}$$

With regard to τ_{trans} in the blends, additional mechanisms such as constraint release,[79] tube dilation effects,[79] and double reptation[80] due to associated effects of the other component in the direct environment surrounding a polymer chain play a role. Even less is known about τ_{seg} in the blends – including the absolute values of relaxation rates, temperature dependences, and broadening of relaxation distributions – despite its importance to the glass transition. Likewise, a

major focus of this work will be on the segmental dynamics in miscible polymer blends and the effect of the dynamically heterogeneous environment surrounding polymer chains.

1.4 Polymers under Nanoconfinement

Increasingly, polymeric materials must function under various conditions of geometric confinement at the nanoscale. Research interest in this area stems from the experimental observations that functional properties such as elastic moduli,[81] ferroelectric properties,[82] and charge carrier mobilities in conjugated polymers[83] can deviate from analogous bulk behavior when these materials are confined to length-scales on the order of which their molecular relaxation processes occur. The driving forces behind this phenomenon are two effects; entropic "packing" and chain conformational effects, together with intermolecular interactions with external interfaces.

In regards to entropic effects, the local packing of segments is perturbed in the vicinity of the interfaces because the density of segment packing is not spatially uniform. For a nanoconfined homopolymer, simulations indicate that the density profile oscillates away from the substrate over a length scale of around $\xi \sim 1$ nanometer.[49,84] In addition, the packing of monomers and their respective orientation change at interfaces, largely manifesting the effects of short-range intermolecular interactions.[85–87] Generally, the dynamics at a "wall" are anisotropic, and the relaxations of the segments normal to the substrate are slow compared to the bulk. This sluggishness is suggested to be due to the long time-scales associated with desorption of segments from the walls, or correspondingly, decreased configurational freedom of the chains in the proximity of the substrate. In essence, interactions of a chain segment in contact with a wall increase the relaxation times of a chain by increasing the activation barriers. Stronger

interactions with the walls lead to longer desorption times and hence slower dynamics.[87] Correspondingly, at a free surface, simulations show that local packing constraints are not as severe (larger configurational freedom) as they are at a hard wall.[85,88–91] These simulations reveal the existence of a mobile surface layer of chains, thickness on the order of nanometers.

Much of these initial predictions are now supported by experimental observations. For freely standing polymer films, the average T_g of the film is decreased in relation to the bulk, provided the film is sufficiently thin.[92–94] The same is generally true for asymmetrically confined films – existence of a free surface and an interface in contact with a substrate – where the polymer interactions with the substrate are weak van der Waals forces.[95–99] This T_g depression is due to the previously mentioned mobile surface layer at the polymer-free surface interface. Even in cases of asymmetrically confined supported films, the additional configurational mobility at the free surface is sufficient to overcome reduced mobility at the polymer-substrate interface. On the other hand, for cases where there exists attractive interactions between the polymer and substrate, for example hydrogen bonding, the average T_g of the film can be greater than that of the bulk[97,100–102] – the strength of the enthalpic interactions dictates the deviation in the glass transition.

Experimental observations show that changes in the glass transition of thin films occur over much longer length-scales *h* than the density fluctuation length-scales ξ. Theoretical work by Schweizer and coworkers[103] provides a molecular perspective for this behavior. They consider a chain segment as caged, such that the size of the cage is the first minimum in the radial distribution function on the order of the monomer size. The requirement of cooperativity reveals that the motions of a chain segment must be facilitated by local volume dilations of the cage. This increase in local volume is accommodated by long-ranged elastic fluctuations,

producing an elastic energy barrier. In the case of a free surface, the number of nearest neighbors is smaller and the elastic energy barrier is likewise weaker. At the substrate, when strong intermolecular interactions exist, there are large energetic barriers for chain cooperative motion. In the case of weak van der Waals interactions at the substrate, the elastic energy barrier is weak, and deviations in T_g are nonexistent.

In addition to T_g deviations, interactions at the substrates can also lead to deviations in various chain relaxation processes (side chain,[104] segmental,[105] end-to-end[106]). Yet there is still some debate as to the extent of these effects:[98,107,108] whereas the length-scales h over which the glass transition appears to be affected by substrate interactions are comparatively large ($h >> \xi$), approaching the order of hundreds of nanometers depending on geometry, the length-scales L over which such effects affect chain dynamics are much smaller ($L \sim \xi$). This connection between thermal measurements such as the glass transition and dynamic measurements such as segmental relaxations under nanoconfinement is still a topic of debate.[109,110] Furthermore, the connection between dynamics and T_g under various confinement conditions remains poorly comprehended. In this dissertation, we further probe the length-scales over which an interface affects polymer chain relaxations, as well as the effects of different types of interfaces.

Chapter 2: Component Dynamics in Polymer/Polymer Blends: Role of Spatial Compositional Heterogeneity

2.1 Introduction

There is significant interest in understanding interrelations between the processing, morphology, properties, and reliability of polymer mixtures for a diverse range of applications. Of particular interest in this study is the manner in which the dynamics of the components A and B of an A/B polymer/polymer blend are influenced by local compositional heterogeneity, a phenomenon by which the composition may remain spatially homogeneous at the macroscopic scale, but heterogeneous at the nanoscale. This is especially prominent in blends whose components are weakly interacting and/or exhibit large differences in glass transition temperatures (T_gs).[53,54,56–58,111,112] Spatial compositional heterogeneity is due to two factors: an intrinsic self-concentration (SC) effect associated with the connectivity of monomers along the chain,[59] and thermally-driven composition fluctuations (TCF).[56,61–63] Due to chain connectivity, the average local compositional environment around a given monomer is enriched with segments

of the same monomer. The relevant length-scale of the self-concentration effect is the polymer's Kuhn length – beyond this length-scale the bulk concentration largely dictates the behavior of the blend. TCF may be understood from the basis of the cooperatively rearranging regions (CRRs), proposed by Adam and Gibbs,[33] to explain the onset of the glass transition – the sizes of the CRRs grow as the temperature T decreases toward the glass transition temperature. Donth[34,35,113] later showed that the size of the CRRs represented a measure of the length-scales of the compositional fluctuations; these length-scales are significantly larger than the Kuhn length. During the last three decades, a number of studies have been devoted to understanding the phenomenon of dynamic heterogeneity;[54,55,57,58,62,64,65,74,76,111,112,114–120] and although recent theoretical models[57,66,89,120–123] have provided important insights into the connection between compositional heterogeneity, dynamics, and the glass transition,[109,110,124,125] a few lingering questions remain.

In this study we report on the temperature and compositional dependencies of the segmental, or α, relaxations of the components in a series of polymer/polymer blends. The temperature dependencies of the chain and segmental dynamics in homogeneous melts, for temperatures not too far above T_g, are generally well described by the Vogel-Fulcher-Tammann equation (VFT)[37] or the analogous Williams-Landel-Ferry equation (WLF).[39] However, the situation involving dynamics of blends is often more complex, largely because spatial compositional heterogeneity can be responsible for the appearance of different component glass transition temperatures $T_g^{(i)}$ (i = A,B) and different temperature-dependent relaxation times $\tau_i(T)$.[59,64,66,126,127] Additionally, the distribution of relaxation times extracted, for example, from the imaginary permittivity $\varepsilon''(\omega)$, measured using broadband dielectric spectroscopy (BDS), is

both temperature and composition-dependent,[62,68,128] manifesting effects of the local compositional environment.

For miscible blends, the effects of compositional heterogeneity on the glass transition and dynamics are most evident when the A/B interactions are comparatively weak and/or there exists a large disparity between the T_gs of each component.[55,64,65,67,68,111,129] Whereas certain miscible A/B systems exhibit two distinct T_gs,[59,64–66,126,127] such as polyisoprene (PI)/ poly(4-tert-butylstyrene) (P4tBS), each associated with one of the components in the mixture, other systems such as poly(vinyl methyl ether) (PVME)/polystyrene (PS) exhibit a single, broad glass transition, as evident from differential scanning calorimetry (DSC) experiments.[58,75,76,112,130] In both cases, spatial compositional differences around a segment *i* creates a distribution of local environments with different compositions φ_i, and leading to a distribution of local T_gs and relaxation times.

With regard to the PVME/PS system, the relaxation rates of both components decrease rapidly, and in a non-linear manner, with decreasing temperature as the temperature is decreased toward the T_g of the blend, $T_g^{(blend)}$; this is known as the typical α processes.[58,74,76,119] However for temperatures $T < T_g^{(blend)}$, the temperature dependence of the segmental dynamics becomes weaker, following approximately Arrhenius behavior. Colmenero and coworkers[68,76,119,120] suggested that this Arrhenius temperature dependence occurs because the dynamics of the lower T_g PVME component occurs within the "frozen" confines of the higher T_g, glassy PS domains, a phenomenon known as dynamically asymmetric confinement. In essence, due to local compositional heterogeneity, and the fact that $T_g^{(PS)} >> T_g^{(PVME)}$, the PS component vitrifies at temperatures at which the PVME chains are still mobile, and thus the PVME chain relaxations occur within the confines of the rigid, localized PS regions. Because the length-scale of

cooperativity is larger than the dimensions of the confined regions, the segmental dynamics is purely thermally activated and necessarily Arrhenius. This was identified as the α' process in order to differentiate it from the conventional α process occurring at high *T*.

Recently Yang and Green[112] showed, based on analyses of BDS frequency-temperature-permittivity (2D contour) plots of the miscible PVME/PS blend, that for temperatures above the blend glass transition temperature the PVME segmental dynamics was characterized by not only the typical α process in the melt ($T > T_g^{(blend)}$) and the α' process in the glass ($T < T_g^{(blend)}$), but also a third, slower α_0 process that occurs in the melt as well ($T > T_g^{(blend)}$). The time-scales of the dynamics associated with this third process decrease at a considerably more rapid rate than those of the α process as *T* decreases toward $T_g^{(blend)}$; they are also significantly slower than the α process.

The consequences of spatial compositional heterogeneity on the dynamics are not manifested in the same way for all blends. For example, in contrast to the miscible PVME/PS blend, the miscible PI/P4tBS blend exhibits two component glass transition temperatures.[65,70,71,117,118] The end-to-end and segmental PI fluctuations were first investigated using BDS by Watanabe et al.[70] and Chen et al.,[71] and later followed by Colmenero et al.;[118] like PVME/PS and other miscible blends, the dielectric loss curves of PI/P4tBS are broad compared to those of the pure components. Additionally, the dielectric strengths change significantly with decreasing *T*, which is in all likelihood the source of slight differences reported between the isochronal and isothermal representations of the relaxation data. Finally, the onset temperature for the increase of the breadths of the distributions for the end-to-end PI relaxations, measured using dielectric spectroscopy and rheology, is associated with the "freezing" of the higher glass transition temperature P4tBS component. This is accompanied by a failure of time-temperature

superposition. Conceptual work by Zhao and Ediger[65] theorize that below the effective T_g of the slow component (P4tBS), both the slow and fast (PI) component dynamics should shift to Arrhenius behavior as the system leaves equilibrium, similar to what is described earlier for PVME/PS and for other blends with large ΔT_gs[131,132]; however, this specific temperature dependent behavior is yet to be confirmed by experiment.

In light of the foregoing, the natural challenge would be to further understand the characteristics of the α' and α_0 processes in blends. To this end, we investigated this issue in further detail in miscible PVME/PS and PI/P4tBS blend systems of different compositions, and additionally in a weakly miscible poly(n-butyl methacrylate) (PnBMA)/PS blend. We determine that the dielectric strengths, loss peak breadths, and correlation factors support a hypothesis that the slower α_0 process manifests a collective phenomenon involving a large number of chains relaxing concurrently. In addition, the faster α' process is associated with the relaxation times of the faster component within the nanoscale "frozen" confines of the higher T_g component. In light of these results, we suggest that the α, α_0, and α' processes would be present in weakly interacting blends, whose component T_gs are sufficiently separated.

2.2 Experimental Section

The dynamics of three blends – PVME/PS, PI/P4tBS, and PnBMA/PS – of varying compositions are investigated in this study: (i) PVME/PS blends containing 5, 15, 25, and 35 weight percent PVME; (ii) PI/P4tBS blends containing 20, 30, and 40 weight percent PI; (iii) PnBMA/PS blends containing 5, 25, and 35 weight percent PnBMA. The homopolymers PVME (number-average molecular weight M_n = 24.4 kg/mol, polydispersity index PDI = 1.08), deuterated polystyrene (dPS) (M_n = 4 kg/mol, PDI = 1.5), PI (M_n = 10.0 kg/mol, PDI = 1.03),

P4tBS (M_n = 32.0 kg/mol, PDI = 1.04) and PS (M_n = 13.5 kg/mol, PDI = 1.06) were purchased from Polymer Source Inc.; PnBMA (M_n = 13.0 kg/mol, PDI = 1.12) was purchased from Pressure Chemical Co. PVME and PI were both refrigerated with desiccants, prior to use. We also note that while deuterated PS was used in place of hydrogenated PS in PVME/PS, it had no effect on the dynamics in the temperature range of interest; in fact these blends are more miscible than the blends containing hPS.[133–135]

Blends were prepared by first dissolving the homopolymers separately in toluene (purchased from Sigma-Aldrich Corp.) at 3 weight percent concentrations, followed by agitation for 24 hours. The solutions were subsequently filtered using PTFE syringe filters with 0.2 μm pore size, then mixed to create the desired weight fractions, again agitated for 24 hours, then dried. Drying occurred first in a laminar flow hood for 72 hours, then under vacuum for 48 hours at 340K for PVME/PS, 383K for PI/P4tBS, and 400K for PnBMA/PS. These temperatures are well below the lower critical solution temperature (LCST) of the mixtures,[136–140] so the components in the blends remained miscible throughout the sample preparation and subsequent measurements, yet they are sufficiently high that while under vacuum the residual moisture was removed. The homopolymer samples were prepared by following the procedures described above without subsequent blending.

The T_gs of the pure component polymers and blends were measured using differential scanning calorimetry (DSC, Q200, TA Instruments) by first heating above the component T_gs and holding isothermally for 10 minutes, cooling at 10 K/min below the component T_gs, and then performing the measurement upon heating at 10 K/min. The glass transition was extracted from the step-like change in the endothermic heat flow baseline, where the baselines before and after the transition were extrapolated to a temperature where the change in heat capacity was at 50%

completion. This result was compared to the peak position in the derivative heat flow in order to ensure accuracy.

Measurements of the dynamics were performed using a broadband dielectric spectrometer (BDS, GmbH, Novocontrol Technologies). The polymer samples were sandwiched between two brass plates 10 mm in diameter; these two plates were used as electrodes in the subsequent experiment. In order to maintain a specific separation distance between the brass plates, especially at higher temperatures when the material viscosity is lower, two silica spacers 50 μm in diameter were placed between the two electrode plates. Because of exposure to air during sample preparation, the samples were annealed again within a BDS cryostat (Active Sample Cell ZGS, Novocontrol Technologies) under a nitrogen (N_2) flow environment at 340K for PVME/PS blends, 383K for PI/P4tBS blends, and 400K for PnBMA/PS blends, all for 10 hours, to ensure than any residual moisture was removed. After in situ annealing, each sample was cooled at a rate of 3 K/min. The BDS sweeps were performed in a frequency range of 0.1 Hz to 1 MHz with an AC voltage of 1.5 V. The temperature ranges were 250K to 325K at a 1K step for PVME/PS and PnBMA/PS and 185K to 440K at a 5K step for PI/P4tBS blends.

2.3 Results and Discussion

2.3.1 BDS Results for PVME/PS

The segmental relaxation rates ($1/\tau$) of the PVME component are plotted as a function of $1/T$ in **Figure 2.1**(a) for the pure PVME homopolymer and for blends of PVME/PS with different PVME concentrations. The glass transition temperature for each sample is identified with a vertical line. We are confident that we are probing solely the dynamics of the PVME chains in each blend for two reasons: (i) the rate of the PS segmental motions is known to be 10^3-

10^4 orders of magnitude slower than that of PVME[74,76] (and thus outside of the carefully chosen temperature and frequency range) and (ii) the dielectric relaxation strength of PS is much weaker than that of PVME.[119] The relaxation times were extracted by fitting the complex dielectric permittivity ε*(ω) at each temperature to a Havriliak-Negami (HN) function,[141] which includes contributions from conductivity:[142]

$$\varepsilon^*_{HN} = \varepsilon_\infty + \frac{\Delta\varepsilon}{(1+(i\omega\tau_{HN})^\beta)^\gamma} - i(\frac{\sigma_0}{\varepsilon_0\omega})^N \quad (2.1)$$

This equation is widely considered to be the most general empirical modeling function for a dielectric relaxation process. The characteristic relaxation time $\tau = 1/2\pi\omega$ is associated with the dielectric loss peak maximum of the imaginary portion of the permittivity ε''(ω); it is identified as the segmental relaxation time at that temperature.[142] The raw dielectric loss curves, including the HN fittings, can be found in **Figure A-1** of Appendix A.

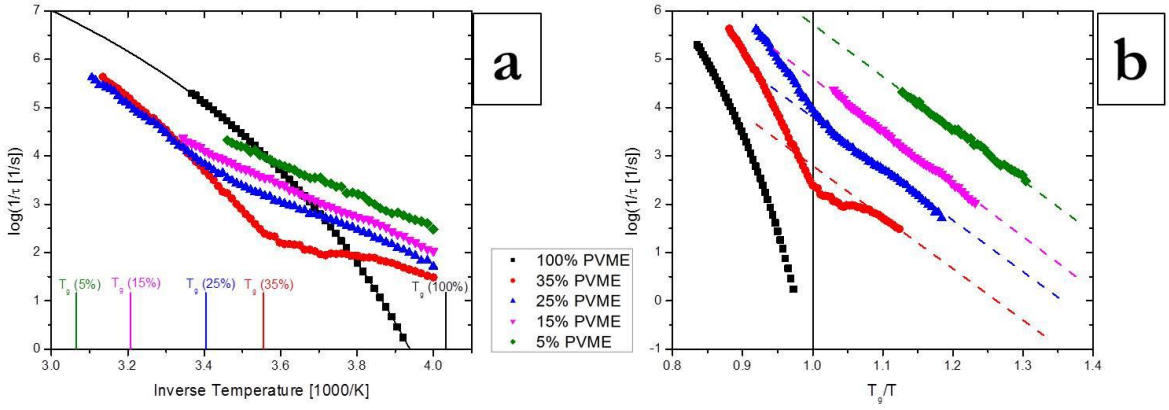

Figure 2.1: (a) Temperature dependencies of the inverse segmental relaxation times of PVME in pure PVME and PVME blends as calculated from frequency sweep (isothermal) dielectric loss curves as a function of inverse temperature. The vertical lines are corresponding to the sample T_gs. (b) Temperature dependencies of the inverse segmental relaxation times of PVME in pure PVME and PVME blends as calculated from frequency sweep (isothermal) dielectric loss curves as a function of T_g/T. The vertical line represents unity (T=T_g), and the dashed lines represent guides to the eye.

In the case of pure PVME (black squares), the temperature dependence of the relaxations is well described by the VFT relation (shown as the solid black line), as is expected for the

segmental, or α, relaxations of a pure homopolymer. With regard to the PVME/PS blends, the temperature dependencies of the PVME relaxations do not follow simple VFT behavior. For $T > T_g^{(blend)}$, the relaxations of the PVME and PS chains are anticipated to be cooperative because they are miscible and are both mobile. This temperature dependence is consistent with VFT-like behavior. Below $T_g^{(blend)}$ however, the PVME relaxation rates begin to follow an Arrhenius temperature dependence, for all blend compositions (note that no data is available in the melt state for the lower composition blends, φ_{PVME} = 15% and 5%). Colmenero and coworkers[68,76,119] first reported that for $T < T_g^{(blend)}$, the Arrhenius relaxation rates are indicative of the lower T_g PVME chains undergoing localized motions within the nanoscale confines of glassy (higher T_g) PS-rich domains ($T_g^{(PS)}$ = 353K and $T_g^{(PVME)}$ = 248K). Cooperativity would be suppressed within such small domains. Small angle neutron scattering experiments provide evidence of the freezing of the PS segments in this temperature range.[68,120,143] Additionally. this type of behavior has been shown experimentally in other dynamically asymmetric blends as well, such as PEO/PMMA[131,132] and PVDF/PMMA.[144]

If the relaxation rates are compared at the same T below $T_g^{(blend)}$, then it is evident that the PVME relaxation times decrease with decreasing φ_{PVME}: $\tau_{PVME}^{(5\%)} < \tau_{PVME}^{(15\%)} < \tau_{PVME}^{(25\%)} < \tau_{PVME}^{(35\%)}$. The compositional dependence is clearer after plotting the relaxation rates as a function of T_g/T in **Figure 2.1**(b) – the temperature difference ($T_g^{(blend)}$-T) influences the extent of freezing of the PS chains and hence the onset of Arrhenius behavior. Typically, the opposite trend in relaxation times is expected in compatible blends because, for lower φ_{PVME}, the PVME chains relax in an environment where the friction coefficient increases due to the higher number of high T_g and stiffer PS host chains. However, we note that although the average macroscopic

concentration decreases, the local – or nanoscopic – PVME concentration within the rigid PS domains increases due to spatial compositional changes.

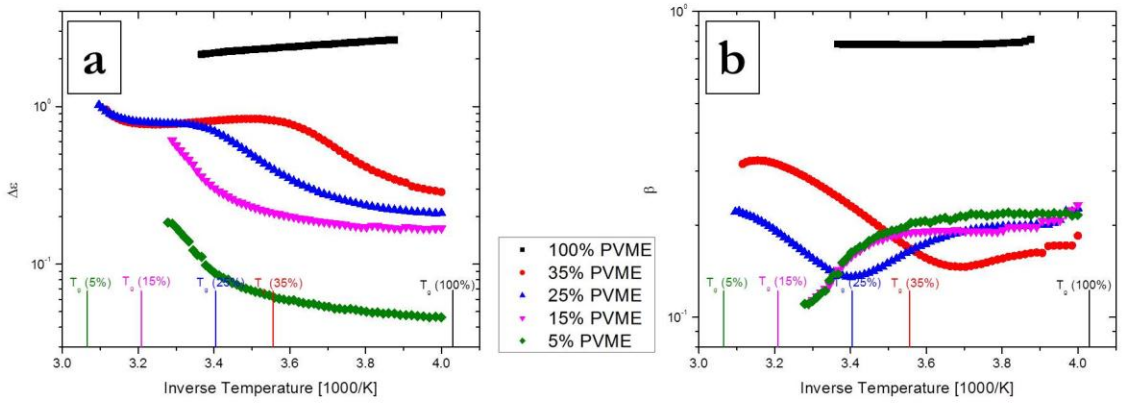

Figure 2.2: (a) Temperature dependencies of the dielectric strengths of PVME segmental relaxations in pure PVME and PVME blends as calculated from HN empirical fittings of frequency sweep (isothermal) dielectric loss curves. The vertical lines are corresponding to the sample T_gs. (b) Temperature dependencies of the β broadening parameter of PVME segmental relaxations in pure PVME and PVME blends as calculated from HN empirical fittings of frequency sweep (isothermal) dielectric loss curves. The vertical lines are corresponding to the sample T_gs.

The breadths and intensities of the dielectric loss curves provide additional information about the dynamics.[142] To begin with, the dielectric strengths, extracted from the HN formulism fittings of the frequency sweep data, are plotted in **Figure 2.2**(a); the strengths increase with increasing PVME concentration due to the larger number of relaxing PVME dipoles. In **Figure 2.2**(b), it is shown that pure PVME, due the absence of compositional heterogeneity, has a relatively narrow peak, as indicated by the comparatively large value of the broadening factor β – β was also extracted from the frequency sweep data using the HN formulism. Below $T_g^{(\text{blend})}$, the breadth of the 5% PVME blend loss peak is the narrowest of the blends and that of the 35% PVME blend is the broadest, indicating that the local environment surrounding the PVME chains trend towards less local compositional diversity with decreasing average (macroscopic) concentration. Moreover, the glass transition peaks characterized by the derivative heat flow (**Figure 2.3**) also trend toward decreasing breadths with decreasing PVME concentration. This is

a further indication that there is strong compositional heterogeneity and spatial separation between the two components in the different concentrations. Similarly, with decreasing average blend concentration, the PVME dynamics is faster because the local PVME concentration increases.

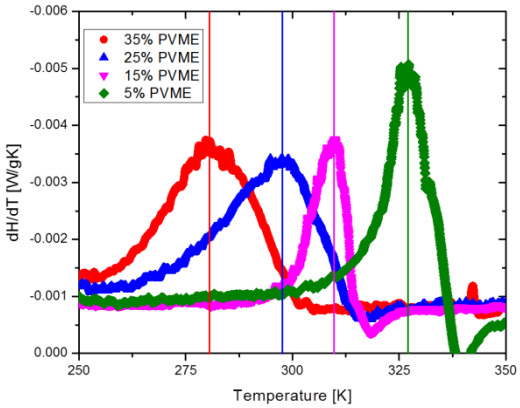

Figure 2.3: Derivative of the heat flow with respect to temperature for PVME blends. Vertical lines represent peak positions at which T_gs are taken.

2.3.2 Frequency versus Temperature-Dependent Experiments

As evident from the temperature-dependent behavior of the dielectric strength and broadening parameters in **Figure 2.2**, the spatial compositional heterogeneities that influence the dynamics are also temperature-dependent. For T above the glass transition, the fluctuations in local composition are rapid, and these fluctuations slow down with decreasing temperature. This may be understood in terms of the previously described Adam and Gibbs phenomenological model,[33] corroborated by simulations of the dynamics of miscible blends.[56,129] These simulations reveal that at high T, the autocorrelation function of end-to-end vector and self-intermediate scattering functions of miscible polymer blends both go to zero as time approaches infinity, indicating that any fluctuations in concentration do not influence the dynamics in different local regions at those temperatures. However for lower temperatures ($0.5 < T^* < 2$, $T^* = k_bT/\varepsilon$), the

compositional fluctuations are sufficiently slow such that they are able to affect the dynamics. This is supported by our experimental data, in which there is a change in the temperature dependence of the relaxation times between high and low *T*.

The isothermal permittivity intensities are strongly temperature-dependent because the dielectric strength is temperature-dependent. For pure PVME, as the temperature approaches T_g from the melt (see **Figure 2.2**(a)), the dielectric strength increases slightly due to a stronger effect of the electric field on the dipoles with less thermal motion. Concerning the blends for which we have data above $T_g^{(\text{blend})}$, the dielectric strength remains relatively constant because of the competing effect of PS vitrification hindering dipole motion. Similarly, the magnitude of the response diminishes with decreasing temperature below $T_g^{(\text{blend})}$ as further PS component vitrification hinders the overall contribution to the dielectric response.

The relaxation rates of miscible blends are both temperature-dependent and spatially composition-dependent. This has important implications regarding measurement of the relaxation processes in these materials. Frequency sweep experiments – isothermal measurement of $\varepsilon''(\omega)$ as a function of *T* – and the temperature sweep experiments – isochronal measurement of $\varepsilon''(T)$ at different ω – have different sensitivities to different features of the dielectric response, and hence to the segmental dynamics. Indeed, the linear response theory, which assumes that the electric field strength is sufficiently small, remains valid, as each type of measurement probes the same time-dependent processes. In a pure homopolymer both types of experiments yield identical results. However for an A/B blend in which the mobilities of the components differ significantly, it is important to perform both frequency and temperature sweep experiments in order to get a complete picture of the temperature and composition-dependent relaxation processes.

Consider the PVME/PS blend, which is characterized by spatial composition heterogeneity. At high temperatures, the dielectric response is strong because both PVME and PS chains are mobile; the magnitude of the dielectric response diminishes with decreasing T below $T_g^{(\text{blend})}$ because of PS vitrification. Since PS possesses a much higher T_g, the dynamics of the PS segments decreases at a much faster rate and virtually vanish when $T = T_g^{(\text{PS})}$. Since the PVME chains remain mobile, they are primarily responsible for the dynamic response. Thus isothermal frequency sweeps are more sensitive to spatially local regions of the blend where the relaxation rates are fastest. In other words, the spatial domains with lower local T_g – containing a higher local PVME concentration – would make the primary contribution to the dielectric intensity. This is the reason PVME relaxation times are slowest in the blend containing the largest average PVME concentrations, decreasing with decreasing φ_{PVME}: $\tau_{\text{PVME}}^{(5\%)} < \tau_{\text{PVME}}^{(15\%)} < \tau_{\text{PVME}}^{(25\%)} < \tau_{\text{PVME}}^{(35\%)}$. In contrast, temperature sweep experiments,[106,117,145] are sensitive to the temperature at which a specific relaxation frequency has the greatest signal intensity, i.e.: the temperature and frequency at which the largest number of dipoles are relaxing. In the absence of compositional heterogeneity (for example a pure homopolymer) all chains relax in the same average environment, so the temperature and frequency scan measurements yield identical results.

Recently Yang and Green[112] showed how measurements of the dielectric response as a function of frequency and temperature (2D analysis) can be effective at identifying multiple relaxations in miscible blends. To illustrate this point, consider the temperature sweep and frequency sweep data points, as overlaid onto the 2D contour map of the same samples, shown in **Figure 2.4**. These data mimic the contours of the map, thereby illustrating the point that both types of experiments should be performed in order to understand all relaxation processes in

miscible blends. Fitting of the peaks measured by the temperature sweep experiments (raw dielectric loss curves at select frequencies are shown in **Figure A-2** of Appendix A) and extracting the characterization parameters was accomplished using a modified version of the HN function.[106] Now consider the relaxation rates of the 35% PVME blend (**Figure 4.4**(a)), as calculated from both the frequency (isothermal) and temperature (isochronal) sweep data, on the respective contour plot. At temperatures sufficiently high above $T_g^{(\text{blend})}$, the compositional fluctuations would presumably be fast compared to the segmental dynamics, so the segments appear to be relaxing in the same average compositional environments. That the temperature sweep and frequency sweep experiments yield comparable relaxation rates and temperature-dependent behaviors in this region is consistent with this notion. However with decreasing temperature, the difference between the rates measured by the two experiments becomes apparent; the frequency sweep experiments preferentially detect the faster relaxation processes, associated with the peaks at the upper part of the plot; the more slowly relaxing species contribute a comparatively small intensity to this overall relaxation spectrum. A temperature sweep experiment will measure the highest signal intensity at temperatures at which the largest numbers of dipoles are relaxing with identical frequency. In this regard, the temperature sweep experiments are sensitive to a slower relaxation process, associated with the peaks at the lower section of the plot, as discussed earlier.

In the isochronal temperature sweep, the segmental relaxations exhibit a strong temperature dependence, decreasing rapidly with decreasing T, as T approaches $T_g^{(\text{blend})}$. This behavior is indicative of a cooperative process associated with the fluctuations of a large number of dipoles. We will refer to this strongly temperature-dependent process as the α_0 process. The isothermal frequency sweep experiments are particularly sensitive to dipolar relaxations in the

local regions of the 35% blend with fast PVME relaxations; moreover the temperature dependence of the dynamics from this experiment is weaker and persists to temperatures far below $T_g^{(\text{blend})}$. As discussed earlier, the PVME molecules here undergo relaxations within the confines of the glassy PS domains. We will refer to this as the α'process.[68,76,119]

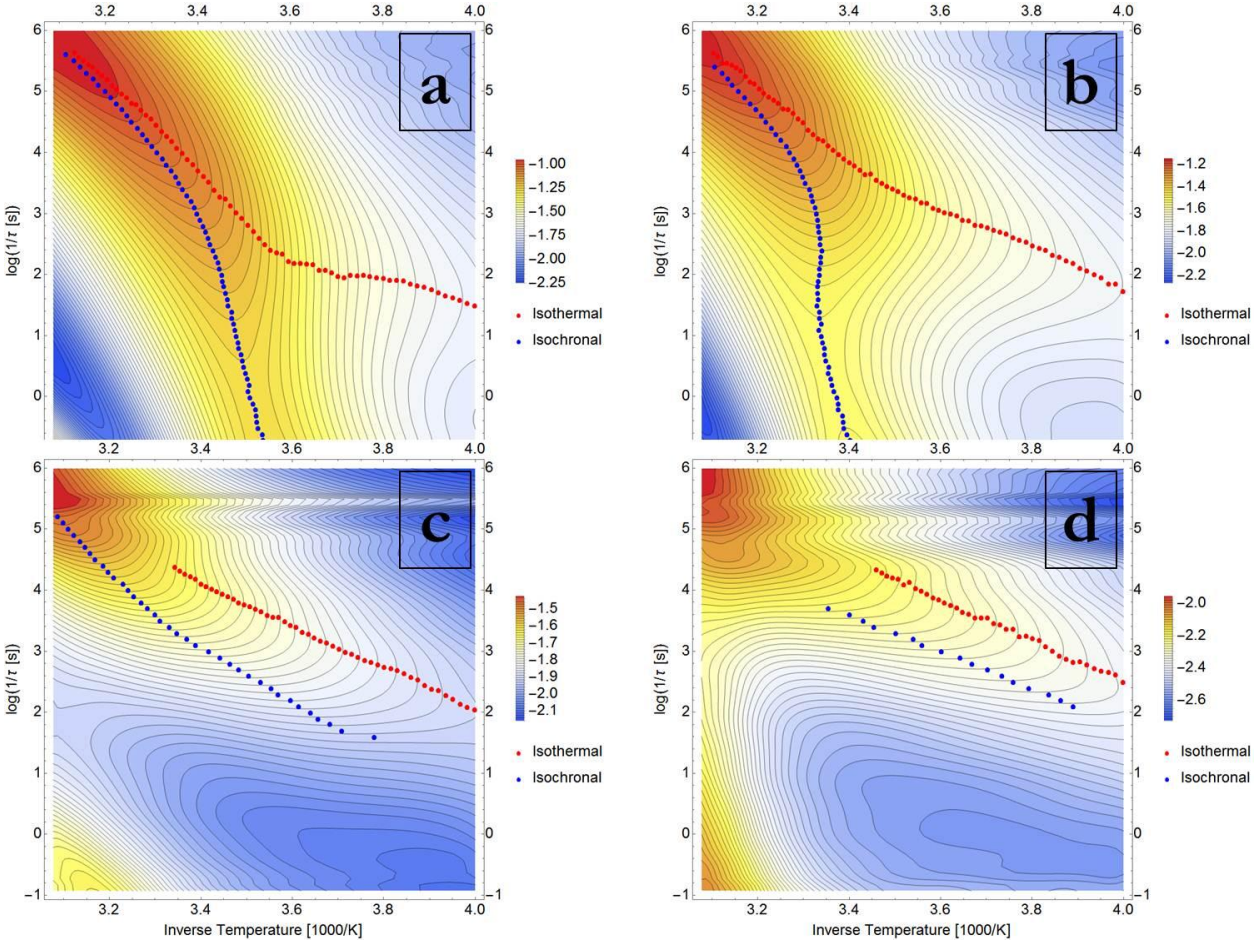

Figure 2.4: Contour maps of (a) 35% (b) 25% (c) 15% (d) 5% PVME made from the frequency sweep experiments as a function of inverse temperature and frequency of the applied electric field. Overlaid are the loss peak maxima as calculated from the frequency sweeps (red circles) and the temperature sweeps (blue circles).

Note that in **Figure 2.4** the isochronal representation of the dynamics reveals that the φ_{PVME} = 35% and 25% blend dynamics exhibit a VFT-like temperature dependency and do not extend below the blend T_g, whereas the data of the φ_{PVME} = 15% and 5% PVME blends are Arrhenius at lower temperatures. Because each of the frequency and temperature sweeps probe

the same time-dependent processes but differ only in sensitivity, we speculate that the α' process becomes more apparent in the temperature sweep experiments with decreasing φ_{PVME} as the tracer limit is approached.

A lingering question one may ask is whether the large variations of the dielectric strength between blend compositions and temperatures would be the cause of the differences detected by the two sweeps. This is evidently not the case for three reasons. First, the expected shift would not be many orders of magnitude as observed; for every order of magnitude shift in dielectric strength, the reciprocal shift in relaxation time would be less than a factor of ten. In the case of the 35% PVME blend, there is a divergence of many orders of magnitude, yet the dielectric strengths remain in the same order of magnitude. Secondly, there would be no change in the temperature dependence of the relaxations if the difference was due solely to an intensity change, in particular a change in inflection as seen in the high φ_{PVME} blends. Finally, one would expect the deviations to become increasingly prominent with decreasing low T_g component concentration, as noted by Colmenero in the PI/P4tBS blend.[117] In PVME/PS, we see the opposite effect – increased deviations with increasing φ_{PVME}.

2.3.3 BDS Results for PI/P4tBS

Now that we have observed this behavior in the well-studied PVME/PS blend, we question to what extent would this type occur in other blend systems? As noted previously, while other blend systems have shown a shift to Arrhenius behavior at low enough temperature,[131,132,144] they have not extended to the identification of an α_0 process. In an attempt to rectify this, PI/P4tBS, a miscible blend which exhibits two component glass transition temperatures that differ by over 200K ($T_g^{(PI)}$ = 206K and $T_g^{(P4tBS)}$ = 419K), is now investigated. While similar experiments have previously been performed on this blend, no evidence of either

the α' nor α_0 process has been reported,[117] although it has been conceptualized.[65] In this system, the two separate T_gs are due to the self-concentration effect; because of the strong connection between T_g and segmental dynamics in the bulk materials, it is of interest to see how this system behaves in comparison with PVME/PS. **Figure 2.5** shows the derivative heat flows as a function of temperature as measured by DSC for different concentration PI/P4tBS blends. It is quite apparent that in addition to the appearance of two T_gs, the PS effective glass transition temperature also shifts more than 50K with a 20% change in macroscopic weight concentration, manifesting the shift in spatial compositional heterogeneity throughout the different blend compositions. Interestingly, the PI component T_g is only influenced by composition slightly, thereby indicating a less compositionally heterogeneous effect with a change in macroscopic blend concentration for this component. In other words, it appears the PI chains are less effected by the host P4tBS chains than vice versa.

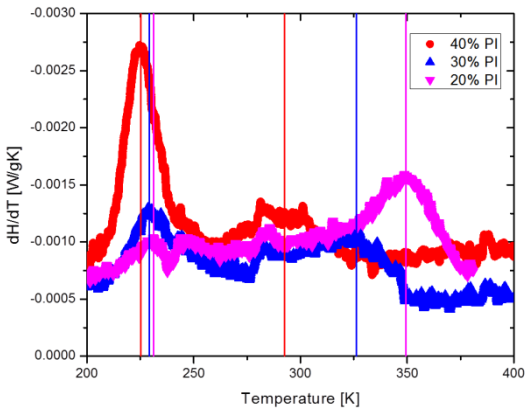

Figure 2.5: Derivative of the heat flow with respect to temperature for PI blends. Vertical lines represent peak positions at which T_gs are taken.

The temperature sweep measurements of the chain relaxations in pure PI, pure P4tBS, and the PI/P4tBS blends are shown in **Figure 2.6**(a). In our BDS studies of the blends, only the PI relaxations are of interest; the P4tBS segmental relaxations (olive diamonds) are both weaker

and well out of the temperature range where the segmental relaxations occur. While both segmental and end-to-end dipolar relaxations are exhibited by polyisoprene, only the segmental relaxations are of interest in this study. From **Figure 2.6**(a), it is apparent that there is an observable separation between the segmental and end-to-end dynamics, allowing for the PI α processes to be isolated. **Figure 2.6**(b) contains both the frequency and temperature sweep measurements of the PI segmental dynamics in the homopolymer and all blend compositions. The raw dielectric data of these measurements may be found in **Figure A-3** and **Figure A-4**, respectively, in Appendix A. One of the two T_gs (the effective glass transition temperature $T_g^{(\varphi PI)}$) of the blends for the different composition blends and pure PI homopolymer is identified as vertical lines in **Figure 2.6**(b). The frequency and temperature sweep experiments yield the same relaxation rates for the pure PI dynamics, as expected for a homopolymer. The PI relaxations are slower in the blends, decreasing with decreasing PI concentration φ_{PI}. As the PI molecules undergo diffusion in an environment where the concentration of higher T_g P4tBS molecules increases, they experience larger intermolecular interactions (friction) that reduce their mobilities. Both the segmental and end-to-end dynamics in **Figure 2.6**(a) corroborate this notion. While anticipated, this is different from the behavior of the PVME/PS blend.

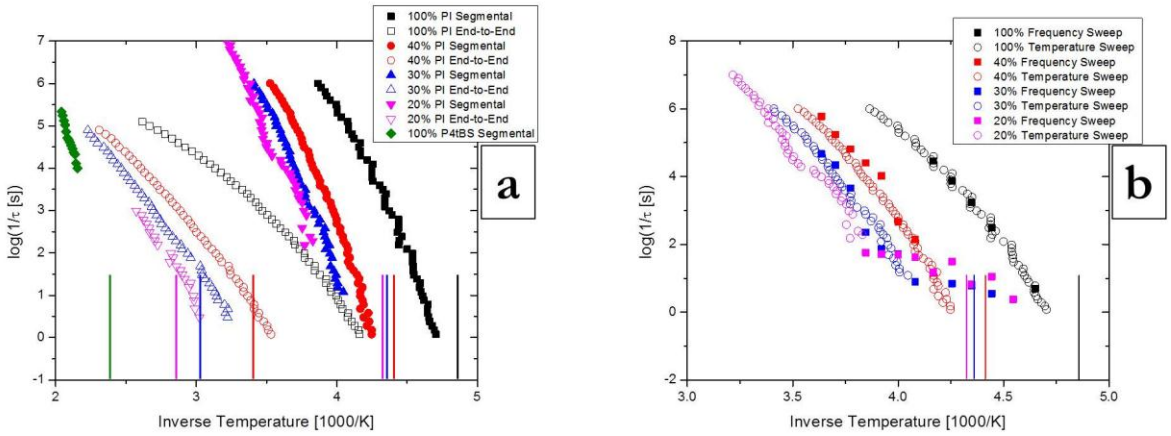

Figure 2.6: (a) Temperature dependencies of the inverse relaxation times of pure PI, pure P4tBS, and PI blends as calculated from the temperature sweep (isochronal) experiments. Vertical lines indicate the two component T_gs. (b) Temperature dependencies of the inverse segmental relaxation times of PI in the pure homopolymer and the PI blends as calculated from both the frequency sweep (isothermal) and temperature sweep (isochronal) measurements. Vertical lines indicate the lower of the two component T_gs.

For all blends, the temperature sweeps reveal that the segmental relaxations exhibit VFT-like temperature dependences, similar to the PVME/PS blends. Because the signal intensities obtained from the frequency sweep measurements in this low temperature regime are small (see raw dielectric loss curves in Appendix A), it was not possible to prepare reliable contour plots. This, along with the noise of the data, is believed to be the same reason that Colmenero and coworkers[117] were unable to detect the Arrhenius relaxation regime when they performed dielectric spectroscopy on these blends. In our analysis, the low temperature relaxations are only determined with HN fittings of the 1D curves.

Consider the frequency sweeps of the lower PI concentrations – 30% and 20%, blue and magenta squares, respectively – in **Figure 2.6**(b). For temperatures $T > T_g^{(\varphi PI)}$, the relaxation rates measured using temperature sweep and frequency sweep experiments are similar, reflecting the notion that the rate of compositional fluctuations are rapid compared to the segmental relaxations. Under these circumstances, the segments relax in the same average environment across the entire system. On the other hand, at lower temperatures in the vicinity of $T_g^{(\varphi PI)}$, where

we now speculate the compositional fluctuations rates are slow compared to the segmental relaxation rates, the segmental dynamics is sensitive to the local compositional environments. The Arrhenius temperature-dependent behavior associated with the α' process is measured by the frequency sweep experiments, which are sensitive to localized motions. The other process, which diminished rapidly in the vicinity of $T_g^{(\varphi PI)}$ would be the α_0 process appearing in the temperature sweeps, which are sensitive to cooperative motions. In the φ_{PI} = 40% PI blend, the isothermal measurements are unable to detect an Arrhenius-like temperature dependence in the segmental dynamics at low temperatures, suggesting that the temperature range is sufficiently high that the concentration fluctuations are fast compared to the segmental relaxations. Evidently, throughout the measured temperature range, the PI segments experience the same average environment, and similarly spatial compositional heterogeneity is not observable in the dynamics.

While this blend exhibits some of the characteristic behavior of the PVME/PS blends, there are some contrasts. For example, the temperature and frequency sweeps do not detect very different relaxation rates associated with two processes; instead the measured rates are comparable for temperatures as low as the $T_g^{(\varphi PI)}$; at lower temperatures an Arrhenius temperature dependence is measured. The latter is likely associated with the transitional α to α' behavior. In PVME/PS, because there is one broad $T_g^{(blend)}$, the transition occurs when the entire system undergoes a glass transition. In PI/P4tBS, where there exists two T_gs while the blend maintains miscibility, the transition occurs near $T_g^{(\varphi PI)}$. This seems to go against the theories and other experiments that show the appearance of an Arrhenius regime in other blends.[65,131,132] Understanding why this occurs is a topic of future work.

2.3.4 BDS Results for PnBMA/PS

As mentioned above, the existence of multiple relaxation processes associated with the same mechanism in the same component is particularly evident in these blends because of the significant asymmetries between the relaxation rates of the individual components. Thus far we have shown that these processes occur in miscible blends. However the manner in which this behavior would be manifested in weakly miscible blends in which spatial compositional heterogeneity occurs at a larger length-scale is yet to be understood. To this end we examine the dynamics of PnBMA in weakly miscible PnBMA/PS blends. We note that full phase separation does not occur until an LCST temperature of 400K, which is beyond our measurement temperature range.[140] This blend exhibits two component glass transition temperatures $T_g^{(PS)}$ = 371K and $T_g^{(PnBMA)}$ = 298K; these component T_gs in the blend do not vary with composition (see **Figure 2.7**). The pure component PnBMA dynamics has been previously investigated[146,147] and it was found that in addition to an α relaxation there is a prominent β relaxation that arises from the rotational motions of the side chain about the carbon-carbon bond connected to the main chain,[148] similar to poly(methyl methacrylate) (PMMA) and poly(ethyl methacrylate) (PEMA).[149,150] Like PMMA and PEMA, the α and β relaxations merge and form what is known as the αβ process; this occurs at high temperatures, at which the time-scales of the two processes are on the same order of magnitude. Typically, it is difficult to deconvolute the two because of the overlapping dielectric loss peaks, though there have previously been some successful attempts through modeling.[151,152] Because of the strength of the PnBMA β relaxation, we can use the origin of the processes to our advantage. Specifically, the β relaxation represents a localized motion, and the α relaxation represents a cooperative motion at the higher temperatures. Similar to PVME/PS, because the rates of the PS segmental motions are over two orders of magnitude

slower than that of PnBMA, and they have a weaker dielectric strength, we are confident that we are probing only the PnBMA relaxations.

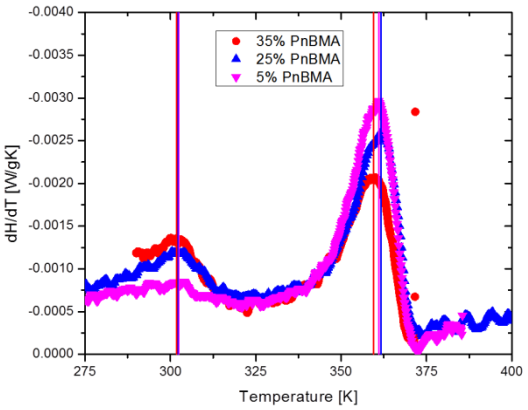

Figure 2.7: Derivative of the heat flow with respect to temperature for PnBMA blends. Vertical lines represent peak positions at which T_gs are taken.

The contour plots of the PnBMA/PS blends of different concentrations, with the isothermal and isochronal representations of the PnBMA segmental dynamics overlaid, are shown in **Figure 2.8** (raw dielectric loss information can be found in **Figure A-5** and **Figure A-6** of Appendix A, respectively). The behavior shown here is identical to that of PVME/PS: the frequency sweeps are sensitive to the faster relaxation processes, and the temperature sweeps show a strong temperature dependence decreasing rapidly as T approaches $T_g^{(\text{blend})}$. The isothermal experiments appear to exclusively detect the localized β relaxations, and the isochronal measurements are exclusively sensing the cooperative α relaxations. The absolute values and temperature dependencies of these relaxation rates are in excellent agreement with results in the literature.[151,152] In addition, the low concentration behavior is similar to the PVME/PS blend as well – the very weak temperature-dependent behavior and lack of a significant signal from the isochronal measurements reveals that the PnBMA component behaves as a tracer. Note that what we are showing here is not the Arrhenius separation between the α and

α' processes, but rather the benefits of both frequency and temperature sweeps at observing and identifying local and cooperative relaxation processes.

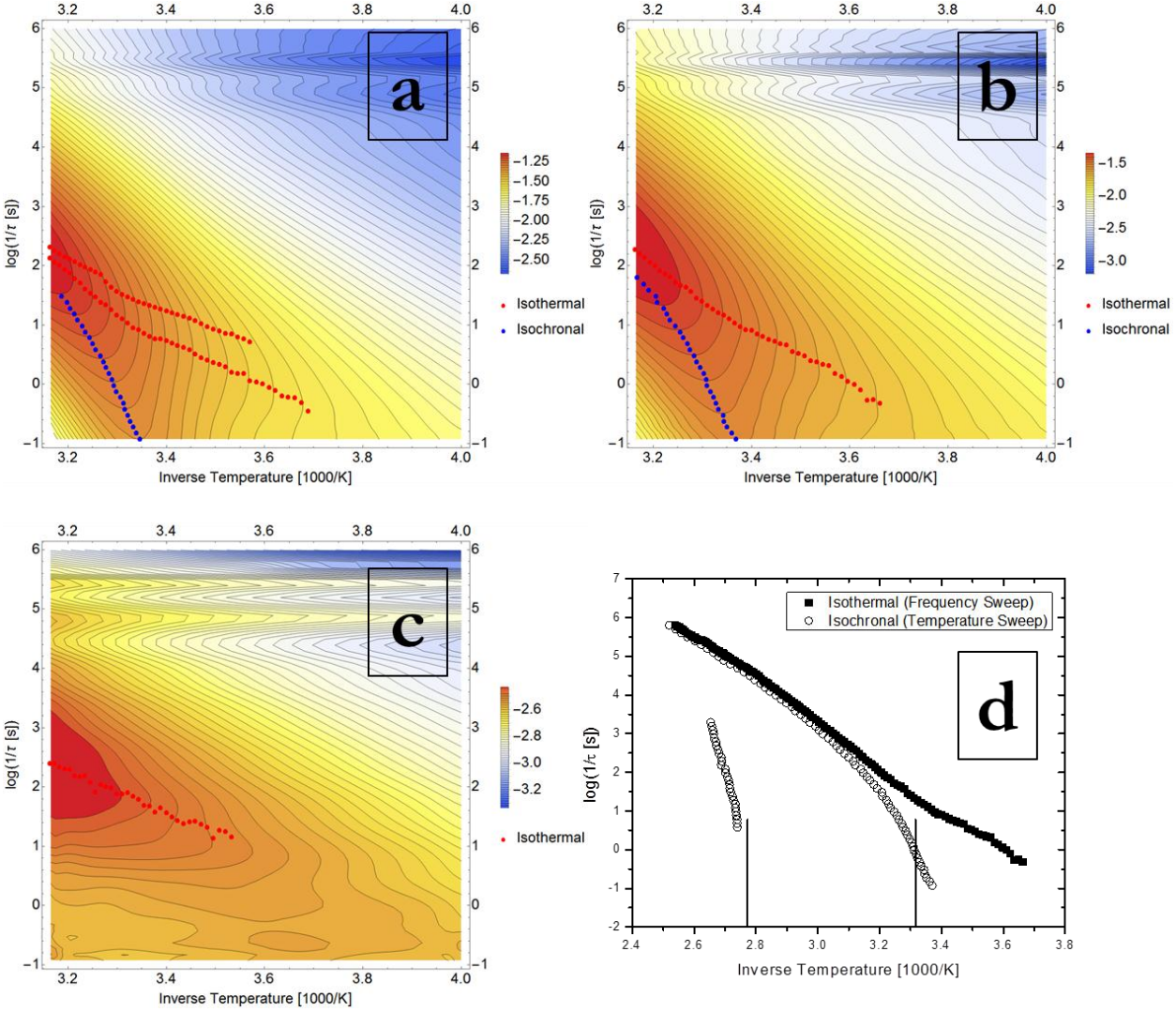

Figure 2.8: Contour maps of (a) 35% (b) 25% (c) 5% PnBMA made from the frequency sweep (isothermal) experiments as a function of inverse temperature and frequency of the applied electric field. Overlaid are the loss peak maxima as calculated from the frequency sweeps (isothermal) and the temperature sweeps (isochronal) experiments, as red and blue circles respectively. (d) Temperature dependencies of the inverse segmental relaxation times of the 25% PnBMA blend as calculated from both the frequency sweep (isothermal) and temperature sweep (isochronal). The vertical lines indicate the two T_gs.

We also show that if the temperature range is increased to higher *T*, the difference between the two measurements (due to experimental sensitivities) becomes marginal within the moderate concentration blends (see **Figure 2.8**(d)). Here we increased the measurement temperature window for the 25% PnBMA blend and learned that the separation between the

relaxation rates occurs at a temperature located between the two component T_gs. With further increasing temperatures, we identify the convoluted αβ process and the frequency and temperature sweep data converging, as shown for the previous two blend systems. It should also be noted that the frequency sweep (isothermal) measurements are unable to detect the PS component –this is another reminder that such an experiment is sensitive to localized motions rather than cooperative. Similarly, the PS segmental relaxations can be identified (left side of **Figure 2.8**(d)) in the temperature sweep experiments.

2.3.5 Theory and Mathematical Analysis of PVME/PS

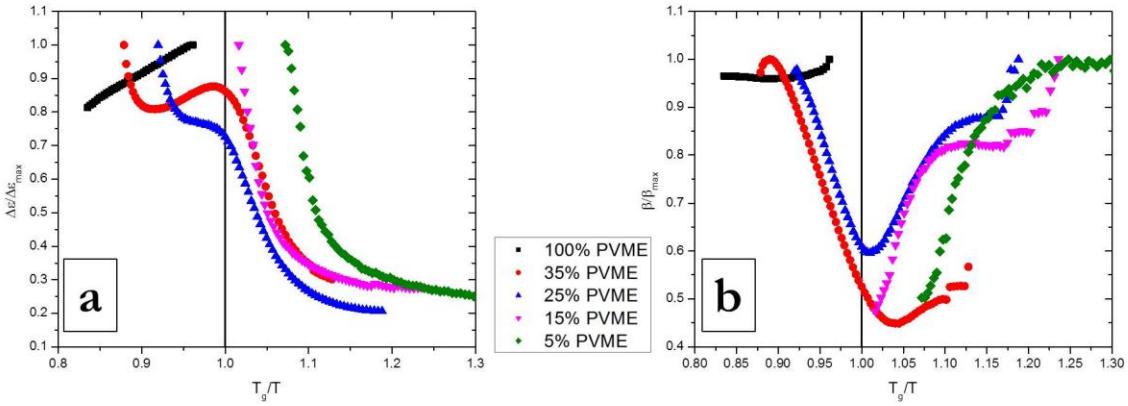

Figure 2.9: (a) Temperature dependencies as a function of T_g/T of the normalized dielectric strengths of PVME segmental relaxations in pure PVME and PVME blends as calculated from HN empirical fittings of frequency sweep (isothermal) dielectric loss curves. The vertical line represents unity ($T_g = T$). (b) Temperature dependencies as a function of T_g/T of the normalized β broadening parameters of PVME segmental relaxations in pure PVME and PVME blends as calculated from HN empirical fittings of frequency sweep (isothermal) dielectric loss curves. The vertical line represents unity ($T_g = T$).

As mentioned previously, the fitting parameters from the HN empirical fits can provide key insights into the dynamics. To further illustrate this, we examine the temperature dependence of the parameters in the PVME/PS blends. Plotted in **Figure 2.9**(a) are the normalized dielectric strengths $\Delta\varepsilon/\Delta\varepsilon_{max}$ for the four blend samples and the pure homopolymer, as a function of T_g/T. Within the context of polymeric materials with permanent dipole moments, the dielectric strength as calculated from the complex dielectric function can be exclusively related to the

change in dielectric permittivity due to orientation (dipole) polarization and written in the form of

$$\Delta\varepsilon = \varepsilon_s - \varepsilon_\infty = \frac{1}{3\varepsilon_0}\frac{\mu^2}{k_B T}\frac{N}{V} \tag{2.2}$$

In this equation $\varepsilon_s = \lim_{\omega\to 0}\varepsilon'(\omega)$ is the relaxed permittivity, accounting for all polarization components; $\varepsilon_\infty = \lim_{\omega\to\infty}\varepsilon'(\omega)$ is the unrelaxed permittivity that accounts for contributions to the dielectric function due to induced polarization (in this case resonance phenomena due to electronic or atomic vibrations). ε_0 is the dielectric permittivity of vacuum, k_BT is the thermal energy, N is the total number of dipoles in the system acting over a volume V, and μ^2 is the mean square dipole moment. A thorough derivation of this can be found elsewhere.[120,142]

For pure PVME (black squares), we noted previously that $\Delta\varepsilon$ increases with decreasing temperature. This is expected because equation (2.2) provides an inverse relation between dielectric strength and temperature. As the temperature is decreased, the effect of the electric field on the dipoles is increased due to less random thermal energy. However, the dependence is stronger than predicted. It is argued[120] that this additional temperature dependence results from an increasing influence of cross-correlation terms in μ^2; in other words, the reorientation of a specific dipole is influenced increasingly by its environment with decreasing T. This is consistent with the cooperativity argument mentioned previously.[33–35,113] This point is especially important for understanding dynamics in the blends, where in all blend compositions we see behavior that indicates a decrease in dielectric strength with decreasing temperature below the blend glass transition temperature. This provides credibility for the localization of motions and decreasing cooperativity with temperature below $T_g^{(\text{blend})}$; as the PS component is vitrified, different blend regions are "frozen in". They are less able to cooperatively relax due to dynamically asymmetric confinement; hence the intermolecular dipole interaction terms in μ^2 also decrease. Essentially,

vitrification hinders dipole motion. Because it is a squared term, its effect on Δε is greater than the linear relation with *T*.

In addition, for samples in which we are able to observe α relaxations above the blend glass transition (25% and 35% PVME, blue up triangles and red circles in **Figure 2.9**(a), respectively), we see rapidly decreasing Δεs at high *T* and a plateau near $T_g^{(blend)}$. For higher concentration blends, at the highest temperatures, increasing Δε with increasing *T* above $T_g^{(blend)}$ represents additional mobility of segments due to the unfrozen PS segments adding to the dielectric response. Further decreasing temperature has the competing effects of PS vitrification and increased electric field effect. For the lower concentration blends, the disappearance of a measureable Δε at the highest measured temperatures represents an interesting phenomenon. The magnitude of Δε is composition-dependent (decreasing with decreasing PVME concentration), as *N* is composition-dependent. Evidently what is occurring is a loss of sensitivity to a subset of chains as $T_g^{(blend)}$ is approached. In other words, a portion of the dynamics of PVME chains is being obscured in the dielectric loss peak curves from the frequency sweep dielectric measurements.

Figure 2.9(b) shows the temperature dependence of the normalized HN broadening parameter β for the four blend samples as well as for the pure homopolymer. As mentioned earlier, the breadth of the loss peaks may be related to a distribution of relaxation frequencies, and likewise a distribution of local environments governing said relaxation rates. The relaxation functions as measured for the blends are considerably broadened compared to the pure polymer.[62,68,128] Our interest is in the temperature dependence. Whereas the pure polymer shows a more or less temperature independent β, the blends show a strong decrease above the blend T_g and a significant increase in β below the blend T_g. This seems to indicate that on opposite sides of

the blend glass transition temperature, there are two different processes occurring. The low temperature behavior is associated with the localized segmental relaxation model; as the PS component becomes vitrified, the distribution of local environments, and the distribution of relaxation times, becomes less broad as the local environments become frozen. Of greater interest is the temperature dependence of the β parameter for the blends in which relaxations occur for $T > T_g^{(\text{blend})}$. Here we note a decrease in β with decreasing *T*, or a broadening of relaxation distribution. Such a rapid decrease in the magnitude of β is indicative of a rapid appearance of a wide distribution of local environments in the blend, which is expected for the strong temperature dependent and cooperative relaxation process seen in this temperature regime.

Returning to the initial assumptions made for analyzing the dielectric data,[120,142] first we assumed that the electric field at the locus of the dipole is equal to the outer electric field. However, because of shielding effects, the electric field at the dipole is not exactly the same as the applied one. These local, or internal reaction, field effects occur because the permanent dipole being measured is surrounded by other polar molecules which, when polarized, can alter the effective field. As such, permanent dipoles in the surrounding environment polarize the measured dipole. This effect has been studied extensively; however the most general extension of the Debye formula for polar molecules is given by Onsager's work on the reaction field.[153] The calculations alter equation (2.2), which now becomes

$$\Delta\varepsilon = \varepsilon_s - \varepsilon_\infty = \frac{1}{3\varepsilon_0}\frac{\mu^2}{k_B T} F \frac{N}{V} \tag{2.3}$$

where *F* is the unspecific correction Onsager factor and is given as:

$$F = \frac{\varepsilon_s(\varepsilon_\infty+2)^2}{3(2\varepsilon_s+\varepsilon_\infty)} \tag{2.4}$$

This works well for estimating dipole moments in a dispersed gas phase, yet it fails to accurately predict dipole moments in associated liquids. We now know that it is because it does not take into account the important role dipole interactions have in condensed systems.

This further problem was treated by Kirkwood[154,155] and by Frohlich.[156] According to statistical mechanics, the contribution of the orientation polarization to the dielectric function is given by

$$\varepsilon_S - \varepsilon_\infty = \frac{1}{3\varepsilon_0 k_B T}\frac{\langle \vec{P}(0)\vec{P}(0)\rangle}{V} = \frac{1}{3\varepsilon_0 k_B T}\frac{\langle \sum_i \overrightarrow{\mu_i}(0)\sum_j \overrightarrow{\mu_j}(0)\rangle}{V} \tag{2.5}$$

where <*P*(0) *P*(0)> is the static correlation function of dipole fluctuations over the whole system, considering all interactions. In practice, this is nearly impossible to compute, and thus a correlation factor *g* was introduced as

$$g = \frac{\langle \sum_i \overrightarrow{\mu_i}\sum_j \overrightarrow{\mu_j}\rangle}{N\mu^2} = \frac{\mu^2_{interact}}{\mu^2} \tag{2.6}$$

where μ^2 is defined previously as the mean square dipole moment for non-interacting, isolated dipoles. More detailed information about this may be found elsewhere.[120] By using data from the dielectric strength, the Frohlich equation[156] enables the effective dipole moment to be written as

$$g\mu^2 = \frac{kT\varepsilon_0}{N}\frac{(\varepsilon_S - \varepsilon_\infty)(2\varepsilon_S + \varepsilon_\infty)}{\varepsilon_S} \tag{2.7}$$

This expression shows that the *g* factor is a measure of the extent to which restricted internal rotations and interactions of neighboring dipoles influence dipole alignment.

Rellick and Runt[157] further applied this to derive an equation for the *g* factor of a polymer blend with respect to its unblended state, showing that for a blend

$$g_{blend} = 9\varepsilon_0 k_B T \frac{\frac{\Delta\varepsilon(2\varepsilon_S + \varepsilon_\infty)}{n\varepsilon_S}}{g_1 n_1 \mu_1^2(\varepsilon_\infty + 2)^2 + g_2 n_2 \mu_2^2(\varepsilon_\infty + 2)^2} \tag{2.8}$$

In this equation n is the overall dipole density of the blend and n_i is the mole fraction of the component i in the blend. The variable g_{blend} is now a measure of the effect of blending on the dipole alignment. As such, g_{blend} is a measure of the polarization in the blend relative to that in the unblended environment. Based on equation (2.8), it is the effective squared moment in the blend over the squared moment that would be obtained if there were no change in interactions. As such, in the blends, we cannot distinguish whether such interactions are parallel or antiparallel in alignment. However, we can relate this to increases or decreases in the effective dipole moment.[157]

The data in **Figure 2.10** reveal that the calculated values of g_{blend} decrease with increasing T_g/T. These data were determined by first calculating $g\mu^2$ for the pure PVME and PS components using equation (2.7) in conjunction with the dielectric data from the HN fitting parameters – obtained from the isothermal experiments at all the experimental temperatures. This information was then used in equation (2.8), along with the blend dielectric data and fitting parameters at each temperature and the appropriately calculated mole fractions. The temperature dependence of g is due to the temperature dependencies of the dielectric strengths.

The decrease of g_{blend} with decreasing temperature is very similar to that of the dielectric strengths. For $T < T_g^{(blend)}$ in all the blends, there is a decrease in g_{blend} with decreasing temperature, indicating a decrease in the effective moment, suggesting less influence by intermolecular interactions. This may suggest the existence of localized and uncorrelated dipole orientations. For the low φ_{PVME} blends in which the VFT to Arrhenius transition is not evident (15% and 5% as the magenta down triangles and olive diamonds of **Figure 2.10**, respectively), the g factor increases with increasing T to the blend glass transition temperature. In the blends in which a temperature-dependent dynamic transition does occur (35% and 25% as the red circles

and blue up triangles of **Figure 2.10**, respectively), the pleateau near $T_g^{(blend)}$ followed by an increasing g factor can be due to large reductions in rotational barriers as the blend approaches its melt state.

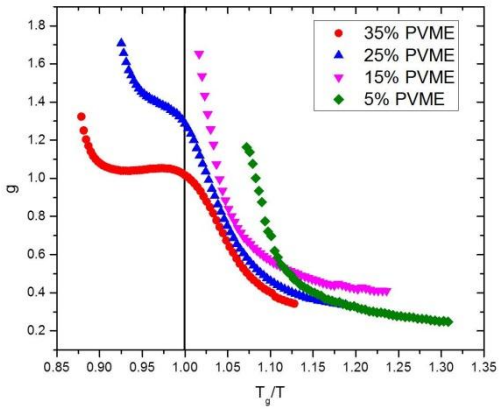

Figure 2.10: Temperature dependencies as a function of T_g/T of the g factor of PVME segmental relaxations in PVME blends as calculated from the frequency sweep (isothermal) experiments. The vertical line represents unity (T_g/T).

2.4 Conclusions

Spatial compositional heterogeneity at the nanoscale is an inherent feature of both miscible and immiscible A/B polymer/polymer blends. The heterogeneity is temperature-dependent, with has important consequences on the dynamics. At high temperatures where the rate of compositional fluctuations is fast compared to the segmental relaxations, the chains would relax in the same average environment. On the other hand, for lower temperatures, the compositional fluctuations are slow compared to the segmental relaxations, and the dynamics of the molecules is sensitive to the local compositional environment. This is particularly evident in weakly interacting blends, in which dynamically asymmetric confinement effects can occur. In order to understand the multiple relaxation processes due to spatial compositional heterogeneity in blends, two types of broadband dielectric spectroscopy experiments were performed: (i) a

frequency sweep experiment (measurement of ε''(ω) at different temperatures) and (ii) a temperature sweep experiment (measurement of ε''(T) at different frequencies).

Segmental dynamics in two miscible polymer blends – PVME/PS and PI/P4tBS – and one weakly miscible blend – PnBMA/PS – are investigated. The PVME/PS system exhibits an average glass transition temperature, $T_g^{(\text{blend})}$, whereas PI/P4tBS and PnBMA/PS each exhibit two separate component T_gs. The main finding is that the faster, lower T_g component of the blends – PVME, PI, or PnBMA – behave similarly. This lower T_g component relaxes in two different, distinctly dominant local compositional environments. Relaxation rates, measured using the BDS frequency sweeps, exhibited Arrhenius temperature dependencies for: (i) $T < T_g^{(\text{blend})}$ in PVME/PS, (ii) $T_g^{(\varphi\text{PS})} < T < T_g^{(\varphi\text{PI})}$ in the PI/P4tBS system, and (iii) $T_g^{(\varphi\text{PS})} < T < T_g^{(\varphi\text{PnBMA})}$ in the PnBMA/PS system. These would be described as localized processes. The dynamics of the slower, collective process involving a large numbers of dipoles relaxing at similar frequencies is apparent from measurements of ε(T). An analysis of the dielectric strengths, broadening parameters from empirical fittings, as well as the Kirkwood g factors for dipole correlation for the PVME/PS blends supports the notion that this collective mechanism is the new α_0 process, which is separate from the typical α process also occurring in the melt state and the α' process occurring at low T. This overall behavior, appearance of the α, α_0, and α' processes, would occur in miscible and weakly miscible blends whose component T_gs differ significantly.

Chapter 3: Role of "Hard" and "Soft" Confinement on Polymer Dynamics at the Nanoscale

3.1 Introduction

Polymer thin films in the nanoscale thickness range play an increasingly important role in a diverse range of technologies, including organic electronics (photovoltaic cells[158] and thin film transistors[159]), coatings,[160] and membranes.[23] Entropic effects associated with unusual chain conformations required to maintain density constraints under thin film confinement,[46] together with enthalpic interactions between the chain segments and external interfaces[161] (free surface, hard or soft confinement), are largely responsible for deviations in the physical properties of such films from the bulk.

Of particular interest in this section is the role of confinement on segmental dynamics in thin film polymer melts. In the bulk, the difference between the measurement temperature T and glass transition temperature T_g, (T-T_g), is generally a good predictor of relative segmental relaxation rates, provided that the Vogel-Fulcher-Tammann[37] (VFT), or equivalent Williams-Landel-Ferry[39] (WLF), relationship holds and the associated physical constants of the polymer

are known. With regard to thin films, the situation can be more complex, due largely to effects associated with the close proximity of the external interfaces.[109,110] Typically, a decrease in the T_g occurs with decreasing film thickness h for sufficiently thin (h ~ tens of nanometers) freely standing films.[95,97] Near a free surface, simulations[88,103,162–164] reveal the existence of a mobile surface layer with thicknesses on the order of nanometers, and significantly faster dynamics than the bulk for linear chain polymers. For asymmetrically confined films (hard substrate-film-air), the T_g increases with decreasing h when the interactions between the polymer chains and the substrate are strong, e.g.: hydrogen bonding;[165,166] interactions of chain segments in contact with a "wall" reduce the relaxation rates of the chains because of the associated increase of activation barriers for torsional relaxations from adsorption. On the other hand, if the polymer and the hard substrate are weakly interacting, e.g.: weak van der Waals interactions, the average T_g of the thin film is comparable or lower than the bulk.[100,167]

Deviations of various chain relaxation processes – side-chain,[104] segmental,[100] and translational[168] – are generally associated with shifts in the T_g from the bulk, though there is growing evidence[98,108,167,169] suggesting that this issue is worth deeper consideration. In this regard, it would be worthwhile to consider the connection between segmental dynamics and T_g of thin films under various conditions of asymmetric – "hard" and "soft" – confinement. To this end, we investigated the segmental dynamics of thin poly(vinyl alcohol) (PVA) films under various conditions of hard and soft confinement: (i) PVA films of varying thicknesses h (25 nm < h < 130 nm) confined between top and bottom Al electrodes (Al/PVA(h)/Al) and (ii) PVA films of varying thicknesses h confined between a bottom Al electrode on one side and polystyrene (PS) films of varying thicknesses L (5 nm < L < 200 nm) on top (Al/PVA(h)/PS(L)/Al) (**Figure 3.1**). Broadband dielectric spectroscopy (BDS) measurements

reveal that the PVA segmental relaxation rates in the Al/PVA(*h*)/PS(*L*)/Al system are much faster, by as much as a factor of six, than in the Al/PVA(*h*)/Al system of the same corresponding *h*. The enhancement effect increased with increasing thickness *L* of the confining PS layer, or decreasing *h*. These results are rationalized in light of recent simulations that implicate the role of the moduli of the confining soft layer.

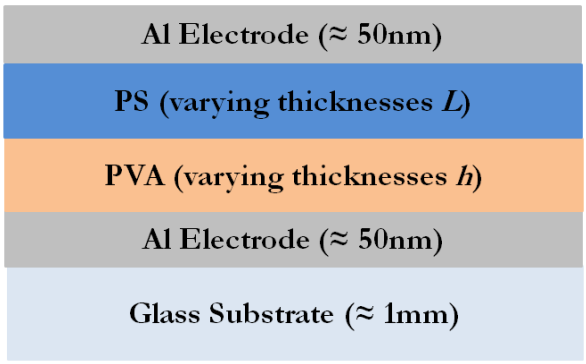

Figure 3.1: Schematic showing the geometric layout of the polymer bilayers (Al/PVA(h)/PS(L)/Al) during the BDS measurement.

3.2 Experimental Section

The polymers used in this study were poly(vinyl alcohol) (PVA) (weight-average molecular weight M_W = 25 kg/mol, polydispersity index PDI = 1.9) purchased from Polysciences Inc. and polystyrene (PS) (M_W = 50 kg/mol, PDI = 1.06) purchased from Pressure Chemical Company. 3% weight concentration PVA solutions were made using deionized (DI) water as the solvent. 3% weight concentration PS solutions were made using toluene as the solvent. The solutions were filtered using polytetrafluoroethylene (PTFE) syringe filters with 0.2 μm pore size, then agitated for 24 hours. Agitation of the PVA solutions were done under elevated temperatures (323K) to ensure thermodynamic mixing.

Thin films of PVA and PS for the dynamics measurements were prepared and confined between two aluminum (Al) electrodes (known as double Al capped/supported). Al electrode strips, 0.5 mm in width and ~100 nm in thickness, were deposited onto glass substrates by thermal evaporation under high vacuum (10^{-7} mbar) in a nitrogen (N_2) environment. Prior to evaporation, the substrates were thoroughly cleaned using DI water, glass detergent, acetone, and toluene under sonication. After Al evaporation, the substrates were brought into ambient air. Films were made by first spin-cleaning (WS-400B-6NPP/LITE/10K, Laurell Technologies) with the used solvent (DI water for PVA), and then spin-coating the previously described solutions at 5000 rpm, 2500 acc for 75 seconds. Typically, BDS film measurements are done with the polymer film confined between hard, electrically conductive electrodes or as a supported film exposing a free surface;[100,170] for the bilayers in this study, a PS film was deposited via spin casting directly on top of the PVA film. Bilayers were made by simply spin-coating one film on top of the other. Film thicknesses and bilayer conformations were confirmed using a spectroscopic ellipsometer (SE) (M-2000, J.A. Woollam). Thickness changes were done by varying the weight percent concentration of the solutions.

Samples were then dried under vacuum at room temperature for 12 hours, followed by subsequent annealing at a temperature of 393K for 24 hours under high vacuum. This temperature is above the bulk T_gs of both PVA and PS. Following annealing, Al strip electrodes of the same geometry were then deposited on top of the films in the counter direction under the same conditions. To ensure that the sample geometry is known (area of film in contact with the electrodes), the Al strip electrodes are cut in such a way to ensure that only the directly overlaying parts of the top and bottom electrodes are available for charge transfer. Further details on sample preparation are described elsewhere.[170]

Measurements of the dynamics were performed using a broadband dielectric spectrometer (BDS) (GmbH, Novocontrol Technologies). Because of probable air and moisture exposure during sample transport, the samples were annealed again within a BDS cryostat (Active Sample Cell ZGS, Novocontrol Technologies) under a N_2 flow environment for 10 hours to ensure that any residual moisture was removed. After in situ annealing, each sample was cooled at a rate of 3 K/min. The BDS sweeps were performed upon step heating in a frequency range of 0.1 Hz to 1 MHz with an AC voltage of 0.3 V per 100 nm of polymer film. The temperature range was 270K to 420K at a 3K step.

The T_gs of the polymers were measured using differential scanning calorimetry (DSC, Q200, TA Instruments) by first heating above the component T_gs and holding isothermally for 10 minutes, cooling at 10 K/min below the component T_gs, and then performing the measurement upon heating at 10 K/min. The glass transition was extracted from the step-like change in the endothermic heat flow baseline, where the baselines before and after the transition were extrapolated to a temperature where the change in heat capacity was at 50% completion. This result was compared to the peak position in the derivative heat flow.

Samples for Fourier transform infrared spectroscopy (FTIR) (Nicolet 6700, Thermo Scientific) were prepared on silicon (Si) substrates with a thin layer of native oxide, thoroughly sonicated with acetone, isopropanol, and water prior to use. Al deposition was done as described previously, except now covering the entire substrate. PVA films were prepared in the same manner as the dynamic samples, including the same annealing conditions. Reflective measurements were done with a resolution of 4.0 cm^{-1} by averaging 128 scans in the range of 4000 – 400 cm^{-1}.

3.3 Results and Discussion

We begin by showing the dielectric loss curves, obtained using BDS, plotted in **Figure 3.2**(a) as a function of frequency for a h = 70 nm PVA film confined between two Al electrodes – Al/PVA(70 nm)/Al. The peaks, due to the segmental, or α, relaxations shift to higher frequencies with increasing temperature; in addition, their intensities modestly increase with increasing T, as expected for pure polymers under isothermal measurement conditions. The relaxation times are extracted by fitting the complex dielectric permittivity ε*(ω) at each temperature to a Havriliak-Negami (HN) function[171] with an included conductivity contribution term[142] (necessary due to electrode and interfacial polarizations in thin films – note the existence of a low frequency tail):

$$\varepsilon^*_{HN}(\omega) = \varepsilon_\infty + \frac{\Delta\varepsilon}{(1+(i\omega\tau_{HN})^\alpha)^\beta} - i\left(\frac{\sigma_0}{\varepsilon_0\omega}\right)^N \tag{3.1}$$

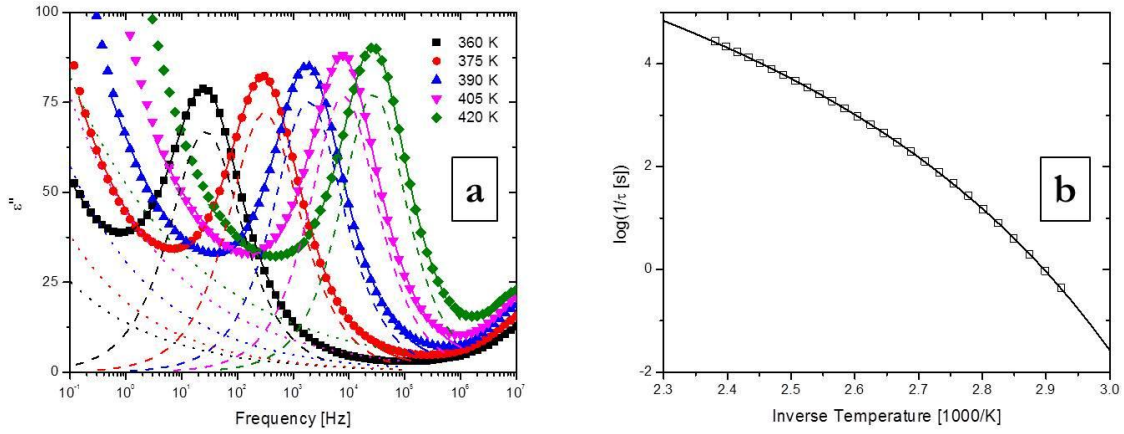

Figure 3.2: (a) Raw dielectric loss curves at different temperatures for a 70 nm PVA film capped between two Al electrodes (Al/PVA(70 nm)/Al). The dashed lines represent the HN peak fittings, the dotted lines represent the conductivity contributions, and the solid lines represent the summation of the two. (b) Temperature dependencies of the inverse PVA segmental relaxation times in Al/PVA(70 nm)/Al as calculated from the peak maxima in the dielectric loss curves. The solid line represents the VFT fitting.

The dashed lines in **Figure 3.2**(a) represent the imaginary portions of the HN peak fittings and the dotted lines represent the imaginary portion of the conductivity contributions. The solid lines represent the summation of the two. Although we model the complex dielectric function, of interest is the characteristic relaxation time τ ($1/2\pi\omega$) associated with the dielectric loss peak maximum of the imaginary portion of the permittivity $\varepsilon''(\omega)$; it is identified as the segmental relaxation time for that temperature. These relaxation rates are plotted as $1/\tau$ vs. $1/T$ in **Figure 3.2**(b). The temperature dependence of the relaxations are well described by the VFT equation,[37] shown as the solid black line. This is consistent with the segmental behavior of a pure homopolymer. Note that an analysis of the data in the temperature (isochronal) representation yields the same results, as expected (see Appendix B).

With regard to preparation of the bilayer samples – Al/PVA(h)/PS(L)/Al (see **Figure 3.1**) – PS, which is immiscible with PVA,[172] films were deposited via spin casting with an orthogonal solvent (water for PVA and toluene for PS) directly on top of the PVA films. Because the permittivity is a capacitive property, we can model the dielectric response $\varepsilon^*_{total}(\omega)$ of this bilayer system in terms of the individual contributions $\varepsilon^*_{PVA}(\omega)$ and $\varepsilon^*_{PS}(\omega)$, for the PVA and PS layers respectively, as:[173]

$$\frac{1}{\varepsilon^*_{total}(\omega)} = \frac{\phi}{\varepsilon^*_{PVA}(\omega)} + \frac{1-\phi}{\varepsilon^*_{PS}(\omega)} \tag{3.2}$$

where φ is the thickness ratio of PVA to that of the bilayer (volume fraction). Thus the PVA dielectric response is not equal to the system total dielectric response (despite a PS dielectric loss signal orders of magnitude lower than that of PVA), but rather

$$\varepsilon^*_{PVA}(\omega) = \phi\left[\frac{1}{\varepsilon^*_{total}(\omega)} - \frac{1-\phi}{\varepsilon^*_{PS}(\omega)}\right]^{-1} \tag{3.3}$$

$\varepsilon^*_{total}(\omega)$ is the measured dielectric response of the bilayer, and $\varepsilon^*_{PS}(\omega)$, whose magnitude is small compared to that of PVA, is determined from measurement of the single layer, double Al

capped PS films – Al/PS(*L*)/Al – of the appropriate thickness. A more thorough analysis of this modeling and its implications may be found in Appendix C.

Shown in **Figure 3.3** are the raw (left – (a), (c), and (e)) and normalized (right – (b), (d), and (f)) dielectric loss curves of PVA films of three thicknesses *h* – 25 nm, 70 nm, and 130 nm – for measurements performed at an arbitrary temperature of 390K. The dashed lines in the raw curves (a), (c), and (e) show the HN peak fittings (conductivity contributions are excluded). Data extracted from the pure confined film Al/PVA(*h*)/Al (black squares) and from the bilayer geometries Al/PVA(*h*)/PS(*L*)/Al of various Ps layer thickness *L* are plotted in this figure. The bilayer geometry data has been corrected as discussed previously to represent the PVA contributions to the total dielectric response. In all cases, the data exhibit a well-defined peak maximum for the segmental relaxation. For each sample, the intensity of the imaginary permittivity (raw dielectric loss curve plots) is proportional to the amount of PS in the bilayer. This may be related to changes in the PVA volume fraction with thickness, as signal intensity is proportional to the total number of relaxing dipoles throughout the entire system. It should be emphasized that with the normalization of the dielectric loss curves, the locations of the maxima change with temperature and film thickness, highlighting a shift in the dynamic response.

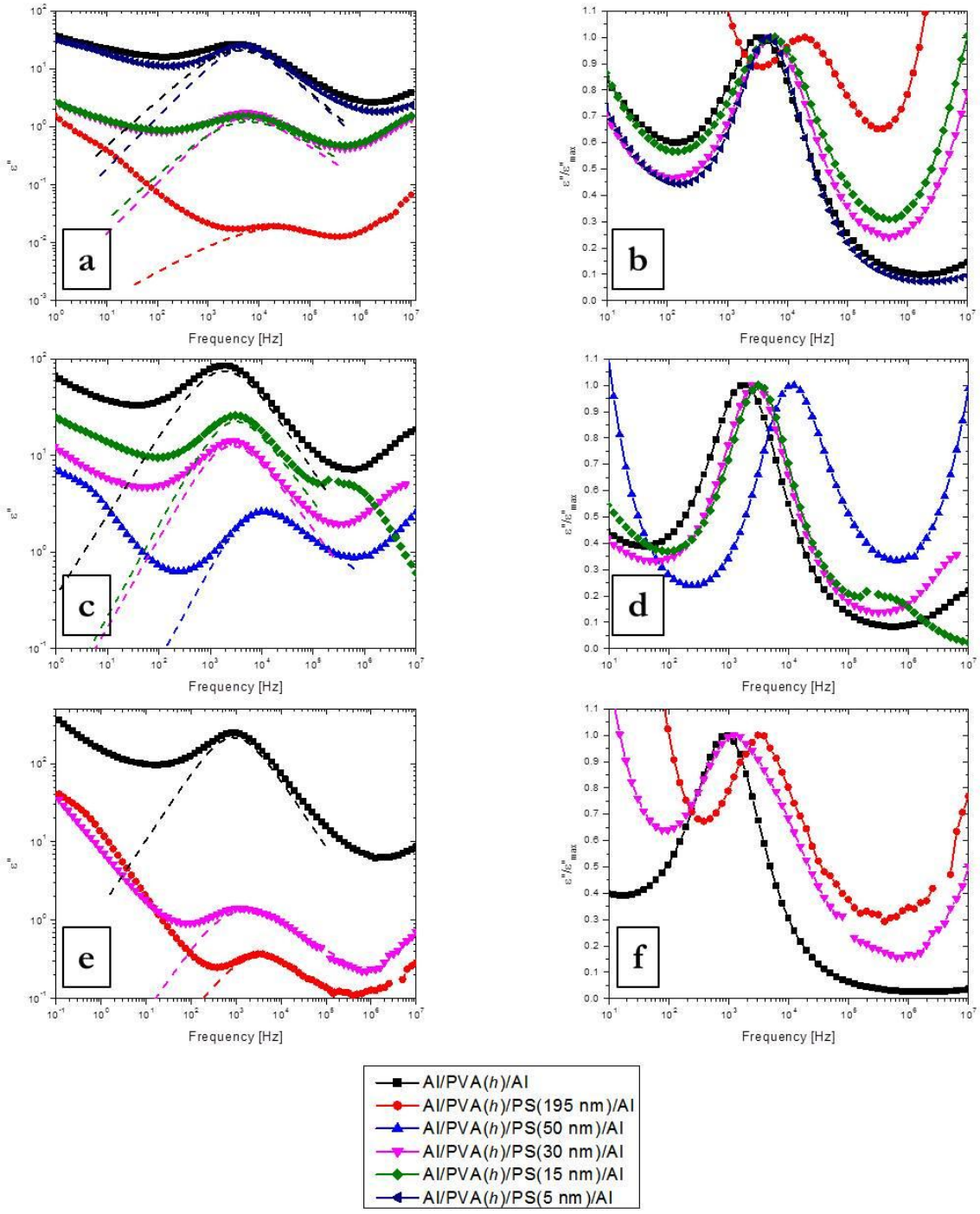

Figure 3.3: Raw and normalized dielectric loss curves at an arbitrary temperature of 390K for the PVA segmental relaxation contribution in PVA films of three thicknesses in double Al capped (Al/PVA(*h*)/Al) and various bilayer (Al/PVA(*h*)/PS(*L*)/Al) geometries (a) 25 nm - raw (b) 25 nm - normalized (c) 70 nm - raw (d) 70 nm - normalized (e) 130 nm - raw (f) 130 nm - normalized. Dashed lines in (a), (c), and (e) represent the HN peak fittings.

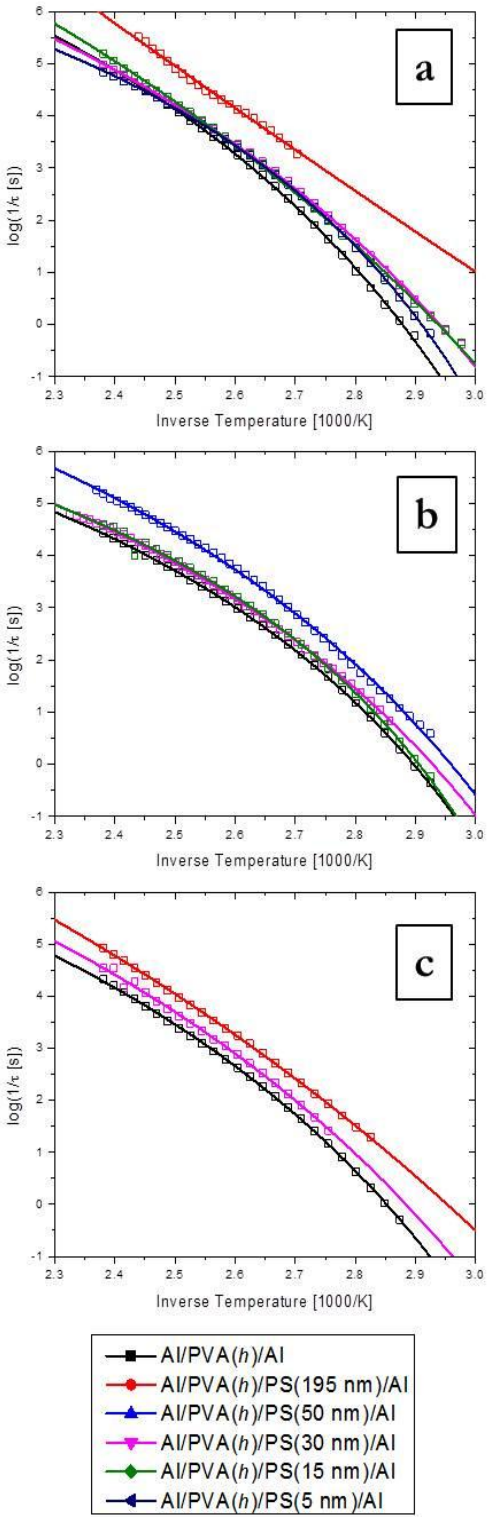

Figure 3.4: Temperature dependencies of PVA inverse segmental relaxation times of PVA films of three thicknesses (a) 25 nm (b) 70 nm, and (c) 130 nm, in double Al capped (Al/PVA(h)/Al) and various bilayer (Al/PVA(h)/PS(L)/Al) geometries.

The temperature dependencies of the characteristic PVA relaxation rates are shown in **Figure 3.4**. It is evident that the PVA dynamics are enhanced in the Al/PVA(*h*)/PS(*L*)/Al samples in comparison to those of the Al/PVA(*h*)/Al samples; this behavior is exhibited for all thicknesses *h* and *L*. The information in **Table 3.1** includes the values of $\tau_{PVA(h)}/\tau_{PVA(h)\text{-}PS(L)}$ for all the samples we investigated, at the arbitrarily chosen temperature of T = 390K. In all cases $\tau_{PVA(h)}/\tau_{PVA(h)\text{-}PS(L)} > 1$, revealing that the PVA segmental relaxations in the bilayers are faster.

Geometry	$\tau_{PVA(h)}$ or $\tau_{PVA(h)\text{-}PS(L)}$	$\tau_{PVA(h)}/\tau_{PVA(h)\text{-}PS(L)}$
Al/PVA(25 nm)/Al	2.50E-04	1.0
Al/PVA(25 nm)/PS(195 nm)/Al	3.97E-05	6.3
Al/PVA(25 nm)/PS(30 nm)/Al	1.78E-04	1.4
Al/PVA(25 nm)/PS(15 nm)/Al	1.70E-04	1.5
Al/PVA(25 nm)/PS(5 nm)/Al	1.43E-04	1.2
Al/PVA(70 nm)/Al	5.37E-04	1.0
Al/PVA(70 nm)/PS(50 nm)/Al	9.05E-05	5.9
Al/PVA(70 nm)/PS(30 nm)/Al	3.65E-04	1.5
Al/PVA(70 nm)/PS(15 nm)/Al	3.20E-04	1.7
Al/PVA(70 nm)/Al	1.15E-03	1.0
Al/PVA(130 nm)/PS(195 nm)/Al	2.93E-04	3.9
Al/PVA(130 nm)/PS(30 nm)/Al	6.79E-04	1.7

Table 3.1: The absolute value of the PVA segmental relaxation time at T = 390K for each of the corresponding geometries is given in the second coluumn: $\tau_{PVA(h)}$ for the pure film or $\tau_{PVA(h)\text{-}PS(L)}$ for the bilayers. The third column gives the ratio $\tau_{PVA(h)}/\tau_{PVA(h)\text{-}PS(L)}$ for the bilayer geometries.

The role of a soft confining layer has been suggested to influence the dynamics of a confined polymer layer under various circumstances. Experiments reveal a depression of T_g[174–177] and increase in physical aging rates[178,179] upon the introduction of soft confinement. The T_g depression is corroborated by simulations performed by Simmons and coworkers.[162,180] Other experiments[181–183] reveal an enhancement of chain dynamics with respect to the bulk in the presence of a fluid-like layer at the interface. Simulations by Lipson and coworkers[88,89] predict that within the interfacial region of a polymer film in contact with a material composed of high-mobility molecules, the segmental mobility in the polymer film is enhanced. This is consistent

with the behavior we observed – enhanced chain mobility of a film in contact with a mobile confining polymer. These simulations also suggest that the length-scales over which a fluid interfacial layer affects the dynamics within the confined film are larger than those due to a free or hard surface. This observation is corroborated by findings of Baglay et al.[177] and by Zhang et al.[175] who examined effects associated with T_g. With regard to the outcomes of these simulations, the effect of the PS layer is observed in PVA films as thick as h = 130 nm, far greater than the few nanometers as seen for homopolymer films with a hard substrate or even a free surface.

We note that Mirigian and Schweizer[103] have pointed out that the length-scale of T_g changes is better rationalized in terms of the effect of a long-ranged elastic field that accommodates localized dynamics; the proximity of a free surface truncates the range of the field, thereby lowering the barrier for displacements in the vicinity of a surface compared to the bulk. This should provide insights into the fact that the length-scales of T_g changes within a film far exceed the thickness of the liquid-like layer at the free surface of a film.

Simmons and coworkers[162,180] showed that an increased softness of the confining layer would have a larger effect on the T_g of the confined polymer film. They moreover suggest that the high frequency shear modulus is a reliable parameter to quantify softness. Our experimental results are consistent with this notion – we see an enhancement in dynamics when replacing Al with PS, the latter of which has a much smaller Debye-Waller factor.[184,185] Our observations also indicate that as the confining PS layer becomes thinner, the dynamics of the confined film more closely approaches the double Al confined case. This is clear from the values of $\tau_{PVA(h)}/\tau_{PVA(h)\text{-}PS(L)}$ in **Table 3.1**: $\tau_{PVA(h)}/\tau_{PVA(h)\text{-}PS(L)}$ is largest for the largest value of L and decreases with decreasing L.

Our observations are consistent with the notion that the thinnest PS layer would have the largest effective modulus. In other words, the effective modulus of the PS layer increases with decreasing *L*. Nanoindentation measurements show that the effective modulus of a thin polymer film supported by a hard substrate increases with decreasing film thickness; this is known as the "substrate effect."[81,186,187] The length-scales of this enhancement of the effective modulus with decreasing film thickness can be from tens to hundreds of nanometers, depending on the polymer.[186,188,189] Incoherent neutron scattering measurements of supported polymer thin films show that the vibrational spring constants (extracted from the Debye-Waller factor) increase with decreasing film thickness, consistent with the increasing effective modulus with decreasing film thickness.[190]

Finally, we note that our dynamics observations are not directly associated with the change in the average T_g of the confining film with film thickness – there are significant shifts in the PVA dynamics even with changing PS film thicknesses (~50 nm to ~195 nm) in which the literature reports no or minimal changes in PS film T_g.[97,100] If the changing PS T_g was causing the shift in PVA dynamics, we would not expect to see a change here, yet this is where we see the biggest change in confined PVA relaxation rates. In addition, because the average T_g of the PS films decreases with decreasing film thickness, it suggests that the thinnest PS film would have the largest effect; this was not the case. These points both show that relating confining layer T_g to neighboring layer dynamic shifts are inconsistent.

3.4 Conclusions

In conclusion, we show an enhancement of the PVA segmental dynamics upon introduction of a soft confining layer, compared to that of a hard support substrate; our

observations are corroborated by independent experiments and by predictive simulations. For the asymmetrically confined system Al/PVA(h)/PS(L)/Al, we show that for a sufficiently large L, the segmental relaxation rates of PVA were more than half an order of magnitude faster than for PVA symmetrically confined by aluminum layers. Upon decreasing the thickness L of the soft confining PS layer, the segmental dynamics of PVA approached that of the hard Al substrate confinement Al/PVA(h)/Al system. This follows from the notion that as the supported polymer film becomes thinner, its mechanical stiffness approaches that of the underlying substrate. A notable observation is that the effects due to soft confinement propagate over longer length-scales than those due to hard confinement or to free surface effects, consistent with simulations and theory.[103,88,89]

Chapter 4: Role of Thickness Confinement on Relaxations of the Fast Component in a Miscible A/B Blend

4.1 Introduction

Interest in the physical properties of polymers at the nanoscale, initially driven in part by the realization that the average glass transition temperature T_g exhibits film thickness-dependent behavior when confined to nanoscale dimensions,[97,191] continues to attract the attention of researchers with much broader interests. Film thickness dependent behaviors are documented in charge carrier mobilities in conjugated polymers,[83,192,193] elastic moduli of polymers,[81,186–188] and ferroelectric properties.[82,194] These length-scale dependent behaviors, which occur for fundamentally different reasons, have major technological implications because thin polymer films are used in a diverse range of applications, including microelectronics,[159] photovoltaic cells,[158] coatings,[160] and membranes.[23] For these reasons, questions related to the behavior of polymers under confinement continue to be a vibrant area of research.

Of particular interest in this study are the issues related to chain dynamics in miscible polymer/polymer thin film blends, an area which has remained largely unexplored. Entropic

effects associated with unusual macromolecular conformations required for the "packing" of chains under confinement conditions, together with the proximity and associated enthalpic interactions between chain segments and external interfaces, influence the overall structure and physical properties of polymer thin films.[46,161,164,195] The average T_g of a sufficiently thin linear chain homopolymer film typically deviates from the bulk because the local T_g near an external interface varies with depth ξ from said interface. When strongly attractive interactions, such hydrogen bonding, exist between the polymer and a hard substrate, the local T_gs in the vicinity of the substrate are enhanced in relation to the bulk; hence the average T_g of a sufficiently thin film confined between two such substrates would be higher than the bulk.[97,165,166,196,197] Additionally, chains in contact with a substrate not only experience reduced configurational entropies, but their relaxations can be hindered because the activation barrier for torsional motions are increased.[101,102,105,106,198–201] With regard to freely standing films, their average T_gs are lower than the bulk.[93,96–98,100,105,175,176,202] The enhanced configurational freedom of chain segments at a free surface, and their associated enhanced segmental mobilities, are responsible for this deviation.[86,88–91,103,164,181] In a sufficiently thin linear chain polymer film in which one interface is free and the other is in contact with a substrate, the average glass transition temperature is lower than the bulk if the effects at the free surface are more dominant than those at the substrate.[203]

The influence of long and short-range intermolecular interactions on the relaxations of chains in thin homopolymer films in contact with various external interfaces is reasonably well understood,[98,101,105,107,108,167,169,170,198–201,204,205] whereas little is known about the component dynamics of binary, miscible, A/B thin film polymer blends. In A/B mixtures, particularly in those in which there exists a large disparity between component T_gs and/or the A/B interactions are comparatively weak, the composition is spatially homogeneous at macroscopic scales, yet

heterogeneous at the nanoscale.[55,64,65,67,111,129] Chain connectivity[59,64] and thermally driven concentration fluctuations[61,62] are responsible for compositional heterogeneities in the bulk mixtures, and they have a profound influence on both the segmental and translational dynamics of the components. This spatial heterogeneity in composition is responsible for local variations of the glass transition temperatures and relaxation processes – characterized by different rates and temperature dependencies – of the individual A and B components throughout the material.[54–56,58,65,68,74,76,111,117,118,129,206]

The effect of the spatial compositional heterogeneity on component dynamics in thin films remains largely unexplored. In thin film polymer mixtures, the composition at the polymer-air and/or polymer-substrate interface generally differs from the bulk, due to the preferential attraction of one component. The component with lower surface energy preferentially adsorbs to a free surface, provided entropic considerations such as asymmetries in chain stiffness are not dominant. Relative intermolecular interactions between a substrate and either component of the blend generally dictate the component that resides preferentially at that substrate.[112,207–210] It would be important to understand (i) the extent to which the preferential segregation of blend components to external interfaces would influence dynamics within the thin film and (ii) the length-scales over which thickness confinement would influence the relaxation rates of the blend components, compared to related length-scales of homopolymer films.

The miscible blend of poly(vinyl methyl ether) (PVME)/polystyrene (PS) offers an ideal system for investigating component dynamics of confined, thin film, polymer mixtures to understand the effects of spatial heterogeneity and interfacial enrichment for the following reasons: (i) it possesses a lower critical solution temperature (LCST) that is well above both component T_gs and thus this system maintains miscibility throughout a wide range of

temperatures[136,137] and (ii) the T_g of PS is over 100 degrees higher than that of PVME – hence the PVME segmental relaxation rates are orders of magnitude faster than those of PS.[74] This, together with the fact that the segmental dipoles in PVME are much stronger than the PS dipoles,[76] make it convenient to investigate the PVME component dynamics. Here we report the relaxation dynamics of the PVME component in thin film PVME/PS blends confined between aluminum (Al) substrates. With regard to the films, it is well known that PVME, the lower surface energy component, preferentially enriches silicon oxide substrates,[209–216] Al substrates,[112] as well as the free surface.[211–213,217] Furthermore, broadband dielectric spectroscopy (BDS),[112,215,216] X-ray photon correlation spectroscopy (XPCS),[211] and specific heat spectroscopy[214,218] all indicate that the existence of a PVME-rich interface would have a significant effect on the overall PVME dynamics. Hence this is an interesting system to understand the effects of nanoconfinement on blend chain dynamics.

We show, using BDS, that with increasing molecular weight *M* of the PS component, the average PVME segmental relaxation rates in 100 nm PVME/PS films increase. Moreover, the thicknesses over which confinement of these miscible blends affects the chain dynamics are well beyond 100 nm; these are significantly larger length-scales than those of confined homopolymer thin films – in homopolymer films the thicknesses where the substrate effects are manifested are generally on the order of nanometers.[109,110] This behavior is due to the existence of spatial compositional heterogeneity in miscible blends and the preferential enrichment of PVME to the external interfaces.

4.2 Experimental Section

The polymers used in this study were poly(vinyl methyl ether) (PVME), with number-average molecular weight M = 22.1 kg/mol and polydispersity index PDI = 1.09, and deuterated polystyrenes (PS) of nearly monodisperse molecular weights M = 3.8, 4, 10.9, 132, 190, 525 kg/mol. All polymers were purchased from Polymer Source Inc.

Each PVME/PS blend investigated in this study contained 25 weight percent PVME and was miscible (in fact, deuterated PS is more miscible with PVME than hydrogenated PS[133–135]). Each blend was prepared by initially dissolving the homopolymers separately in toluene at 3 weight percent concentration, followed by agitation for 24 hours. The solutions were then filtered using PTFE syringe filters with 0.2 μm pore sizes, before mixing to create the desired 25% blend compositions, and finally agitated for 24 hours. The final blends are known as: PVME/PS(3.8k), PVME/PS(4k), PVME/PS(10.9k), PVME/PS(132k), PVME/PS(190k), and PVME/PS(525k).

Thin film PVME/PS samples for BDS were confined between Al electrode strips, top and bottom, 0.5 mm in width and ~100 nm in thickness. The bottom Al electrodes were deposited onto glass substrates by thermal evaporation under high vacuum (10^{-7} mbar). Prior to evaporation, the substrates were thoroughly cleaned using deionized (DI) water, glass detergent, acetone, and toluene under sonication. The previously described polymer solutions were spin-coated (WS-400B-6NPP/LITE/10K, Laurell Technologies) onto the clean Al/glass substrates at 5000 rpm, 2500 acc for 75 seconds to fabricate 100 nm thick films. A spectroscopic ellipsometer (SE) (M-2000, J.A. Woollam) was used to confirm the film thicknesses. Samples were then dried under vacuum at room temperature for 12 hours, followed by subsequent annealing at temperatures at least 50K above the bulk blend T_gs and also above the bulk component T_gs, for

24 hours. Top Al strip electrodes were then deposited on top of the films in the counter direction. To ensure that the sample geometry is known (area of film in contact with the electrodes), the Al strip electrodes are cut in such a way to ensure that only the directly overlaying parts of the top and bottom electrodes are available for charge transfer. Further details on sample preparation are described elsewhere.[170]

Measurements of the dynamics were performed using a broadband dielectric spectrometer (BDS) (GmbH, Novocontrol Technologies). Because of probable exposure to air during sample preparation, the samples were annealed again within a BDS cryostat (Active Sample Cell ZGS, Novocontrol Technologies) under a nitrogen (N_2) flow environment for 10 hours to ensure than any residual moisture was removed. After in situ annealing, each sample was cooled at a rate of 3 K/min. The BDS sweeps were performed upon step heating in a frequency range of 0.1 Hz to 1 MHz with an AC voltage of 0.3 V. The temperature range was 250K to 325K at a 1K step. Measurements were performed with the previously described Al strips in contact with gold probes.

The T_gs of the polymer films were measured using capacitive dilatometry in the BDS film setup as described above. The temperature is taken at the kink-like change in the temperature dependence of the real permittivity $\varepsilon'(\omega)$ at 10^5 Hz of the applied electric field, a frequency sufficiently high enough to guarantee that the values are not affected by relaxation processes. This allows for the monitoring of the temperature dependence of the film density.[26,38] A cooling rate of 1 K/min was used; we note no difference in the T_g between heating and cooling at the same rate.

The depth profiles of PVME/PS(3.8k) and PVME/PS(525k) were determined using dynamic secondary ion mass spectrometry (DSIMS). We note that while the films used for the

dynamics studies were sandwiched between two Al electrodes, the samples prepared for DSIMS were spin-coated on an Al substrate (100 nm thick), exposing the other surface. A sacrificial hydrogenated polystyrene (hPS) (purchased from Pressure Chemical Co., M = 143.4 kg/mol, PDI = 1.06) layer 50 nm in thickness was placed on top of the films by first floating off a silicon substrate onto heated deionized water and then placing onto the thin film blend. These samples are prepared with a sacrificial PS layer on top in order to (i) determine the ion beam sputtering rate and (ii) protect the film while the beam stabilized. All other film preparations were kept consistent with the dynamics study. The DSIMS measurements were performed by Dr. Tom Mates of the University of California, Santa Barbara, using a Physical Electronics 6650 Quadrupole instrument. A Cs^+ primary ion beam (6 keV and 50 nA) was used to sputter the samples with a 350 μm x 450 μm raster area, and negative secondary ions of hydrogen (H), deuterium (D), aluminum (Al), and silicon (Si) were monitored from the center 15% of the crater area. SE measurements were used to convert the sputtering time axis to the appropriate depth scale.

Samples for variable angle spectroscopic ellipsometry (VASE) measurements were made with three different substrates; one with a thin layer of native silicon oxide and the other two with layers of thermally grown SiO_2 that are 300 nm and 500 nm thick (purchased from Encompass Inc.). To match the substrate interfaces with the dynamics studies, a thin layer of Al (10 nm) was evaporated on the substrates. The blends and pure homopolymers were subsequently spin-cast on top, with all annealing conditions matching those done in the dynamic studies. Ellipsometric measurements were performed in reflection mode at 5 angles: 55°, 60°, 65°, 70°, and 75°. Measurements were performed both prior and post Al deposition in order to correctly determine the optical constants for the homopolymers and thickness of the Al layers.

Optical constants of the Si, native oxide, and thermally grown SiO_2 were taken from CompleteEASE software's library database. Optical constants of PVME and PS were measured by fitting the VASE data of neat films. It is evident that while no noticeable differences are observed across the different PS molecular weights, the refractive indices of PVME and PS are significantly different – this difference enables ellipsometric identification of PVME and PS at different depths into the film. The blend data were then fit simultaneously using the CompleteEASE software (J. A. Woollam Co.) to determine the depth/concentration profiles of the different PVME/PS blends. This multi-sample analysis is necessary to increase the uniqueness of the fits due to the strong correlations between the fitting parameters.[219,220]

4.3 Results and Discussion

The dielectric loss curves extracted from the broadband dielectric spectroscopy (BDS) frequency sweep (isothermal) experimental data for 100 nm thick PVME/PS(3.8k) and PVME/PS(525k) films are plotted in **Figure 4.1**(a) and **Figure 4.1**(b), respectively. Due to the significantly stronger dipole moment in the PVME segments, in addition to the large time-scale of separation between PVME and PS relaxation rates, these curves readily describe the relaxations of the PVME segments. These BDS experiments, in which the temperature is kept constant and the frequency is changed many orders of magnitude, are most sensitive to the fastest relaxing PVME segments, as shown in previous work.[206] The maximum of each curve shifts to higher frequencies with increasing temperature in a non-linear manner, as expected for molecular relaxation processes.

The curves are well described by the Havriliak-Negami (HN) function with conductivity contributions (fits shown as solid lines in **Figure 4.1**(a) and **Figure 4.1**(b)):[171]

$$\varepsilon^*_{HN}(\omega) = \varepsilon_\infty + \frac{\Delta\varepsilon}{(1+(i\omega\tau_{HN})^\alpha)^\beta} - i(\frac{\sigma_0}{\varepsilon_0\omega})^N \quad (4.1)$$

This equation is widely considered to be the most general empirical modeling function for a dielectric relaxation process. The characteristic relaxation time $\tau = (1/2\pi\omega)$ associated with the dielectric loss peak maximum of the imaginary portion of the permittivity $\varepsilon''(\omega)$ is identified as the segmental relaxation time at that temperature.[142] The segmental relaxation rates $(1/\tau)$ of the PVME component are plotted as a function of $1/T$ in **Figure 4.1**(c) for the two thin film samples. In contrast to the pure PVME homopolymer,[206] the temperature dependencies of the PVME relaxations do not follow the simple Vogel-Fulcher-Tammann (VFT) behavior.[37] Colmenero et al.[68,76,119] showed that the PVME segmental relaxation rates decrease rapidly, and in a non-linear manner, with decreasing temperature for $T > T_g^{(blend)}$. However, for temperatures $T < T_g^{(blend)}$, the segmental dynamics of PVME exhibits a weak, approximately Arrhenius temperature dependence with further decreasing T. This, as Colmenero and collaborators have shown, is because for $T < T_g^{(blend)}$, the low T_g PVME chains relax within the "frozen" confines of the high T_g, glassy PS domains. In other words, the PS component vitrifies, while the still mobile PVME component relaxes. This Arrhenius dependence is believed to be due to the fact that the length-scale of cooperativity – as described by Adam and Gibbs[33] and further by Donth[34,36,113] – of the PVME chains would be suppressed due to confinement between the PS domains. Whereas this phenomena has been shown in the bulk blends before,[68,76,119,206] we show here that the behavior also occurs in films with thicknesses at least up to 100 nm.

In **Figures 4.1**(c), the onset of the low temperature relaxation behavior, where localized PVME relaxations occur in "frozen" PS domains, occurs at an onset temperature T_o, which differs from $T_g^{(blend)}$; this is in contrast to the bulk where $T_o = T_g^{(blend)}$. This is potentially one of the effects of confinement on the structure, and hence PVME segmental dynamics, of the films.

The preferential segregation of PVME to the Al substrates, which we show later, is due to a preferential attraction between the PVME and the Al and a decreased entropy of mixing with the PS with increased PS chain length (scales as $1/N$). In these films, the structure is such that the segregation of the PVME forms sufficiently thick layers at the Al substrates, thereby altering the average blend composition within the interior of the sample. This effective blend composition within the interior differs from the average blend composition of the sample. The consequences of this effect on the PVME dynamics is of specific interest in the remainder of this chapter.

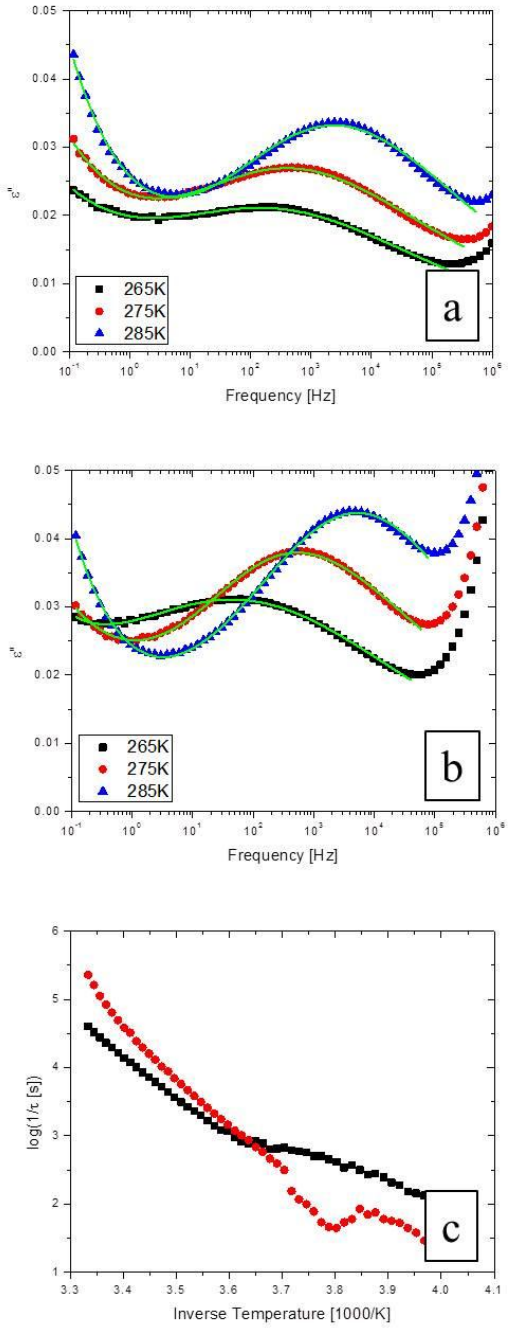

Figure 4.1: Raw dielectric loss curves of ε" vs frequency of the applied AC voltage, at select temperatures, for (a) 100 nm PVME/PS(3.8k) and (b) 100 nm PVME/PS(525k). Green solid lines represent the HN peak fittings. (c) Temperature dependencies of the inverse segmental relaxation rates of PVME/PS(3.8k) (black squares) and PVME/PS(525k) (red circles). Relaxation times are calculated from the maxima in the frequency sweep dielectric loss curves.

Recently Yang and Green,[112] and subsequently Sharma and Green,[206] showed that the PVME chains in bulk PVME/PS blends exhibited different relaxation processes characterized by distinct relaxation times, and very different temperature dependencies, manifesting the influence of spatial compositional heterogeneity. At high temperatures where the compositional fluctuations are fast compared to the PVME chain relaxation rates, the temperature dependence is VFT-like. For temperatures $T < T_g^{(blend)}$, the phenomenon occurs where the PS component undergoes a component glass transition and the PVME chains relax within the "frozen" PS domains. This *T* dependence is Arrhenius, as mentioned earlier – this was identified as the α' process. Another relaxation process, more strongly temperature-dependent, occurs wherein the PVME chains undergo a slower, collective relaxation process, identified at the α_0 process. This identification was achieved using a contour plot representation, where the abscissa and ordinate are $1/T$ and $\log(1/\tau)$, respectively; the contours are dependent on log(ε"). These plots were created by fitting the data to a two variable polynomial (ω and *T* are independent variables and ε" is the dependent variable) and recalculating the permittivity using the generated function at every temperature and frequency. Note here that a typical isochronal measurement (temperature sweep measurement of ε"(*T*) for different values of ω) exhibits a maximum when the largest number of dipoles relax at the same frequency. Such a measurement is sensitive to the α_0 process. Because the most rapidly relaxing dipoles provide the largest signal, the isothermal experiments (frequency sweep measurement of ε"(ω) over a range of frequencies, at constant *T*) are more sensitive to the faster α' process.

The contour plots of the two thin film blends, PVME/PS(3.8k) and PVME/PS(525k), are shown in **Figure 4.2**(a) and **Figure 4.2**(b) respectively, with the frequency and temperature sweeps overlaid as the red and blue circles, respectively. The α_0 and α' dynamic processes,

occurring at low temperatures, reported earlier by our group for bulk PVME/PS blends, are now also identified separately by the frequency and temperature sweep experiments.[112,206] Recall that for temperatures well above the $T_g^{(blend)}$, the fluctuations in local composition are rapid, compared to the relaxation rates. However at lower *T*, the fluctuations are slow compared to the relaxation rates; in other words, the PVME relaxation rates are sensitive to the local compositional environment, as discussed by Sharma and Green.[206] It is readily apparent from **Figure 4.2** that the separation time-scales between the isothermal and isochronal measurements are significant. However, this separation between experimental data is larger than that observed in the bulk analogs. Recall that the dielectric loss peaks of the bulk blends are much broader than the homopolymers;[101,200,221,222] the loss peak maxima for the thin films are broader than the bulk due to the segregation of PVME chains to the external interfaces.

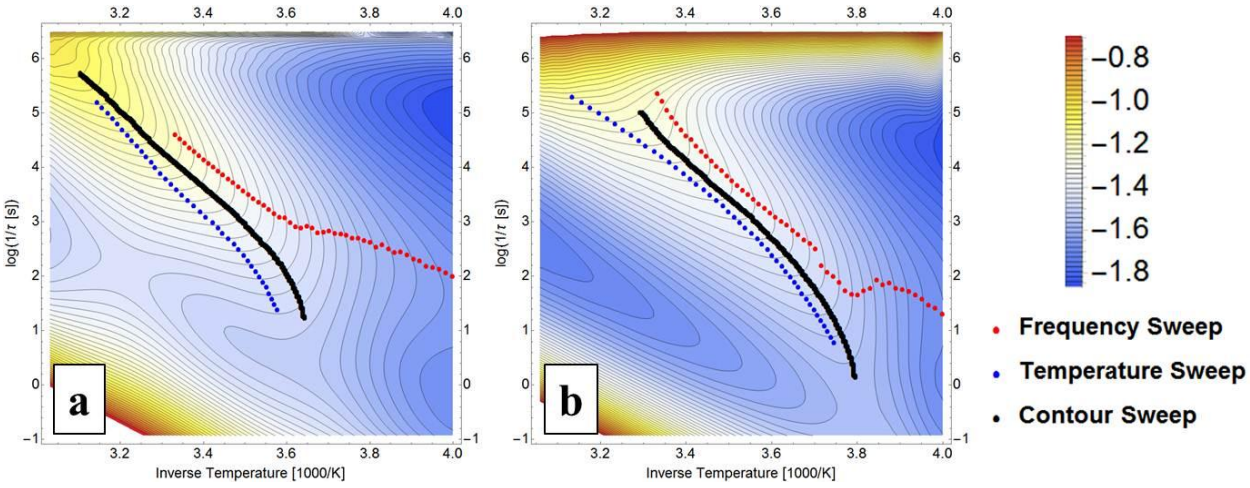

Figure 4.2: Contour plots of log(ε'') vs AC electric field frequency 1/τ and inverse temperature 1/*T* for 100 nm films of (a) PVME/PS(3.8k) and (b) PVME/PS(525k). Overlaid on the plot are the relaxations from the frequency sweep (red circles), temperature sweep (blue circles), and contour sweep (black circles).

In order to compare the PVME relaxation rates in the films of varying compositions, the extremum of each contour curve is identified in **Figure 4.2**; these extrema are represented by the black symbols. It is recognized that PVME segments are mixed with PS in the bulk of the film as

well as residing within the external interfacial regions, so their dielectric responses would be different; i.e.: the electric field strengths differ throughout the sample. The use of the contour plot, or the contour ridgelines, as a function of both temperature and frequency, as described in further detail in Appendix H, mitigates this concern.

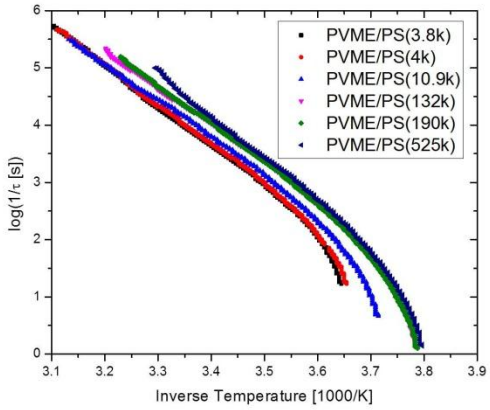

Figure 4.3: Temperature dependencies of the inverse segmental relaxation rates of PVME/PS(*M*), including all six measured PS molecular weights. Relaxations are calculated from the contour sweeps.

The data in **Figure 4.3** depict the temperature dependencies of the characteristic PVME relaxations for six 100 nm films of different PS molecular weights (the raw dielectric loss curves and contour data for all these films may be found in Appendix E, **Figure E-1** and **Figure E-2**). These data reveal that, for all temperatures, the PVME segmental relaxation rates increase with increasing PS molecular weight *M* in the blend. This appears to be counterintuitive because the relaxations of the PS chains are extremely slow – by orders of magnitude – in comparison to those of the PVME chains; therefore one might anticipate that the relaxation rates of the PVME chains, occurring in a comparatively static environment, would be constant. We further note that even if the PVME relaxations are affected by the PS dynamics, the higher *M* PS chains, with

higher T_gs and friction coefficients, should serve to slow the PVME relaxations down; yet the opposite is observed – PVME relaxation rates increase with increasing *M*.

In light of these observations, it would be prudent to investigate the role of thickness confinement. As such, it would be important to examine the depth-dependent composition profile of PVME in the samples. To this end dynamic secondary ion mass spectrometry (DSIMS) measurements of PVME/PS(3.8k) and PVME/PS(525k) are shown in **Figure 4.4**(a) **and Figure 4.4**(b), respectively. Because deuterated PS is used in the blends rather than hydrogenated PS, secondary ions from hydrogen and deuterium originate from PVME and PS, respectively. Unsurprisingly, the DSIMS measurements reveal that the segregation of PVME to the external aluminum interfaces is significant.[112,137,209,211] This is apparent from the peak in the secondary count for PVME hydrogen ions on the right hand side of both plots, revealing a buildup of PVME at that interface. It is noteworthy that the ion count is stronger and larger, indicating a thicker PVME interfacial layer, for the PVME/PS(525k) sample, revealing a PS molecular weight effect on interfacial enrichment.

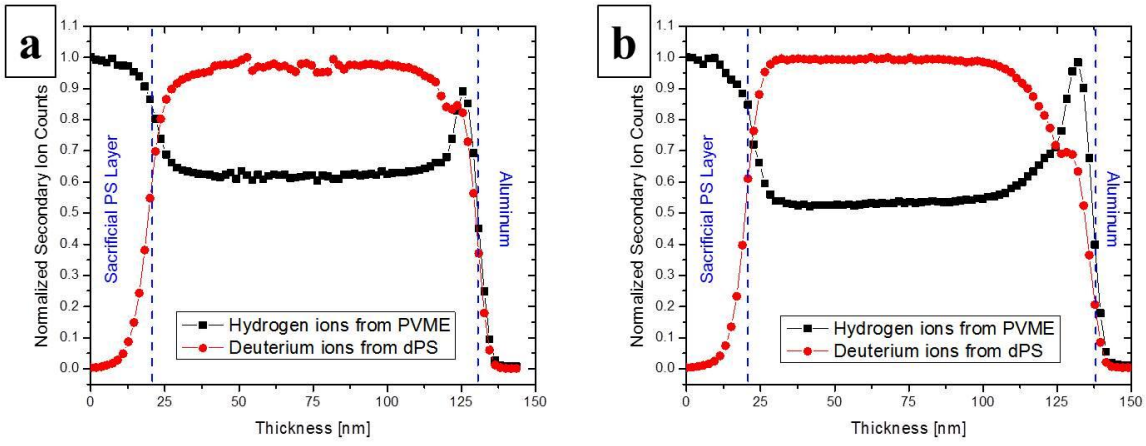

Figure 4.4: SIMS generated depth profiles of normalized ion count versus thickness into the film of 100 nm (a) PVME/PS(3.8k) and (b) PVME/PS(525k). The two interfaces are a sacrificial hPS layer (left) and an aluminum substrate (right). Because deuterated polystyrene is used in the blends, hydrogen ions indicate PVME and deuterium ions indicate PS.

In order to gain further information about the layer thicknesses and concentrations in these samples of varying PS chain length, variable angle spectroscopic ellipsometry (VASE) experiments were performed. This was accomplished by building a model consisting of 3 effective medium approximation (EMA) layers in order to describe the ellipsometric data. Since the refractive indices of PS and PVME in the blends remain the same as in the neat films, we used the fit to calculate the thicknesses and compositions of each EMA layer in the film (the difference between refractive indices of the two components is large). In agreement with both previous studies[112,211] and our DSIMS measurements, our results indicate (**Figure 4.5**) that the PVME/PS films consist of PVME-rich layers at the polymer-Al interfaces. These layers are determined to be nearly 100% PVME in concentration. Of particular relevance here is that the thickness of the interfacial layer at the Al substrate increases with increasing *M* (**Figure 4.5**(a)). Consequently, the PVME concentration in the interior also reduces with increasing PS molecular weight, as shown in **Figure 4.5**(b). It is now clear that with increasing PS chain length in thin film PVME/PS(*M*) blends, the interior of the blend is depleted in PVME; in other words the PVME resides, increasingly, at the external interfaces. These layers are each nanometers in thickness and sufficiently thick to deplete the amount of PVME mixed with PS. This is also consistent with the notion that the transition from the α to the α' process does not occur near $T_g^{(\text{blend})}$, because the composition within the interior of the sample is no longer the average composition of the material. It would be richer in PS and presumably with higher T_g.

It is apparent from the foregoing that the increased PVME relaxation rates with increasing *M* is due to the fact that the PVME external layer thicknesses, due to the preferential enrichment of the component to the Al substrates and decreasing entropy of mixing, increase with increasing *M*. An increase in the wetting layer thickness means that PVME at the surface

takes up a greater fraction of the film's dielectric response; hence the increase of the average PVME dynamics, as a greater number of PVME chains are relaxing in a PVME-rich environment. These layers are nanometers in thickness, sufficient such that the PVME concentration within the interior of the film is depleted. It is important to note that the interaction between the PVME chains and the Al would remain constant, regardless of *M*, because the PVME-Al interactions should be short-ranged. It is the decreasing entropy of mixing, associated with the increase of *M* that is responsible for increasing the effective driving force for segregation of PVME to the external interfaces.

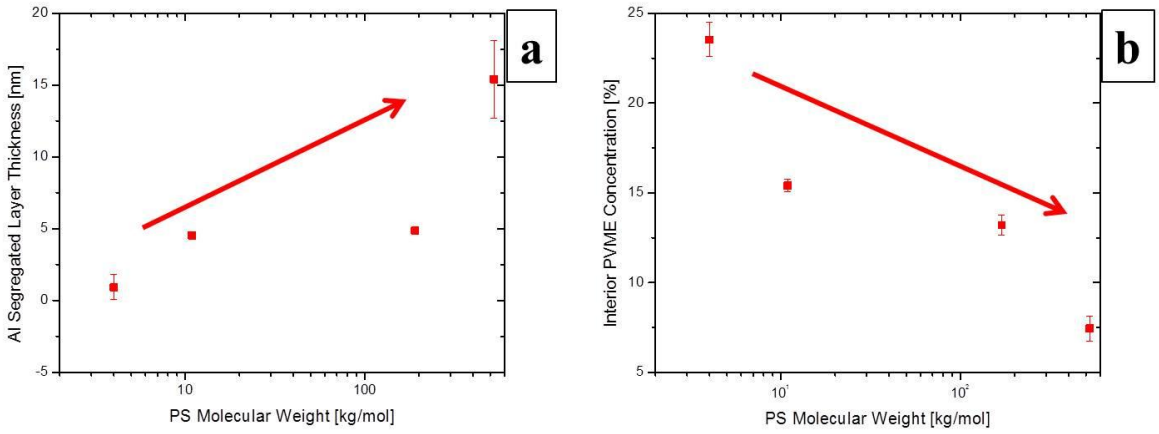

Figure 4.5: (a) Thickness of the PVME-rich layer segregated to the Al interface as a function of PS *M*, as measured through VASE. (b) Concentration of PVME in the interior of film as a function of PS *M*, as measured through VASE.

An important implication of these findings is that the length-scales over which the dynamics of a component of a miscible blend is influenced by thickness confinement are large compared to those that characterize the response of a homopolymer film.[109,110] For example, some experiments show the nanoconfinement effects on dynamics saturating by a thickness of 15 nm;[200] others even show no noticeable effect at all.[98] It is shown here that if a component

exhibits a tendency to preferentially enrich an external interface, the confinement effect length-scale would be large.

To this end, it would be useful to gain insight into the potential length-scales over which the confinement effects would influence the dynamics of thin film PVME/PS blends. The temperature dependencies of PVME segmental relaxations in PVME/PS(4k) blends of different thicknesses, as calculated from the contour sweeps (contour plots shown in **Figure G-1** of Appendix G) are plotted in **Figure 4.6**. It is apparent from these data that the PVME segmental relaxation rates decrease with increasing film thickness. The decrease of the relaxation rates occurs for the following reason. Begin by recalling that the BDS contour sweep measurements manifest the average relaxation rates of the contributions from PVME molecules mixed with the PS within the interior of the sample and PVME molecules in the wetting layers at the external interfaces. As the overall film thickness increases, the relative contributions of the PVME chains in the wetting layers decrease – the ratio of wetting layer thickness to overall film thickness decreases. This is connected to a corresponding increase in T_g with increasing film thickness; which is manifested in the truncation of relaxations at lower temperatures.

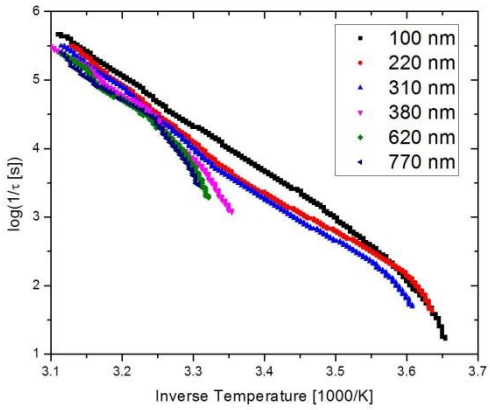

Figure 4.6: Temperature dependencies of the segmental relaxation rates of PVME/PS(4k), at different film thicknesses. Relaxations are calculated from the contour sweeps.

4.4 Conclusions

Bulk miscible blends are spatially heterogeneous and this influences the dynamics of their components. Such influence in miscible A/B systems is especially apparent when the lower T_g component relaxes within the vitrified confined of the higher T_g component; this phenomenon produces the so-called α' process to differentiate it from the normal α process which occurs at sufficiently high T. Another α_0 process has been identified and associated with a collective and slower, yet stronger T-dependent process.[112,206] This behavior is characteristic of the bulk, miscible PVME/PS system, where the transition from the α to the α' process occurs for $T < T_g^{(\text{blend})}$.

In thin film, 100 nm thick, PVME/PS mixtures confined between aluminum substrates, the segmental relaxation times of PVME chains increase with increasing PS molecular weight M. This increase is associated with the preferential segregation of PVME chains to the Al interfaces to form wetting layers many nanometers in thickness; the layer thicknesses increase with increasing M. This increase in layer thickness is accompanied by a depletion of PVME chains mixed with PS in the interior of the film. Therefore, the overall relaxation rates of the sample increases. When the film thickness increased, the thickness of the wetting layer stayed constant relative to the overall film thickness, and the overall rate of the dynamics decreases. The surprising finding is the large thickness confinement length-scales, hundreds of nanometers, over which the component dynamics are affected. The length-scale of this confinement is primarily determined by the extent to which the wetting layers deplete one component from the mixture, thereby changing the local mixture composition and hence the dynamics. Spatial compositional heterogeneity in this system is partly responsible for this large wetting layer formation. In light of this, the length-scales of confinement effects in miscible blends would be system dependent,

i.e.: dependent on factors that include the extent of spatial compositional heterogeneity (dictated in part by component T_g differences and disparities in component relaxation rates), component-substrate interactions, and chain lengths (entropy of mixing).

Chapter 5: Conclusions

5.1 Summary

The secret to controlling and tuning material properties lies in the structure; likewise, the establishment of the structure-property relationship is key to the understanding and improvement of various materials and complex condensed matter systems in application. Considerable efforts have been invested towards understanding this interrelation in functional polymeric materials because of their wide use in applications, such as microelectronics,[159] organic electronics (photovoltaic cells[158] and thin film transistors[223]), coatings,[160] and membranes.[23] In these systems, due to complex intermolecular interactions, lack of long-range order, and heterogeneous nanostructuring, it is difficult to predict and understand properties. This dissertation develops a stronger understanding of how the mesoscale dynamic responses of polymers are influenced by morphological/structural changes, imposed via the local environment surrounding the polymer chains. Understanding and solving these problems may provide means and ideas to enhancing and tailoring specific properties in these complex systems.

In Chapter 2, the absolute values and temperature dependences of the segmental relaxation times τ_A and τ_B of the components in miscible, binary A/B polymer/polymer blends are investigated. It is shown that for weakly miscible A/B blends, the segmental relaxations of the faster A component occur via separate and distinct mechanisms. In the melt state, τ_A increases in a nonlinear manner as temperature *T* decreases toward the blend glass transition

temperature $T_g^{(blend)}$; this is the typical α relaxation process. For temperatures below $T_g^{(blend)}$, $1/\tau_A$ exhibits an Arrhenius temperature dependence; this is identified as the α' process. A third relaxation process, a so-called α_0 process, also occurs in the melt state; it is slower than the α process and exhibits a significantly stronger dependence on temperature. Each of these relaxation processes, characterized by different relaxation rates and dependencies on temperature, occurs via the same mechanism (segmental fluctuations) but differing associated local composition surrounding the chains. This behavior, the existence of the α' and α_0 relaxations that accompany the α relaxations, would occur in miscible and weakly miscible blends whose component T_gs differ significantly.

In Chapter 3, the segmental dynamics of asymmetrically confined polymer films are investigated, and an unusual phenomenon is reported in which the presence and thickness of a soft confining layer is responsible for significant changes in the segmental dynamics of the confined films. Specifically, τ_{PVA} of poly(vinyl alcohol) (PVA) thin films asymmetrically confined between hard aluminum (Al) and soft polystyrene (PS) films is shown to shift by as much as half an order of magnitude upon changes in the thicknesses of the confining PS layer. These effects are more significant than those due to symmetric confinement between hard Al substrates, or exposure to a free surface. These observations, partially rationalized in terms of recent simulations and theory, implicate the role of the moduli and mechanical properties of the confining layers.

Chapter 4 shows the average segmental relaxation times τ_{PVME} of the PVME component in 100 nm thick films of miscible PVME/PS blends confined between Al electrodes decrease with increasing molecular weight *M* of the PS component. These relaxation rates are film thickness dependent up to a few hundred nanometers. In contrast, thickness confinement length-

scales are on the order of nanometers for neat homopolymer films. This behavior is associated with spatial compositional heterogeneity that characterizes the structure of this miscible blend, in conjunction with the preferential interfacial enrichment – wetting layer formation – of the PVME component at the external Al interfaces. The behavior is dependent on factors that include spatial compositional heterogeneity, component-substrate interactions, and chain lengths.

Although the above-mentioned systems are all different in their own right, the studies are all focused on the same goal – understanding how and why the environment surrounding a polymer chain as it relaxes significantly influences both the relaxation rates and the associated temperature dependences. Because many polymer material properties are dependent on the chain dynamics, this connects back to the structure-property relationship. Showing that the polymer chains and their interactions behave very differently on the nanoscale molecular level from what we are familiar with macroscopically tells us that their mesoscopic structures and properties are also affected. These results will provide new insights to polymer processing-property and nanostructuring-property relations for future use in application.

5.2 Future Work and Outlooks

The findings presented in this dissertation provide several important insights into the influence of local intermolecular environments on chain relaxation processes, but also raise a number of new questions that warrant further investigation. The following is an outline of several directions for future research projects, some of which are already in progress.

Chapter 2 deals with an examination of how the local heterogeneous environment in a polymer blend affects polymer segmental relaxations τ_{seg} of the components. There are a number of theoretical and computational models to predict this behavior, such as the simple lattice model

by Colby and Lipson,[121] the self-concentration model by Lodge and McLeish,[59] and the generalized entropy theory by Freed.[66] As for the experimental side, to date most of the work on this phenomenon has been done on binary, dynamically asymmetric polymer blends;[54,55,57,58,62,64,65,74,76,111,112,114–120] the large separation in component dynamic time-scales amplifies the dynamic heterogeneity because of distinct differences in component friction factors at the same temperature. However we predict that this type of behavior can be extended to all miscible blends – this includes both dynamically symmetric blends and multiple component blends. However, identification of the dynamic heterogeneous effect on τ_{seg} is difficult in such systems due to the magnitude and macroscopic scales over which most spectroscopy experiments are performed.

One interesting approach that has been developed in our research group is using a newly developed atomic force microscopy (AFM) tool for measuring local dielectric relaxations, a technique known as local, or nanoscale, dielectric spectroscopy.[224–226] In this technique, a cantilever in an AFM is oscillated at its resonant frequency. The nanoscopic tip is situated about 50 nm above a polymer film, and a sinusoidal voltage is then applied to it. If the tip is kept in a region where the force gradients are much smaller than the spring constant of the cantilever, the resulting electrostatic forces between the tip and the polymer cause a shift in the resonant frequency of the cantilever. The measured frequency shifts can be related to a complex capacitance. The data obtained in this measurement has been shown to correspond well with the loss tangent in bulk dielectric spectroscopy measurements, and can be used to obtain information about the dynamics of polymers at localized regions underneath the tip.[227,228] This can be useful for identifying the nanoscopic regions within blends of varying local composition to understand to what extent and length-scales dynamic heterogeneity occurs.

For bulk polymer systems, a further avenue to explore from this work is on polymer nanocomposites (PNCs) and understanding how the introduction of nanoparticles (NPs) into polymer matrices affects the relaxations and dielectric properties of the polymers, due to their proximity to the NPs. This has attracted considerable interest in soft matter research due to the wide array of technological applications; high refractive index materials,[229] light-emitting diodes,[230] photocatalysts,[231] solid polymer electrolytes,[232] and photovoltaic solar cells[233] all call upon physiochemical properties that can be provided by polymer nanocomposites (PNCs). These can include mechanical,[234] optical,[235] or electronic[236] properties, the likes of which may be tailored through control of the nano- and meso- scale spatial distribution of the nanoparticles within the polymer host. One effective strategy to control the organization of NPs within a polymer host is the grafting of molecules onto the surfaces of the nanoparticles, introducing a so-called brush layer, before incorporation into the host. In this scenario, the NP organization throughout the polymer host is dictated by a complex interplay of enthalpic and entropic interactions between the grafted layer and the polymer host chains. Simulations and experimental studies have revealed PNC anisotropic structures are sensitivity to the degree of polymerization N of the host, the surface grafting density Σ, and the nanoparticle sizes and shapes.[237–246]

While much of the experimental work has focused on the case where the matrix and the graft have the same chemical structure, the use of a matrix polymer that is different than the brush remains a relatively unexplored subject. For example, one could choose a scenario in which the graft is thermodynamically compatible with the host – the enthalpic interactions offer a new level of complexity.[244] Because we know that it is the interactions with and/or the vicinity to the interfaces that drive property deviations from bulk behavior,[109,110] a more potentially interesting case is that in which the host and the grafted chains are immiscible. The dielectric

interface formed between two dissimilar but uniform material phases will be substantially different than when sufficiently strong graft-host interactions occur. In particular, the dielectric properties of the composite will be modified due to the additional contributions to polarization from charge carrier blockage at these dielectric boundary layers, known as the Maxwell-Wagner (MW) effect.[247,248]

In preliminary work in this area, we are interested in how the interfaces formed in immiscible host and graft ligand PNCs affect the dielectric properties of the composite. To examine this, we use broadband dielectric spectroscopy (BDS) to examine dielectric properties and polymer relaxations in PNCs of polyisoprene (PI) and poly(vinyl acetate) (PVAc) with immiscible PS-grafted gold nanoparticles. We have seen no changes in τ_{seg} or τ_{trans}; however there is a significant change in the secondary relaxations of the host, becoming more prominent with increasing nanoparticle concentration. Modeling for Maxwell-Wagner effects in a particle suspension with a dielectric shell, it can be shown that this change in secondary relaxation is due to a convolution with a second, Debye-type process due to space-charge polarization at the interface. These results can be utilized for further control of properties in polymer nanocomposites.

Additional precursory work on bulk PNCs shows that the type of NP can have a substantial effect on polymer chain dynamics. Studies of PVAc systems show no change in relaxation rates or temperature dependencies of τ_{seg} upon introduction of C_{60} or Au NPs, regardless of concentration, despite significant particle dispersion. However, introduction of a collapsible particle, such as POSS, with surface groups that can form enthalpic interactions with the host polymer, such as PEG, manifests shifts in τ_{seg} with concentration. Understanding the source and magnitude of this effect is an area of future work.

Chapter 3 (and to an extent Chapter 4) focuses on polymers under nanoconfinement, particularly in understand the role that the type of interface has on polymer dynamics. In this field, there is still much to be done both experimentally and theoretically. Experimentally, additional experimental techniques should be utilized in order to measure the dynamics directly and locally. For example, the above-mentioned nanoscale dielectric spectroscopy can provide insights into not only laterally localized behavior, but also localization with depth. Because the voltage is applied to the tip and radiated out, there is a volume gradient of the electric field; the further from the tip the sample is, the less of an electric field the polymer chains in that area feel, and the smaller the localized permittivity response would be. Carefully designed experiments can utilize this experimental implication to study layer-by-layer dielectric properties as a function of distance from an interface, providing information about the length-scales of interfacial effect propagation.

Another powerful technique useful for characterizing polymer dynamics under nanoconfinement is X-ray photon correlation spectroscopy (XPCS).[249] In this technique, high energy, coherent x-rays interact with a polymer film at an angle of grazing incidence. When energy of coherent wavelength scatters from a disordered system, it gives rise to a diffraction pattern known as a speckled scattering signal giving the exact spatial arrangement of the scatterers in the system. Because these systems are dynamic and constantly in motion, these patterns change with time – likewise an intensity-intensity autocorrelation function of the speckle pattern as it changes with time gives information about the movement of the chains in a polymer film. Because of the high energy of the x-rays, the length-scales being probed are smaller than what can be achieved by traditional dynamic light scattering experiments. Depending of the angle of grazing incidence, these measurements can probe either surface fluctuations[211] or

different depths into the film, even the buried interfaces.[250] Because of this potential for depth probing of dynamics, one would be able to probe dynamics specifically at different interfaces.

On the theoretical side, additional insights are needed to resolve the apparent discrepancies between experiments and simulations of nanoconfinement effects. A number of studies show that confinement-induced shifts in T_g as measured through pseudo-thermodynamic measurements are not accompanied by a shift in the dielectric relaxation spectra, as shown in the bulk.[98,108,204] This equivalency between thermodynamic and dynamic measurements in nanoconfined polymers remains an open question in the field,[109] and simulation work has not yet answered this question; for example, recent work by Fakhraai and Forrest[181] presents experimental measurements of surface relaxation times that show an extrapolated convergence to bulk, whereas the segmental relaxation times at the surface computed from simulations show substantial deviations from the bulk. It remains unanswered whether this represents a physical difference between the experimental and simulated systems or a difference between the relaxation processes being probed. Future simulation work would be useful for addressing the coupling (or lack thereof) between relaxation processes and thermodynamic variables in confined polymers.

Another area of future theoretical and simulation work on polymer nanomaterials is on the hypothesis that a polymer's fragility determines its susceptibility to confinement effects on τ_{seg} and T_g.[251,252] This theory suggests that glass-formers with greater fragility exhibit greater dynamic and thermodynamic alterations under nanoconfinement because they have a greater degree of cooperativity. However, beyond the experimental observations, none of the recent theories regarding polymer fragility provide insight into the reasoning behind this. Further simulations are necessary to establish a generality of this hypothesis.

Appendices

Appendix A. Raw Dielectric Loss Curves of the Bulk Blends

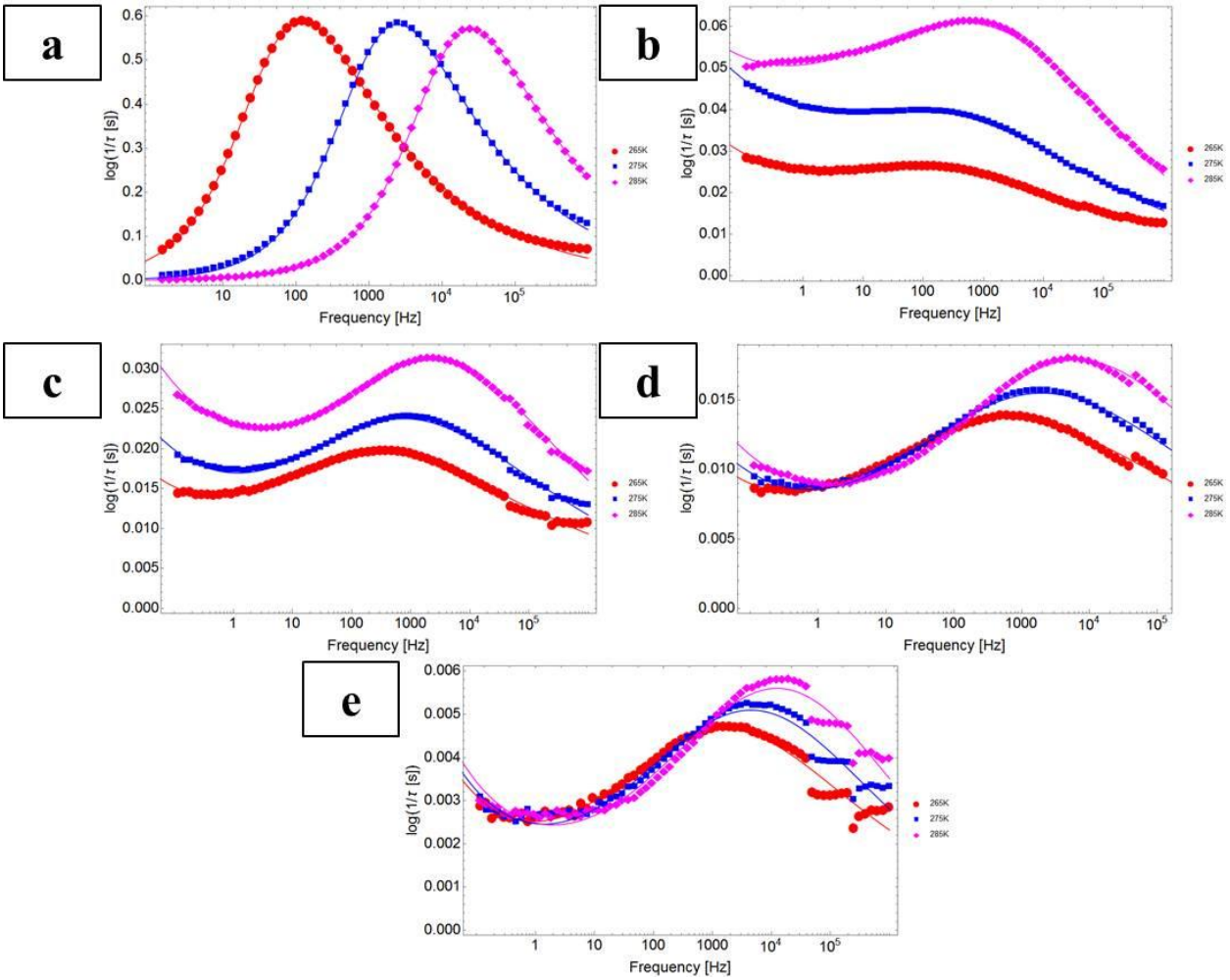

Figure A-1: Raw BDS data of ε" versus frequency of the applied AC voltage (frequency sweep) at select temperatures for (a) pure PVME, (b) 35% PVME blend, (c) 25% PVME blend, (d) 15% PVME blend, (e) 5% PVME blend. HN empirical fittings are shown as solid lines of the same color.

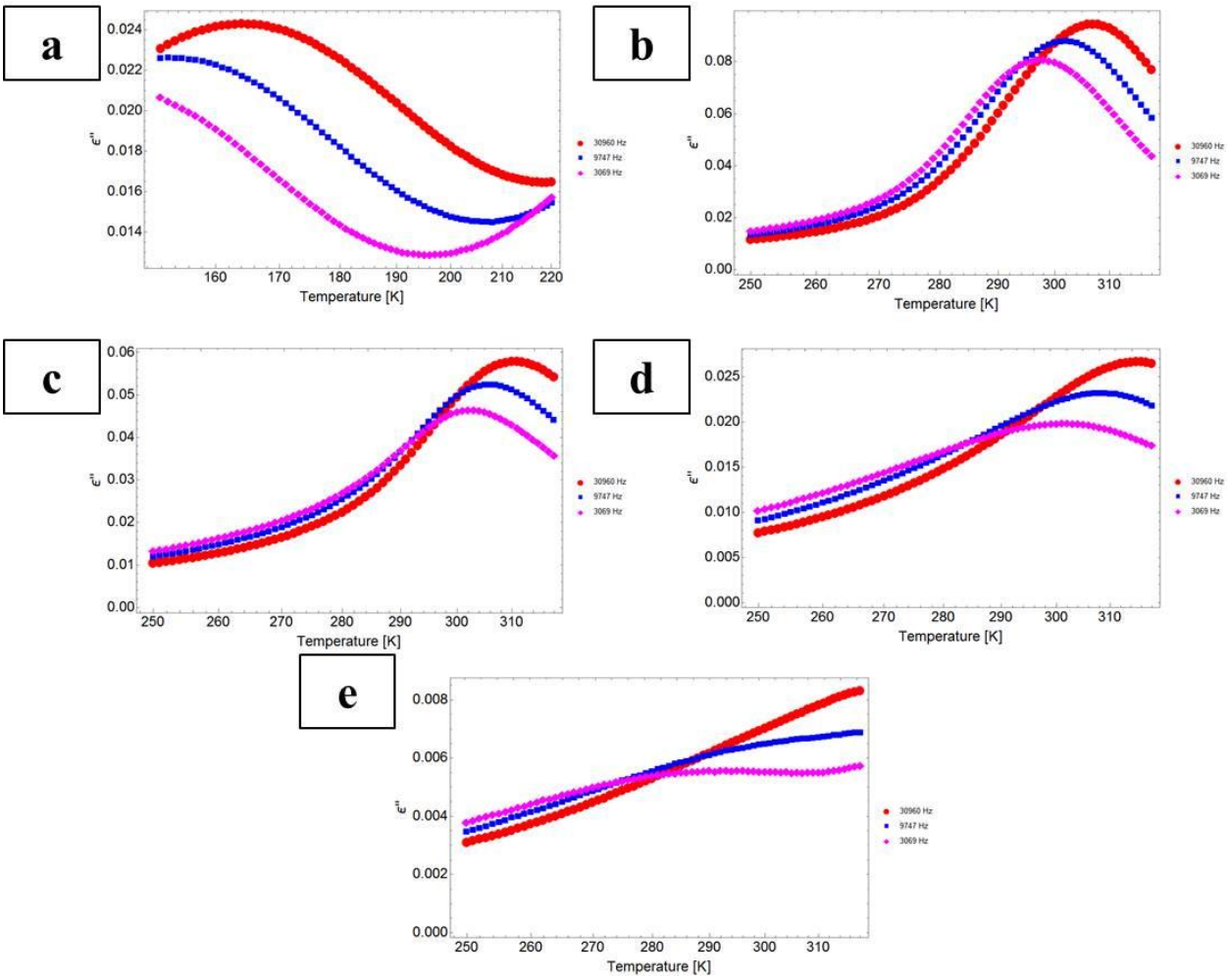

Figure A-2: Raw BDS data of ε" versus temperature (temperature sweep) at select frequencies of the applied AC voltage for (a) pure PVME, (b) 35% PVME blend, (c) 25% PVME blend, (d) 15% PVME blend, (e) 5% PVME blend.

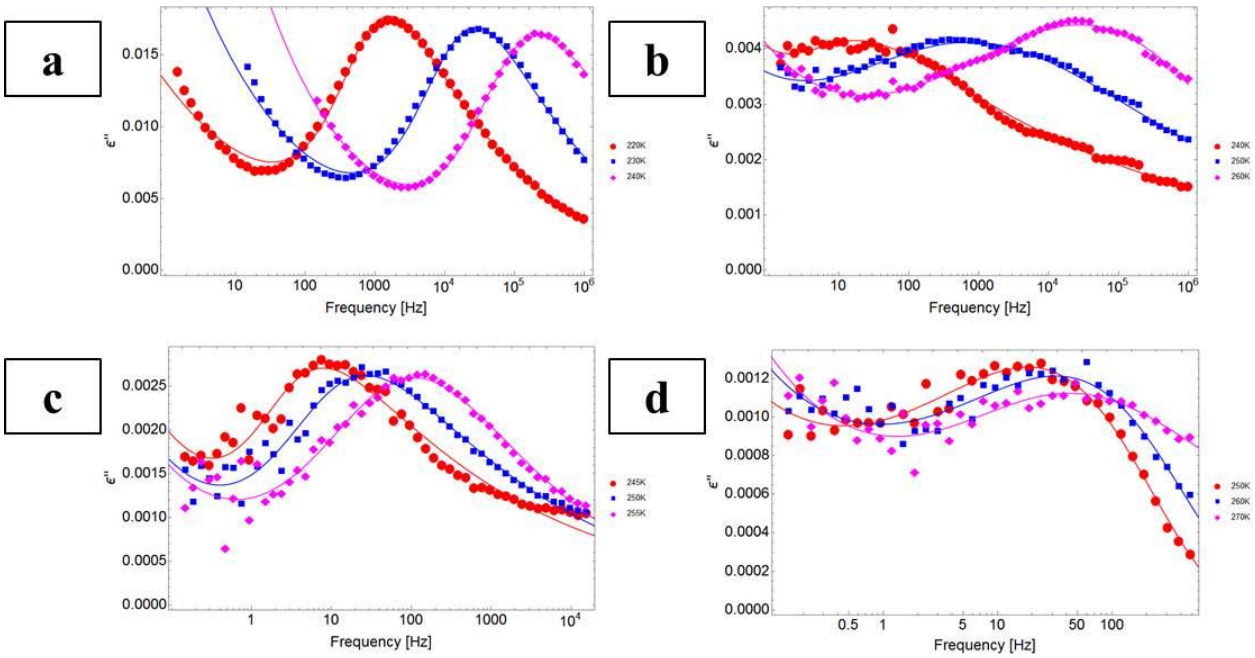

Figure A-3: Raw BDS data of ε" versus frequency of the applied AC voltage (frequency sweep) at select temperatures for (a) pure PI, (b) 40% PI blend, (c) 30% PI blend, (d) 20% PI blend. The PI relaxations observed are the segmental relaxations. HN empirical fittings are shown as solid lines of the same color.

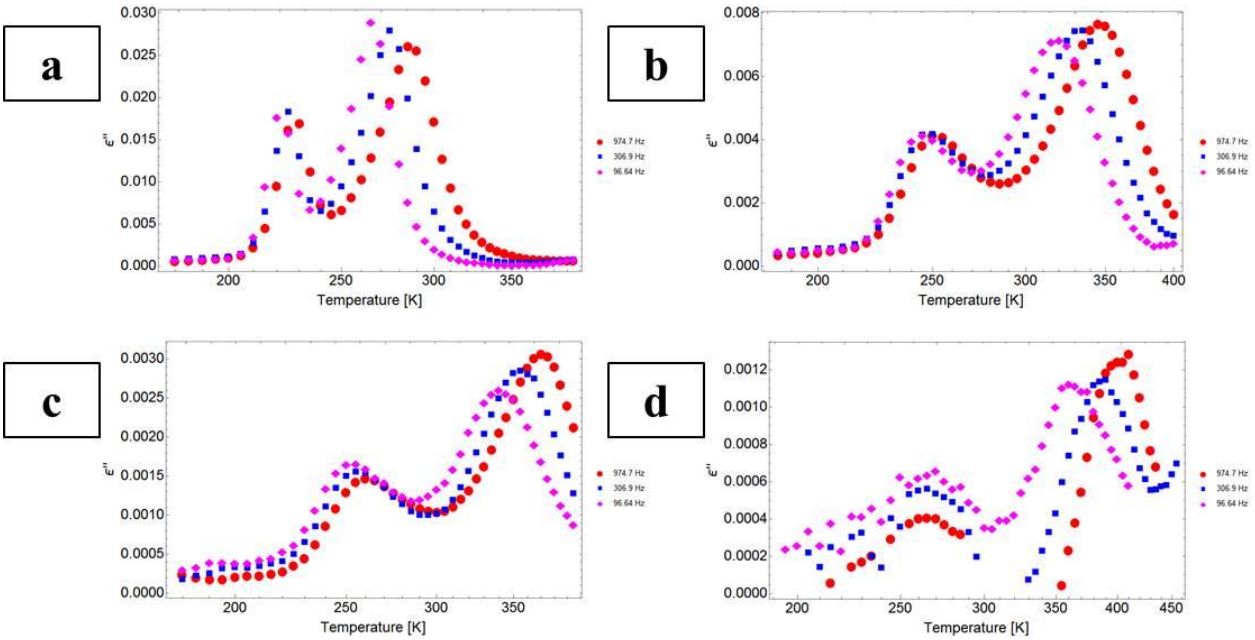

Figure A-4: Raw BDS data of ε" versus temperature (temperature sweep) at select frequencies of the applied AC voltage for (a) pure PI, (b) 40% PI blend, (c) 30% PI blend, (d) 20% PI blend. Both the segmental and end-to-end relaxations are observed.

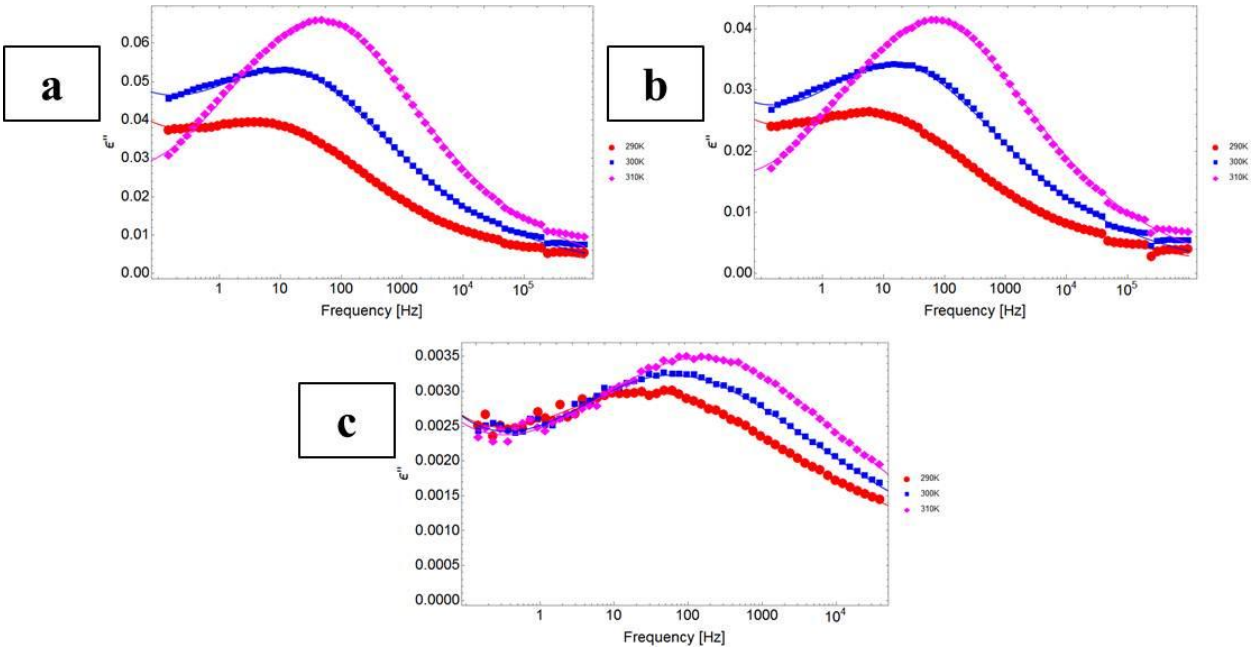

Figure A-5: Raw BDS data of ε" versus frequency of the applied AC voltage (frequency sweep) at select temperatures for (a) 35% PnBMA blend, (b) 25% PnBMA blend, (c) 5% PnBMA blend. HN empirical fittings are shown as solid lines of the same color.

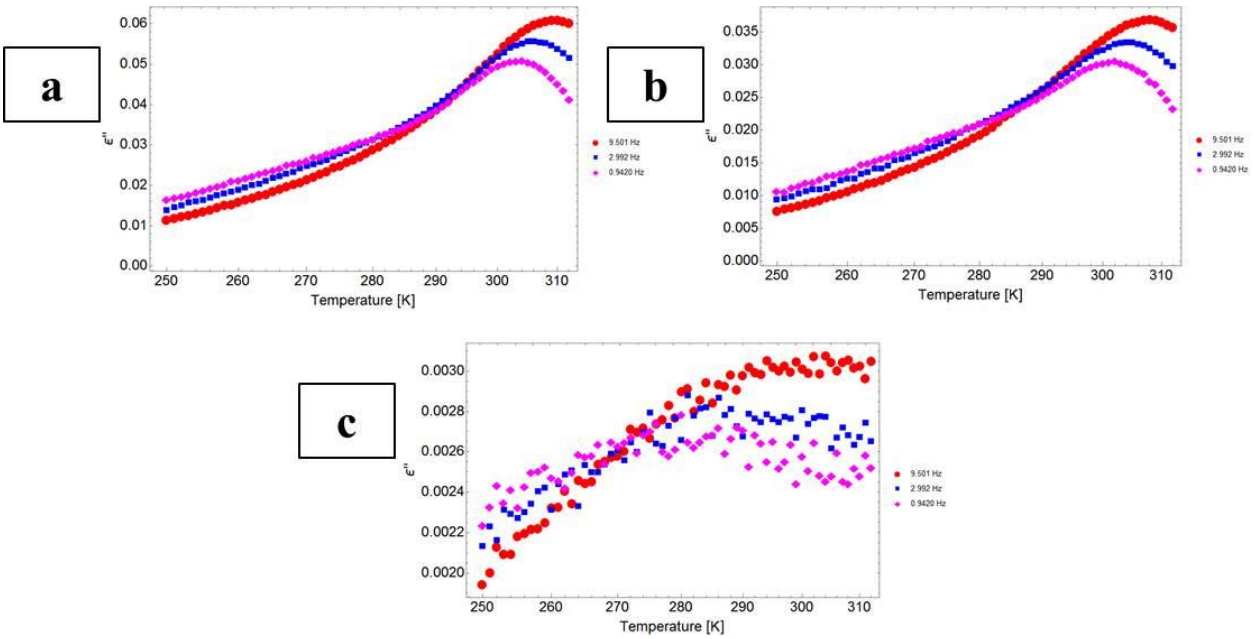

Figure A-6: Raw BDS data of ε" versus temperature (temperature sweep) at select frequencies of the AC applied voltage for (a) 35% PnBMA blend, (b) 25% PnBMA blend, (c) 5% PnBMA blend.

Appendix B. Analysis of BDS Data in the Temperature Representation

In Chapter 3, the dynamic data is displayed as a typical frequency sweep experiment - ε''(ω) is measured at constant *T*. As long as the experiment is conducted within the linear response regime (small electric field strengths and a time-dependent response based solely on linearity and causality), representation as a temperature sweep – ε''(*T*) at constant ω – provides identical dielectric information.[142] The temperature sweep experiments can be noted for the relative ease of identification of the relaxation processes; in addition, frequency sweep measurements, particularly in thin films, can suffer from electrode and interfacial polarization, which convolutes the dielectric response at low frequencies and/or high temperatures.[142]

An example of the raw dielectric loss curves as a function of temperature for a h = 70 nm PVA film confined between two Al electrodes – Al/PVA(70 nm)/Al – obtained using BDS is shown in **Figure B-1**(a). As with its corresponding frequency representation (**Figure 2.2**(a)), the peak that appears is due to the segmental, or α, relaxation process, and shifts to lower temperatures with decreasing frequencies of the applied AC voltage, as expected for a pure polymer under isochronal measurement conditions. These curves are well described using a modified version[106] of the Havriliak –Negami (HN) function (not shown). From this empirical fit to the data, a characteristic relaxation temperature associated with the dielectric loss peak maximum of the imaginary portion of the permittivity ε''(*T*) can be identified. The relaxation

rates as calculated from both the frequency and temperature representations are plotted as $1/\tau$ vs. $1/T$ in **Figure B-1**(b). The results are in excellent agreement, confirming that both types of experiments yield the same results.

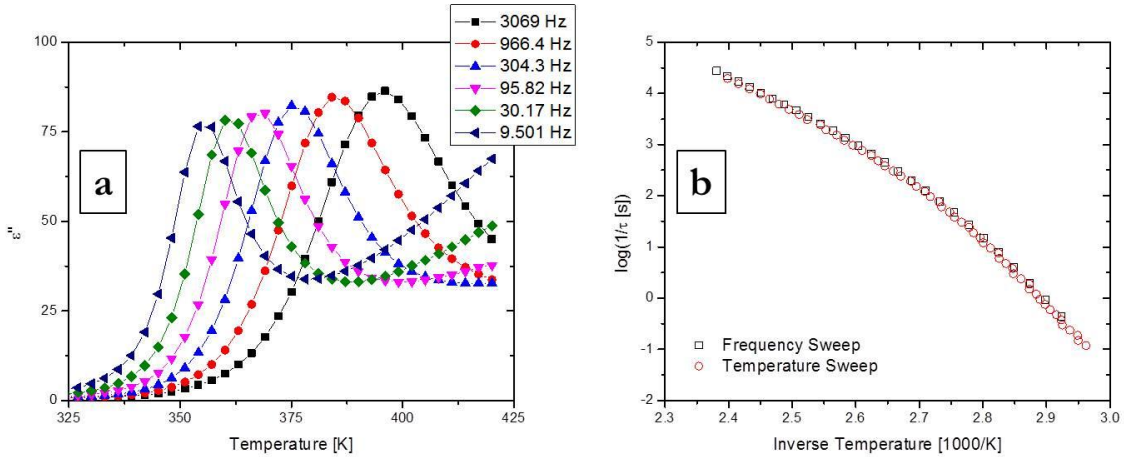

Figure B-1: (a) Raw dielectric loss curves at different frequencies of the applied AC electric field for a 70 nm PVA film capped between two Al electrodes (Al/PVA(70 nm)/Al). (b) Temperature dependencies of the inverse PVA segmental relaxation times in Al/PVA(70 nm)/Al as calculated from the peaks in the dielectric loss curves of both the frequency sweep and the temperature sweep.

Appendix C. Modeling for Dielectric Properties in Series

The simplest model to describe the inhomogeneous bilayer system is as a double layer arrangement where each layer is characterized by a complex dielectric permittivity. It is well known that capacitive properties can be modelled in the following manner:

$$\frac{1}{C_{equivalent}} = \frac{1}{C_1} + \frac{1}{C_2} \tag{C.1}$$

Of course, the relationship between parallel plate capacitance and permittivity is defined as follows:

$$C = \varepsilon \frac{A}{D} \tag{C.2}$$

where A is area of the capacitor perpendicular to current flow and D is the spacing between the plates (in our case the thickness of the layer). Because the area is unchanged throughout the sample, the complex permittivity can be defined as:

$$\frac{1}{\varepsilon^*_{total}(\omega)} = \frac{\phi}{\varepsilon^*_{PVA}(\omega)} + \frac{1-\phi}{\varepsilon^*_{PS}(\omega)} \tag{C.3}$$

where $\varepsilon^*_{total}(\omega)$ is the dielectric response of the entire bilayer system, $\varepsilon^*_{PVA}(\omega)$ and $\varepsilon^*_{PS}(\omega)$ are the contributions from the PVA and PS layers respectively, and φ is the thickness ratio of PVA to the whole bilayer. Algebraic manipulation can get the PVA dielectric response as:[173]

$$\varepsilon^*_{PVA}(\omega) = \phi\left[\frac{1}{\varepsilon^*_{total}(\omega)} - \frac{1-\phi}{\varepsilon^*_{PS}(\omega)}\right]^{-1} \tag{C.4}$$

In the experimental analysis in the study, equation (C.4) is applied for all the bilayer systems across all measured frequencies at all the temperatures. The PS contribution used in this equation is obtained by measuring double Al capped PS films – Al/PS(L)/Al – of the appropriate thickness. These PS films are measured under different experimental conditions than exist in the bilayer – double Al cap rather than asymmetric Al and PVA confining interfaces.

For modelling purposes, we are interested in two effects: (i) how does the PVA dielectric response compare to the total bilayer dielectric response and (ii) what effect does the PS dielectric response have on the PVA dielectric response. As such, consider a model bilayer system in which the film thicknesses are equal ($\varphi = 0.5$). Each component response in our frequency and temperature range is modelled as a single relaxation described by the HN function:

$$\varepsilon^*(\omega) = \varepsilon_\infty + \frac{\Delta\varepsilon}{(1+(i\omega\tau)^\alpha)^\beta} \tag{C.5}$$

Relative values for the parameters for the total bilayer response and PS contribution can be estimated from the bilayer and single PS film experimental data, respectively, at an arbitrary temperature. These complex permittivities can then be applied to equation (C.4) to calculate the corresponding PVA dielectric contribution. Note that, for this particular model, we consider material conductance to be equal and therefore negligible for all samples and focus solely on dielectric properties.

Figure C-1 shows the frequency dependent dielectric losses peaks of the bilayer, PS with varying parameters, and the correspondingly calculated PVA at an arbitrary temperature. First note that the PVA response is shifted from the total bilayer response in both peak and permittivity – despite the much stronger PVA signal, the PS permittivity still has a contribution and therefore should be taken into account. However, note what happens when the PS dielectric

strength or relaxation time is varied – even varying these parameters by an order of magnitude leaves the PVA dielectric response as extracted from the same total bilayer dielectric response relatively unchanged. Thus, even though in our analysis we use the experimental data from PS films under double aluminum confinement rather than asymmetric confinement, in which the interface change may have effects on the PS dynamics, such changes appear to be negligible for the extraction of PVA dynamics.

It is noteworthy that, because there is an inner dielectric boundary layer, Maxwell/Wagner polarization will occur due to a buildup of charge carries at said boundary layer. This gives rise to an additional conductivity contribution and a relaxation process due to charge build-up, creating an internal dipole moment. However, because charge carrier transport is a temperature dependent process that takes place at higher temperatures than molecular relaxation processes, it does not affect the measurements in our temperature and frequency range.

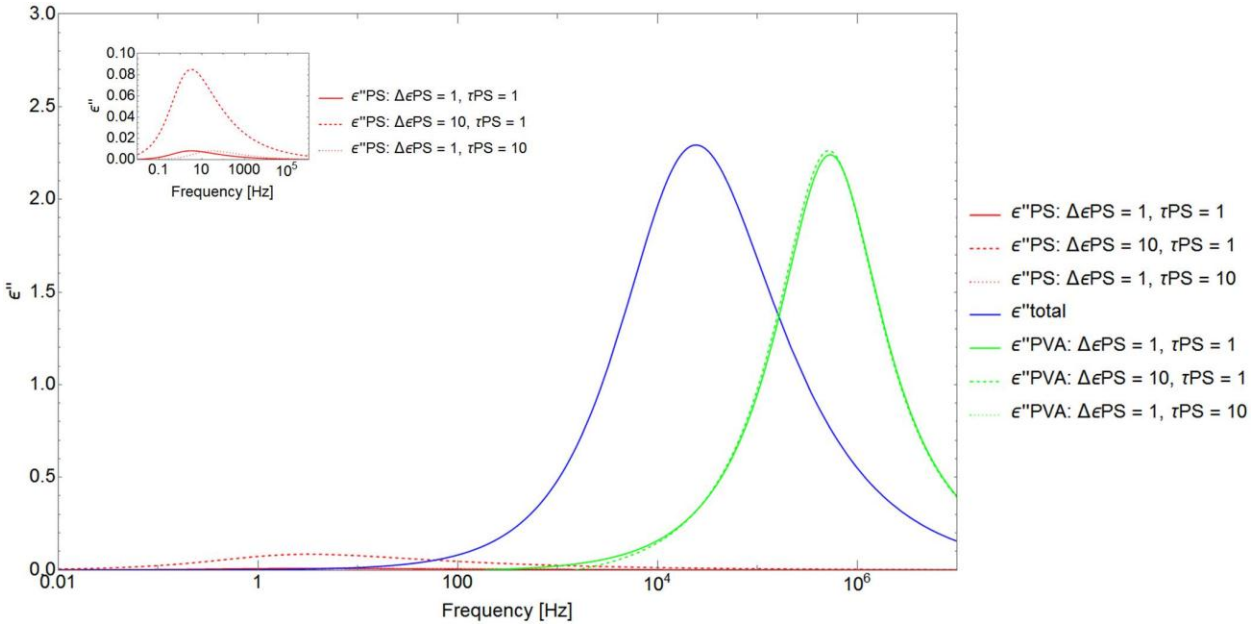

Figure C-1: Model of the dielectric loss response of 0.5 PS film and 0.5 PVA film in series. Red lines represent the PS dielectric loss, green lines represent the PVA dielectric loss, and the blue line represents the series total dielectric loss. Model is based on equation (C3), in which the complex permittivities of PS and the bilayers are inputs and the PVA contribution is calculated. Red dashed and dotted lines represent shifts of one order of magnitude in the PS dielectric strength and characteristic relaxation time, respectively, and corresponding green dashed and dotted lines show how the PVA dielectric loss is affected. Inset plot shows an enlarged version of the PS dielectric loss.

Appendix D. PVA Moisture and Crystallinity Concerns

We address the potential effects that moisture and changes in the degree of crystallinity might have on the reliability of our measurements of PVA dynamics. It has been suggested that moisture, if not carefully eliminated, could lead to a shift in the relaxation times and the appearance of a secondary Arrhenius relaxation.[253] These were determined to not be issues in our study – we used a more stringent annealing procedure than proposed in the literature to remove moisture from our samples: 393K for at least 24 hours under high vacuum, followed by additional in situ annealing. Only a single VFT-type relaxation was observed in the dynamics, which is consistent with the absence of moisture. Moreover, confirmation of the removal of moisture was evident by the absence of a BDS signal associated with water.[254] Certain studies suggest that deviations of the dynamics might be due to improper annealing conditions;[98,108,167] we have observed no unusual changes or fluctuations that would be due to annealing in our experiments.

The second factor that has been suggested to be potentially problematic is the crystallinity of PVA. Fourier-transform infrared spectroscopy (FTIR) was used to identify quantitative correlations between the intensity of the crystalline band normalized to the intensity of the C-O stretching band (see **Figure D-1**).[255] Our measurements indicate a degree of crystallinity of roughly 57%, which is well within literature values for dried PVA[256] and does not vary across all PVA film thicknesses.

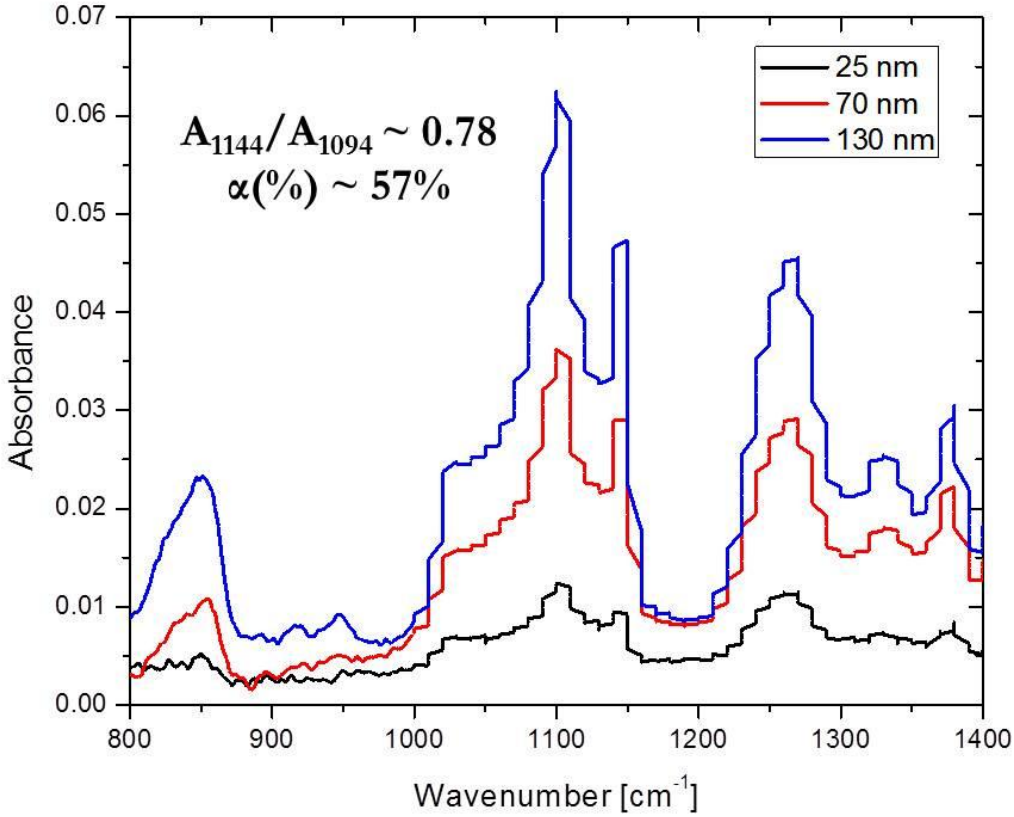

Figure D-1: IR spectrum of 3 different PVA films showing the C-C stretching band (A_{1144}) and the C-O stretching band (A_{1094}). The ratio between the two relates to the degree of crystallinity, giving a value of roughly 57%.

Appendix E. Raw Dielectric Loss Curves of PVME/PS Films

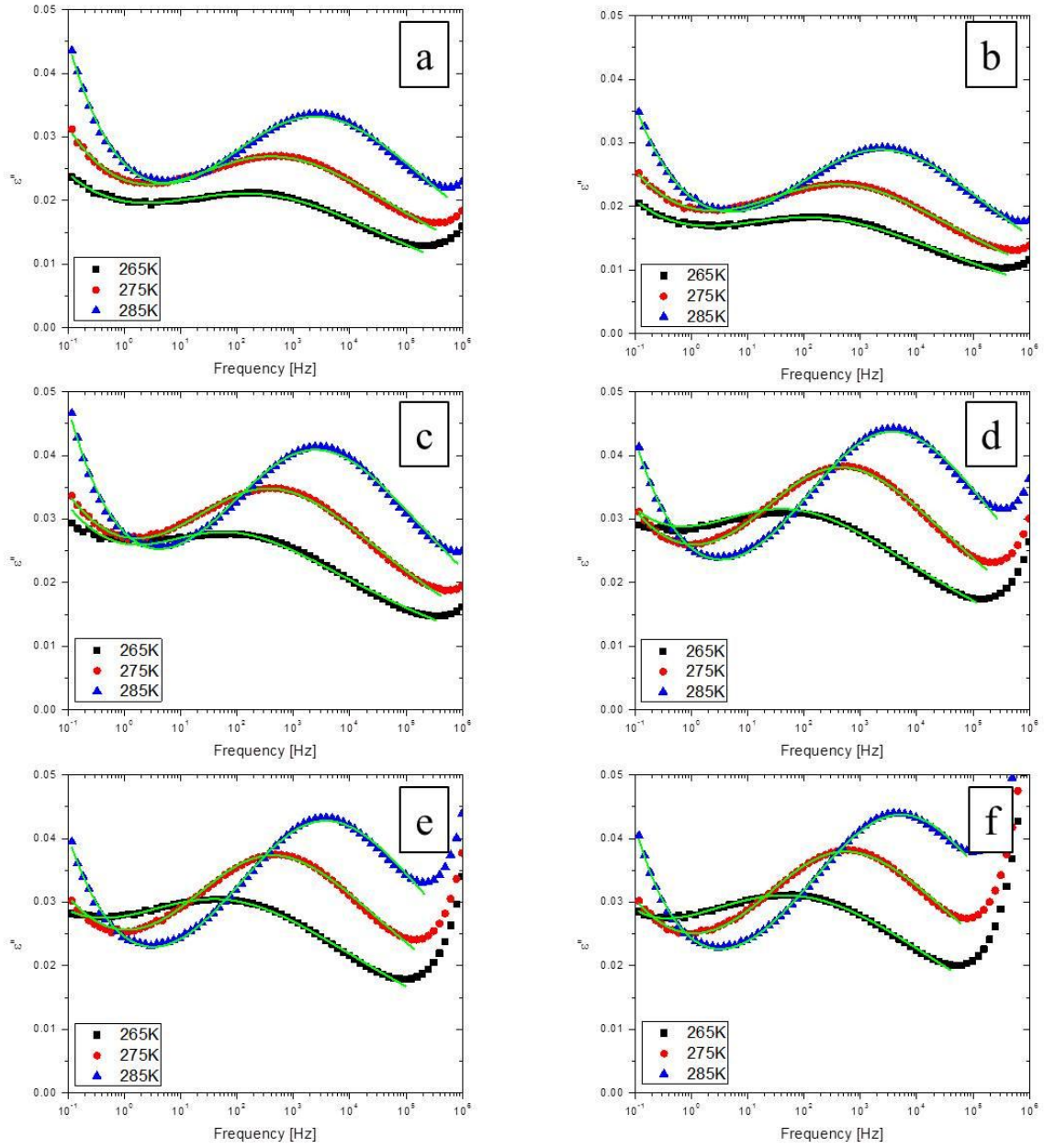

Figure E-1: Raw dielectric loss curves of ε" vs frequency of the applied AC voltage, at select temperatures, for 100 thin films of (a) PVME/PS(3.8k), (b) PVME/PS(4k), (c) PVME/PS(10.9k), (d) PVME/PS(132k), (e) PVME/PS(190k), (f) PVME/PS(525k). Solid green lines represent the HN empirical fittings.

Appendix F. Contour Plots of 100 nm PVME/PS(*M*) Films

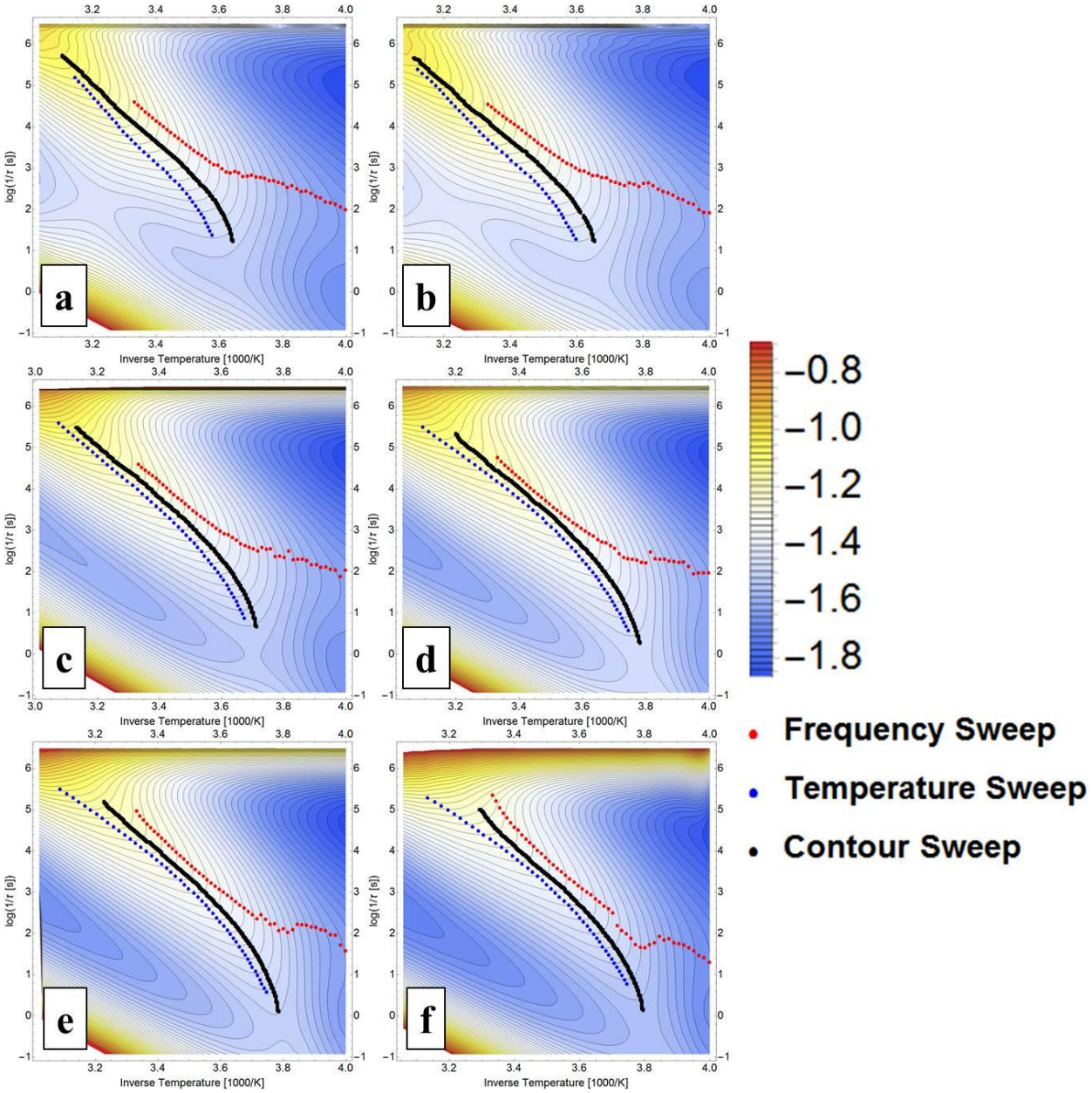

Figure F-1: Contour plots of log(ε'') vs inverse relaxation rate 1/τ and inverse temperature 1/T for 100nm films of (a) PVME/PS(3.8k), (b) PVME/PS(4k), (c) PVME/PS(10.9k), (d) PVME/PS(132k), (e) PVME/PS(190k), (f) PVME/PS(525k). Overlaid on the plot are the relaxations from the frequency sweep (red circles), temperature sweep (blue circles), and contour sweep (black circles).

Appendix G. Thickness Dependent Contour Plots of PVME/PS Films

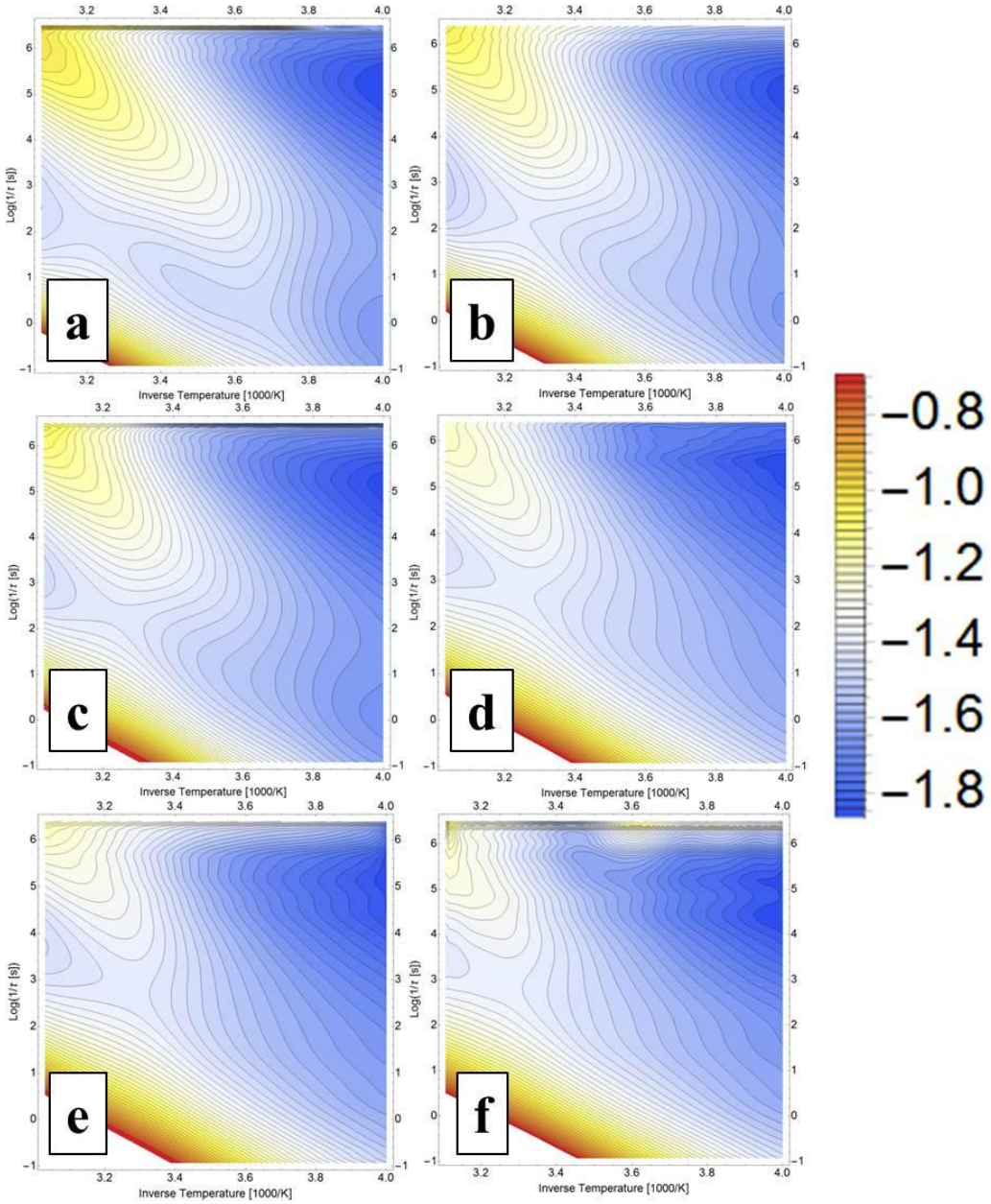

Figure G-1: Contour plots of log(ε'') vs inverse relaxation time 1/τ and inverse temperature 1/T for PVME/PS(4k) films of thicknesses (a) 100 nm (b) 220 nm (c) 310 nm (d) 380 nm (e) 620 nm (f) 770 nm.

Appendix H. Considerations for the Reaction Field Strength Between the Surface Layer and Interior

Because of the difference in concentration between the wetted surface layer and the interior of the film (and significant length-scales of the wetting surface layer thickness comparative to the bulk interior), these regions have different electric field strengths because the dielectric loss (amount of energy absorbed to dissipate the field) is changing – different shielding effects creating different internal reaction fields. This has important implications for a typical isothermal BDS measurement because more mobile dipoles are able to rotate more in response to an external electric field, increasing the internal reaction field and producing a higher dielectric strength. This relationship is apparent in the Onsager factor's dependence on dielectric strength. This is why, as previously described, frequency sweep experiments are sensitive to more mobile regions in compositionally heterogeneous environments at lower temperatures.

However, because the PVME dipole moment strengths are the same in all areas of the blend due to intrinsic chain chemistry, isochronal experiments have a frequency dependent sensitivity in favor of lower frequencies. Isochronal experiments are specifically sensitive to temperatures at which a specific relaxation frequency has the highest intensity (largest number of dipoles relax at that frequency). In other words, assuming that all PVME segments have time to react to the field, this is sensitive to the largest number of chains relaxing at the same frequency, and thus lower frequency (slower relaxing) segments.

The introduction of the contour sweeps is an attempt to rectify this. As a function of both temperature and frequency, this type of data analysis accounts for sensitivities of both types of experiments – frequency and temperature sweeps. In this regard, the contour sweep calculations should not have a bias in terms of electric field strength changes.

Bibliography

(1) Suter, U. W. Why Was the Macromolecular Hypothesis Such a Big Deal? In *Hierarchical Macromolecular Structures: 60 Years after the Staudinger Nobel Prize I*; Advances in Polymer Science; Springer, Cham, 2013; pp 61–80.

(2) Mazza, P. P. A.; Martini, F.; Sala, B.; Magi, M.; Colombini, M. P.; Giachi, G.; Landucci, F.; Lemorini, C.; Modugno, F.; Ribechini, E. A New Palaeolithic Discovery: Tar-Hafted Stone Tools in a European Mid-Pleistocene Bone-Bearing Bed. *J. Archaeol. Sci.* **2006**, *33* (9), 1310–1318.

(3) R C Thompson. *A Dictionary Of Assyrian Chemistry And Geology 1936*; 1936.

(4) Nicholson, P. T.; Shaw, I. *Ancient Egyptian Materials and Technology*; Cambridge University Press, 2000.

(5) Pizzi, A.; Mittal, K. L. *Handbook of Adhesive Technology, Revised and Expanded*; CRC Press, 2003.

(6) Regnault, M. V. De l'Action Du Chlore Sur La Liqueur Des Hollandais et Sur Le Chlorure d'Aldéhydène. *Ann Chim Phys* **1838**, *69*, 151–169.

(7) Simon, E. Ueber Den Flüssigen Storax (Styrax Liquidus). *Ann. Pharm.* **1839**, *31*, 265–277.

(8) Staudinger, H. *From Organic Chemistry to Macromolecules: A Scientific Autobiography Based on My Original Papers*; John Wiley & Sons Canada, Limited, 1970.

(9) Staudinger, H. Über Polymerisation. *Eur. J. Inorg. Chem.* **1920**, *53* (6), 1073–1085.

(10) Staudinger, H.; Fritschi, J. Über Isopren Und Kautschuk. 5. Mitteilung. Über Die Hydrierung Des Kautschuks Und Über Seine Konstitution. *Helv. Chim. Acta* **1922**, *5* (5), 785–806.

(11) Carothers, W. H. STUDIES ON POLYMERIZATION AND RING FORMATION. I. AN INTRODUCTION TO THE GENERAL THEORY OF CONDENSATION POLYMERS. *J. Am. Chem. Soc.* **1929**, *51* (8), 2548–2559.

(12) Kuhn, W. Über Die Gestalt Fadenförmiger Moleküle in Lösungen. *Kolloid-Z.* **1934**, *68* (1), 2–15.

(13) Flory, P.; Volkenstein, M. *Statistical Mechanics of Chain Molecules*; Wiley Online Library, 1969.

(14) Rouse Jr, P. E. A Theory of the Linear Viscoelastic Properties of Dilute Solutions of Coiling Polymers. *J. Chem. Phys.* **1953**, *21* (7), 1272–1280.

(15) Zimm, B. H. Dynamics of Polymer Molecules in Dilute Solution: Viscoelasticity, Flow Birefringence and Dielectric Loss. *J. Chem. Phys.* **1956**, *24* (2), 269–278.

(16) Edwards, S. F. The Statistical Mechanics of Polymers with Excluded Volume. *Proc. Phys. Soc.* **1965**, *85* (4), 613.

(17) De Gennes, P.-G. *Scaling Concepts in Polymer Physics*; Cornell university press, 1979.

(18) Doi, M.; Edwards, S. F. *The Theory of Polymer Dynamics*; oxford university press, 1988; Vol. 73.
(19) Lam, C. X. F.; Mo, X. M.; Teoh, S. H.; Hutmacher, D. W. Scaffold Development Using 3D Printing with a Starch-Based Polymer. *Mater. Sci. Eng. C* **2002**, *20* (1), 49–56.
(20) Takeyama, H.; Soeda, Y.; Kawaguchi, G.; Kawazura, T.; Ozawa, O.; Watanabe, G.; Kuroda, N.; Ikawa, M. Polymer Composition for Tire and Pneumatic Tire Using Same. US6079465 A, June 27, 2000.
(21) Facchetti, A. π-Conjugated Polymers for Organic Electronics and Photovoltaic Cell Applications. *Chem. Mater.* **2011**, *23* (3), 733–758.
(22) Zocco, A. T.; You, H.; Hagen, J. A.; Steckl, A. J. Pentacene Organic Thin-Film Transistors on Flexible Paper and Glass Substrates. *Nanotechnology* **2014**, *25* (9), 094005.
(23) Yave, W.; Car, A.; Wind, J.; Peinemann, K.-V. Nanometric Thin Film Membranes Manufactured on Square Meter Scale: Ultra-Thin Films for CO 2 Capture. *Nanotechnology* **2010**, *21* (39), 395301.
(24) Freiberg, S.; Zhu, X. X. Polymer Microspheres for Controlled Drug Release. *Int. J. Pharm.* **2004**, *282* (1), 1–18.
(25) McKenna, G. B.; Simon, S. L. 50th Anniversary Perspective: Challenges in the Dynamics and Kinetics of Glass-Forming Polymers. *Macromolecules* **2017**, *50* (17), 6333–6361.
(26) Deschenes, L. A.; Bout, D. A. V. Single-Molecule Studies of Heterogeneous Dynamics in Polymer Melts Near the Glass Transition. *Science* **2001**, *292* (5515), 255–258.
(27) Ediger, M. D. Spatially Heterogeneous Dynamics in Supercooled Liquids. *Annu. Rev. Phys. Chem.* **2000**, *51* (1), 99–128.
(28) Glotzer, S. C. Spatially Heterogeneous Dynamics in Liquids: Insights from Simulation. *J. Non-Cryst. Solids* **2000**, *274* (1), 342–355.
(29) Berthier, L.; Biroli, G. Theoretical Perspective on the Glass Transition and Amorphous Materials. *Rev. Mod. Phys.* **2011**, *83* (2), 587–645.
(30) Biroli, G.; Garrahan, J. P. Perspective: The Glass Transition. *J. Chem. Phys.* **2013**, *138* (12), 12A301.
(31) Angell, C. A. Liquid Fragility and the Glass Transition in Water and Aqueous Solutions. *Chem. Rev.* **2002**, *102* (8), 2627–2650.
(32) Kunal, K.; Robertson, C. G.; Pawlus, S.; Hahn, S. F.; Sokolov, A. P. Role of Chemical Structure in Fragility of Polymers: A Qualitative Picture. *Macromolecules* **2008**, *41* (19), 7232–7238.
(33) Adam, G.; Gibbs, J. H. On the Temperature Dependence of Cooperative Relaxation Properties in Glass-Forming Liquids. *J. Chem. Phys.* **1965**, *43* (1), 139–146.
(34) Donth, E. Characteristic Length of the Glass Transition. *J. Polym. Sci. Part B Polym. Phys.* **1996**, *34* (17), 2881–2892.
(35) Donth, E. Does Temperature Fluctuate? The Fluctuation-Dissipation Theorem Considered as an Equation Describing Quantum Mechanical Experiments, and Application to the Dynamic Glass Transition. *J. Phys. Condens. Matter* **2000**, *12* (50), 10371.
(36) Donth, E.-J. *The Glass Transition*, 2001 edition.; Springer: Berlin ; New York, 2001.
(37) Fulcher, G. S. Analysis of Recent Measurements of the Viscosity of Glasses. *J. Am. Ceram. Soc.* **1925**, *8* (6), 339–355.

(38) Doolittle, A. K. Studies in Newtonian Flow. II. The Dependence of the Viscosity of Liquids on Free-Space. *J. Appl. Phys.* **1951**, *22* (12), 1471–1475.
(39) Williams, M. L.; Landel, R. F.; Ferry, J. D. The Temperature Dependence of Relaxation Mechanisms in Amorphous Polymers and Other Glass-Forming Liquids. *J. Am. Chem. Soc.* **1955**, *77* (14), 3701–3707.
(40) Freed, K. F. Influence of Monomer Molecular Structure on the Glass Transition in Polymers I. Lattice Cluster Theory for the Configurational Entropy. *J. Chem. Phys.* **2003**, *119* (11), 5730–5739.
(41) Freed, K. F. Communication: The Simplified Generalized Entropy Theory of Glass-Formation in Polymer Melts. *J. Chem. Phys.* **2015**, *143* (5), 051102.
(42) Xu, W.-S.; Freed, K. F. Influence of Cohesive Energy and Chain Stiffness on Polymer Glass Formation. *Macromolecules* **2014**, *47* (19), 6990–6997.
(43) Battezzati, L. Is There a Link between Melt Fragility and Elastic Properties of Metallic Glasses? *Mater. Trans.* **2005**, *46* (12), 2915–2919.
(44) Angell, C. A. Formation of Glasses from Liquids and Biopolymers. *Science* **1995**, *267* (5206), 1924–1935.
(45) Debenedetti, P. G.; Stillinger, F. H. Supercooled Liquids and the Glass Transition. *Nature* **2001**, *410* (6825), 259–267.
(46) Long, D.; Lequeux, F. Heterogeneous Dynamics at the Glass Transition in van Der Waals Liquids, in the Bulk and in Thin Films. *Eur. Phys. J. E* **2001**, *4* (3), 371–387.
(47) Kohlrausch, R. Theorie Des Elektrischen Rückstandes in Der Leidener Flasche. *Ann. Phys.* **1854**, *167* (1), 56–82.
(48) Williams, G.; Watts, D. Non-Symmetrical Dielectric Relaxation Behaviour Arising From a Simple Empirical Decay Function. *Trans. Faraday Soc.* **1970**, *66*.
(49) Hanakata, P. Z.; Douglas, J. F.; Starr, F. W. Local Variation of Fragility and Glass Transition Temperature of Ultra-Thin Supported Polymer Films. *J. Chem. Phys.* **2012**, *137* (24), 244901.
(50) White, R. P.; Lipson, J. E. G. Polymer Free Volume and Its Connection to the Glass Transition. *Macromolecules* **2016**, *49* (11), 3987–4007.
(51) White, R. P.; Lipson, J. E. G. How Free Volume Does Influence the Dynamics of Glass Forming Liquids. *ACS Macro Lett.* **2017**, *6* (5), 529–534.
(52) Hiemenz, P. C.; Lodge, T. P. *Polymer Chemistry, Second Edition*, 2 edition.; CRC Press: Boca Raton, 2007.
(53) Kant, R.; Kumar, S. K.; Colby, R. H. What Length Scales Control the Dynamics of Miscible Polymer Blends? *Macromolecules* **2003**, *36* (26), 10087–10094.
(54) Roland, C. M.; Ngai, K. L. Dynamical Heterogeneity in a Miscible Polymer Blend. *Macromolecules* **1991**, *24* (9), 2261–2265.
(55) Chung, G.-C.; Kornfield, J. A.; Smith, S. D. Compositional Dependence of Segmental Dynamics in a Miscible Polymer Blend. *Macromolecules* **1994**, *27* (20), 5729–5741.
(56) Kamath, S. Y.; Colby, R. H.; Kumar, S. K. Evidence for Dynamic Heterogeneities in Computer Simulations of Miscible Polymer Blends. *Phys. Rev. E Stat. Nonlin. Soft Matter Phys.* **2003**, *67* (1 Pt 1), 010801.
(57) Leroy, E.; Alegría, A.; Colmenero, J. Segmental Dynamics in Miscible Polymer Blends: Modeling the Combined Effects of Chain Connectivity and Concentration Fluctuations. *Macromolecules* **2003**, *36* (19), 7280–7288.

(58) Pathak, J. A.; Colby, R. H.; Floudas, G.; Jérôme, R. Dynamics in Miscible Blends of Polystyrene and Poly(Vinyl Methyl Ether). *Macromolecules* **1999**, *32* (8), 2553–2561.
(59) Lodge, T. P.; McLeish, T. C. B. Self-Concentrations and Effective Glass Transition Temperatures in Polymer Blends. *Macromolecules* **2000**, *33* (14), 5278–5284.
(60) Cangialosi, D.; Schwartz, G. A.; Alegría, A.; Colmenero, J. Combining Configurational Entropy and Self-Concentration to Describe the Component Dynamics in Miscible Polymer Blends. *J. Chem. Phys.* **2005**, *123* (14), 144908.
(61) Kumar, S. K.; Colby, R. H.; Anastasiadis, S. H.; Fytas, G. Concentration Fluctuation Induced Dynamic Heterogeneities in Polymer Blends. *J. Chem. Phys.* **1996**, *105* (9), 3777–3788.
(62) Zetsche, A.; Fischer, E. w. Dielectric Studies of the α-Relaxation in Miscible Polymer Blends and Its Relation to Concentration Fluctuations. *Acta Polym.* **1994**, *45* (3), 168–175.
(63) Katana, G.; Fischer, E. W.; Hack, T.; Abetz, V.; Kremer, F. Influence of Concentration Fluctuations on the Dielectric .Alpha.-Relaxation in Homogeneous Polymer Mixtures. *Macromolecules* **1995**, *28* (8), 2714–2722.
(64) Lodge, T. P.; Wood, E. R.; Haley, J. C. Two Calorimetric Glass Transitions Do Not Necessarily Indicate Immiscibility: The Case of PEO/PMMA. *J. Polym. Sci. Part B Polym. Phys.* **2006**, *44* (4), 756–763.
(65) Zhao, J.; Ediger, M. D.; Sun, Y.; Yu, L. Two DSC Glass Transitions in Miscible Blends of Polyisoprene/Poly(4-Tert-Butylstyrene). *Macromolecules* **2009**, *42* (17), 6777–6783.
(66) Dudowicz, J.; Douglas, J. F.; Freed, K. F. Two Glass Transitions in Miscible Polymer Blends? *J. Chem. Phys.* **2014**, *140* (24), 244905.
(67) Colby, R. H. Breakdown of Time-Temperature Superposition in Miscible Polymer Blends. *Polymer* **1989**, *30* (7), 1275–1278.
(68) Colmenero, J.; Arbe, A. Segmental Dynamics in Miscible Polymer Blends: Recent Results and Open Questions. *Soft Matter* **2007**, *3* (12), 1474–1485.
(69) Watanabe, H.; Chen, Q.; Kawasaki, Y.; Matsumiya, Y.; Inoue, T.; Urakawa, O. Entanglement Dynamics in Miscible Polyisoprene/Poly(p-Tert-Butylstyrene) Blends. *Macromolecules* **2011**, *44* (6), 1570–1584.
(70) Watanabe, H.; Matsumiya, Y.; Takada, J.; Sasaki, H.; Matsushima, Y.; Kuriyama, A.; Inoue, T.; Ahn, K. H.; Yu, W.; Krishnamoorti, R. Viscoelastic and Dielectric Behavior of a Polyisoprene/Poly(4-Tert-Butyl Styrene) Miscible Blend. *Macromolecules* **2007**, *40* (15), 5389–5399.
(71) Chen, Q.; Matsumiya, Y.; Masubuchi, Y.; Watanabe, H.; Inoue, T. Component Dynamics in Polyisoprene/Poly(4-Tert-Butylstyrene) Miscible Blends. *Macromolecules* **2008**, *41* (22), 8694–8711.
(72) Matsumiya, Y.; Rakkapao, N.; Watanabe, H. Entanglement Length in Miscible Blends of Cis-Polyisoprene and Poly(p-Tert-Butylstyrene). *Macromolecules* **2015**, *48* (21), 7889–7908.
(73) Gill, L.; Damron, J.; Wachowicz, M.; White, J. L. Glass Transitions, Segmental Dynamics, and Friction Coefficients for Individual Polymers in Multicomponent Polymer Systems by Chain-Level Experiments. *Macromolecules* **2010**, *43* (8), 3903–3910.

(74) Cendoya, I.; Alegría, A.; Alberdi, J. M.; Colmenero, J.; Grimm, H.; Richter, D.; Frick, B. Effect of Blending on the PVME Dynamics. A Dielectric, NMR, and QENS Investigation. *Macromolecules* **1999**, *32* (12), 4065–4078.
(75) Arbe, A.; Alegría, A.; Colmenero, J.; Hoffmann, S.; Willner, L.; Richter, D. Segmental Dynamics in Poly(Vinylethylene)/Polyisoprene Miscible Blends Revisited. A Neutron Scattering and Broad-Band Dielectric Spectroscopy Investigation. *Macromolecules* **1999**, *32* (22), 7572–7581.
(76) Lorthioir, C.; Alegría, A.; Colmenero, J. Out of Equilibrium Dynamics of Poly(Vinyl Methyl Ether) Segments in Miscible Poly(Styrene)-Poly(Vinyl Methyl Ether) Blends. *Phys. Rev. E* **2003**, *68* (3), 031805.
(77) De Gennes, P. G. Dynamics of Entangled Polymer Solutions. I. The Rouse Model. *Macromolecules* **1976**, *9* (4), 587–593.
(78) de Gennes, P. G. Reptation of a Polymer Chain in the Presence of Fixed Obstacles. *J. Chem. Phys.* **1971**, *55* (2), 572–579.
(79) Viovy, J. L.; Rubinstein, M.; Colby, R. H. Constraint Release in Polymer Melts: Tube Reorganization versus Tube Dilation. *Macromolecules* **1991**, *24* (12), 3587–3596.
(80) Cloizeaux, J. des. Double Reptation vs. Simple Reptation in Polymer Melts. *EPL Europhys. Lett.* **1988**, *5* (5), 437.
(81) Stafford, C. M.; Vogt, B. D.; Harrison, C.; Julthongpiput, D.; Huang, R. Elastic Moduli of Ultrathin Amorphous Polymer Films. *Macromolecules* **2006**, *39* (15), 5095–5099.
(82) Prabu, A. A.; Kim, K. J.; Park, C. Effect of Thickness on the Crystallinity and Curie Transition Behavior in P(VDF/TrFE) (72/28) Copolymer Thin Films Using FTIR-Transmission Spectroscopy. *Vib. Spectrosc.* **2009**, *49* (2), 101–109.
(83) Huang, B.; Glynos, E.; Frieberg, B.; Yang, H.; Green, P. F. Effect of Thickness-Dependent Microstructure on the Out-of-Plane Hole Mobility in Poly(3-Hexylthiophene) Films. *ACS Appl. Mater. Interfaces* **2012**, *4* (10), 5204–5210.
(84) Yelash, L.; Virnau, P.; Binder, K.; Paul, W. Three-Step Decay of Time Correlations at Polymer-Solid Interfaces. *EPL Europhys. Lett.* **2012**, *98* (2), 28006.
(85) Varnik, F.; Baschnagel, J.; Binder, K. Glassy Dynamics in Thin Polymer Films: Recent MD Results. *J. Non-Cryst. Solids* **2002**, *307–310* (Supplement C), 524–531.
(86) Solar, M.; Mapesa, E. U.; Kremer, F.; Binder, K.; Paul, W. The Dielectric α -Relaxation in Polymer Films: A Comparison between Experiments and Atomistic Simulations. *EPL Europhys. Lett.* **2013**, *104* (6), 66004.
(87) Yelash, L.; Virnau, P.; Binder, K.; Paul, W. Slow Process in Confined Polymer Melts: Layer Exchange Dynamics at a Polymer Solid Interface. *Phys. Rev. E Stat. Nonlin. Soft Matter Phys.* **2010**, *82* (5 Pt 1), 050801.
(88) DeFelice, J.; Milner, S. T.; Lipson, J. E. G. Simulating Local Tg Reporting Layers in Glassy Thin Films. *Macromolecules* **2016**, *49* (5), 1822–1833.
(89) Tito, N. B.; Lipson, J. E. G.; Milner, S. T. Lattice Model of Dynamic Heterogeneity and Kinetic Arrest in Glass-Forming Liquids. *Soft Matter* **2013**, *9* (11), 3173–3180.
(90) Lin, F.-Y.; Steffen, W. Capillary Wave Dynamics of Thin Liquid Polymer Films. *J. Chem. Phys.* **2014**, *141* (10), 104903.
(91) Peter, S.; Meyer, H.; Baschnagel, J. Thickness-Dependent Reduction of the Glass-Transition Temperature in Thin Polymer Films with a Free Surface. *J. Polym. Sci. Part B Polym. Phys.* **2006**, *44* (20), 2951–2967.

(92) Dalnoki-Veress, K.; Forrest, J.; G De Gennes, P.; Dutcher, J. Glass Transition Reductions in Thin Freely-Standing Polymer Films: A Scaling Analysis of Chain Confinement Effects. *J. Phys. IV Proc.* **2000**, *10*, Pr7-221.
(93) Roth, C. B.; Dutcher, J. R. Glass Transition Temperature of Freely-Standing Films of Atactic Poly(Methyl Methacrylate). *Eur. Phys. J. E* **2003**, *12*, 103–107.
(94) Wang, J.; McKenna, G. B. Viscoelastic and Glass Transition Properties of Ultrathin Polystyrene Films by Dewetting from Liquid Glycerol. *Macromolecules* **2013**, *46* (6), 2485–2495.
(95) Ellison, C. J.; Torkelson, J. M. The Distribution of Glass-Transition Temperatures in Nanoscopically Confined Glass Formers. *Nat. Mater.* **2003**, *2* (10), 695–700.
(96) Forrest, J. A. Effect of Free Surfaces on the Glass Transition Temperature of Thin Polymer Films. *Phys. Rev. Lett.* **1996**, *77* (10), 2002–2005.
(97) Keddie, J. L.; Jones, R. A. L.; Cory, R. A. Size-Dependent Depression of the Glass Transition Temperature in Polymer Films. *EPL Europhys. Lett.* **1994**, *27* (1), 59.
(98) Boucher, V. M.; Cangialosi, D.; Yin, H.; Schönhals, A.; Alegría, A.; Colmenero, J. Tg Depression and Invariant Segmental Dynamics in Polystyrene Thin Films. *Soft Matter* **2012**, *8*, 5119.
(99) Forrest, J. A.; Dalnoki-Veress, K. The Glass Transition in Thin Polymer Films. *Adv. Colloid Interface Sci.* **2001**, *94* (1–3), 167–195.
(100) Fukao, K. Glass Transitions and Dynamics in Thin Polymer Films: Dielectric Relaxation of Thin Films of Polystyrene. *Phys. Rev. E* **2000**, *61* (2), 1743–1754.
(101) Priestley, R. D.; Broadbelt, L. J.; Torkelson, J. M.; Fukao, K. Glass Transition and $\ensuremath{\alpha}$-Relaxation Dynamics of Thin Films of Labeled Polystyrene. *Phys. Rev. E* **2007**, *75* (6), 061806.
(102) Yin, H.; Napolitano, S.; Schönhals, A. Molecular Mobility and Glass Transition of Thin Films of Poly(Bisphenol A Carbonate). *Macromolecules* **2012**, *45* (3), 1652–1662.
(103) Mirigian, S.; Schweizer, K. S. Communication: Slow Relaxation, Spatial Mobility Gradients, and Vitrification in Confined Films. *J. Chem. Phys.* **2014**, *141* (16), 161103.
(104) Hsu, D. D.; Xia, W.; Song, J.; Keten, S. Glass-Transition and Side-Chain Dynamics in Thin Films: Explaining Dissimilar Free Surface Effects for Polystyrene vs Poly(Methyl Methacrylate). *ACS Macro Lett.* **2016**, *5* (4), 481–486.
(105) Lupaşcu, V.; Picken, S. J.; Wübbenhorst, M. Cooperative and Non-Cooperative Dynamics in Ultra-Thin Films of Polystyrene Studied by Dielectric Spectroscopy and Capacitive Dilatometry. *J. Non-Cryst. Solids* **2006**, *352* (52–54), 5594–5600.
(106) Kipnusu, W. K.; Elmahdy, M. M.; Tress, M.; Fuchs, M.; Mapesa, E. U.; Smilgies, D.-M.; Zhang, J.; Papadakis, C. M.; Kremer, F. Molecular Order and Dynamics of Nanometric Thin Layers of Poly(Styrene-b-1,4-Isoprene) Diblock Copolymers. *Macromolecules* **2013**, *46* (24), 9729–9737.
(107) Mapesa, E. U.; Tress, M.; Schulz, G.; Huth, H.; Schick, C.; Reiche, M.; Kremer, F. Segmental and Chain Dynamics in Nanometric Layers of Poly(Cis-1,4-Isoprene) as Studied by Broadband Dielectric Spectroscopy and Temperature-Modulated Calorimetry. *Soft Matter* **2013**, *9* (44), 10592–10598.
(108) Kremer, F.; Tress, M.; Mapesa, E. U. Glassy Dynamics and Glass Transition in Nanometric Layers and Films: A Silver Lining on the Horizon. *J. Non-Cryst. Solids* **2015**, *407*, 277–283.

(109) Priestley, R. D.; Cangialosi, D.; Napolitano, S. On the Equivalence between the Thermodynamic and Dynamic Measurements of the Glass Transition in Confined Polymers. *J. Non-Cryst. Solids* **2015**, *407*, 288–295.
(110) Ediger, M. D.; Forrest, J. A. Dynamics near Free Surfaces and the Glass Transition in Thin Polymer Films: A View to the Future. *Macromolecules* **2014**, *47* (2), 471–478.
(111) Chung, G. C.; Kornfield, J. A.; Smith, S. D. Component Dynamics Miscible Polymer Blends: A Two-Dimensional Deuteron NMR Investigation. *Macromolecules* **1994**, *27* (4), 964–973.
(112) Yang, H.; Green, P. F. Role of Spatial Compositional Heterogeneity on Component Dynamics in Miscible Bulk and Thin Film Polymer/Polymer Blends. *Macromolecules* **2013**, *46* (23), 9390–9395.
(113) Donth, E.; Huth, H.; Beiner, M. Characteristic Length of the Glass Transition. *J. Phys. Condens. Matter* **2001**, *13* (22), L451.
(114) Le Menestrel, C.; Kenwright, A. M.; Sergot, P.; Laupretre, F.; Monnerie, L. Carbon-13 NMR Investigation of Local Dynamics in Compatible Polymer Blends. *Macromolecules* **1992**, *25* (12), 3020–3026.
(115) Alegria, A.; Colmenero, J.; Ngai, K. L.; Roland, C. M. Observation of the Component Dynamics in a Miscible Polymer Blend by Dielectric and Mechanical Spectroscopies. *Macromolecules* **1994**, *27* (16), 4486–4492.
(116) Smith, G. D.; Bedrov, D. Dynamics of a Poly(Isoprene)/Poly(Vinyl Ethylene) Blend Revisited: Component Polymer Relaxation and Blend Behavior. *Eur. Polym. J.* **2006**, *42* (12), 3248–3256.
(117) Arrese-Igor, S.; Alegría, A.; Colmenero, J. Comparison of Calorimetric and Dielectric Single Component Glass Transitions in PtBS−PI Blends. *Macromolecules* **2010**, *43* (15), 6406–6413.
(118) Arrese-Igor, S.; Alegría, A.; Moreno, A. J.; Colmenero, J. Effect of Blending on the Chain Dynamics of the "Low-Tg" Component in Nonentangled and Dynamically Asymmetric Polymer Blends. *Macromolecules* **2011**, *44* (9), 3611–3621.
(119) Schwartz, G. A.; Colmenero, J.; Alegría, Á. Single Component Dynamics in Miscible Poly(Vinyl Methyl Ether)/Polystyrene Blends under Hydrostatic Pressure. *Macromolecules* **2007**, *40* (9), 3246–3255.
(120) Yin, H.; Schönhals, A. Broadband Dielectric Spectroscopy on Polymer Blends. *ResearchGate* **2014**.
(121) Colby, R. H.; Lipson, J. E. G. Modeling the Segmental Relaxation Time Distribution of Miscible Polymer Blends: Polyisoprene/Poly(Vinylethylene). *Macromolecules* **2005**, *38* (11), 4919–4928.
(122) Schwartz, G. A.; Cangialosi, D.; Alegría, Á.; Colmenero, J. Describing the Component Dynamics in Miscible Polymer Blends: Towards a Fully Predictive Model. *J. Chem. Phys.* **2006**, *124* (15), 154904.
(123) Schwartz, G. A.; Alegría, Á.; Colmenero, J. Adam-Gibbs Based Model to Describe the Single Component Dynamics in Miscible Polymer Blends under Hydrostatic Pressure. *J. Chem. Phys.* **2007**, *127* (15), 154907.
(124) Götze, W. *Complex Dynamics of Glass-Forming Liquids: A Mode-Coupling Theory*; OUP Oxford, 2008.
(125) Anderson, P. W. Through the Glass Lightly. *Science* **1995**, *267* (5204), 1615–1616.

(126) Gaikwad, A. N.; Wood, E. R.; Ngai, T.; Lodge, T. P. Two Calorimetric Glass Transitions in Miscible Blends Containing Poly(Ethylene Oxide). *Macromolecules* **2008**, *41* (7), 2502–2508.
(127) Herrera, D.; Zamora, J.-C.; Bello, A.; Grimau, M.; Laredo, E.; Müller, A. J.; Lodge, T. P. Miscibility and Crystallization in Polycarbonate/Poly(ε-Caprolactone) Blends: Application of the Self-Concentration Model. *Macromolecules* **2005**, *38* (12), 5109–5117.
(128) Wetton, R. E.; MacKnight, W. J.; Fried, J. R.; Karasz, F. E. Compatibility of Poly(2,6-Dimethyl-1,4-Phenylene Oxide) (PPO)/Poly(Styrene-Co-4-Chlorostyrene) Blends. 2. Dielectric Study of the Critical Composition Region. *Macromolecules* **1978**, *11* (1), 158–165.
(129) Shenogin, S.; Kant, R.; Colby, R. H.; Kumar, S. K. Dynamics of Miscible Polymer Blends: Predicting the Dielectric Response. *Macromolecules* **2007**, *40* (16), 5767–5775.
(130) Leroy, E.; Alegría, A.; Colmenero, J. Quantitative Study of Chain Connectivity Inducing Effective Glass Transition Temperatures in Miscible Polymer Blends. *Macromolecules* **2002**, *35* (14), 5587–5590.
(131) Genix, A.-C.; Arbe, A.; Alvarez, F.; Colmenero, J.; Willner, L.; Richter, D. Dynamics of Poly(Ethylene Oxide) in a Blend with Poly(Methyl Methacrylate): A Quasielastic Neutron Scattering and Molecular Dynamics Simulations Study. *Phys. Rev. E* **2005**, *72* (3), 031808.
(132) Tyagi, M.; Arbe, A.; Colmenero, J.; Frick, B.; Stewart, J. R. Dynamic Confinement Effects in Polymer Blends. A Quasielastic Neutron Scattering Study of the Dynamics of Poly(Ethylene Oxide) in a Blend with Poly(Vinyl Acetate). *Macromolecules* **2006**, *39* (8), 3007–3018.
(133) White, R. P.; Lipson, J. E. G.; Higgins, J. S. Effect of Deuterium Substitution on the Physical Properties of Polymer Melts and Blends. *Macromolecules* **2010**, *43* (9), 4287–4293.
(134) Buckingham, A. D.; Hentschel, H. G. E. Partial Miscibility of Liquid Mixtures of Protonated and Deuterated High Polymers. *J. Polym. Sci. Polym. Phys. Ed.* **1980**, *18* (4), 853–861.
(135) Yang, H.; Shibayama, M.; Stein, R. S.; Shimizu, N.; Hashimoto, T. Deuteration Effects on the Miscibility and Phase Separation Kinetics of Polymer Blends. *Macromolecules* **1986**, *19* (6), 1667–1674.
(136) Nishi, T.; Kwei, T. K. Cloud Point Curves for Poly(Vinyl Methyl Ether) and Monodisperse Polystyrene Mixtures. *Polymer* **1975**, *16* (4), 285–290.
(137) Ubrich, J. M.; Larbi, F. B. C.; Halary, J. L.; Monnerie, L.; Bauer, B.; Han, C. C. Molecular Weight Effects on the Phase Diagram of Polystyrene-Poly(Vinyl Methyl Ether) Blends. *Macromolecules* **1986**, *19* (3), 810–815.
(138) Yurekli, K.; Krishnamoorti, R. Thermodynamic Interactions in Blends of Poly(4-Tert-Butyl Styrene) and Polyisoprene by Small-Angle Neutron Scattering. *J. Polym. Sci. Part B Polym. Phys.* **2004**, *42* (17), 3204–3217.
(139) Kiran, E.; Sengers, J. M. H. L. *Supercritical Fluids: Fundamentals for Application*; Springer Science & Business Media, 1994.
(140) Watkins, J. J.; Brown, G. D.; Pollard, M. A.; Ramachandrarao, V. S.; Russell, T. P. Phase Transitions in Polymer Blends and Block Copolymers Induced by Selective Dilation with

Supercritical CO2. In *Supercritical Fluids*; Kiran, E., Debenedetti, P. G., Peters, C. J., Eds.; NATO Science Series; Springer Netherlands, 2000; pp 277–289.
(141) Havriliak, S.; Negami, S. A Complex Plane Representation of Dielectric and Mechanical Relaxation Processes in Some Polymers. *Polymer* **1967**, *8*, 161–210.
(142) Kremer, F.; Schönhals, A. *Broadband Dielectric Spectroscopy*; Springer Berlin Heidelberg: Berlin, Heidelberg, 2003.
(143) Koizumi, S. Gel-like Aspect of a Miscible Polymer Mixture Studied by Small-Angle Neutron Scattering. *J. Polym. Sci. Part B Polym. Phys.* **2004**, *42* (17), 3148–3164.
(144) Sy, J. W.; Mijovic, J. Reorientational Dynamics of Poly(Vinylidene Fluoride)/Poly(Methyl Methacrylate) Blends by Broad-Band Dielectric Relaxation Spectroscopy. *Macromolecules* **2000**, *33* (3), 933–946.
(145) Schlosser, E.; Schoenhals, A.; Carius, H. E.; Goering, H. Evaluation Method of Temperature-Dependent Relaxation Behavior of Polymers. *Macromolecules* **1993**, *26* (22), 6027–6032.
(146) Dudognon, E.; Bernès, A.; Lacabanne, C. Comparative Study of Poly(n-Butyl Methacrylate) by Thermo-Stimulated Currents and Dynamic Dielectric Spectroscopy. *J. Phys. Appl. Phys.* **2002**, *35* (1), 9.
(147) Dantras, E.; Dudognon, E.; Bernes, A.; Lacabanne, C. Study of Polymers with Various Chemical Structures and Chain Architectures by Thermo-Stimulated Currents and Broadband Dielectric Spectroscopy. In *Proceedings. 11th International Symposium on Electrets*; 2002; pp 235–242.
(148) McCrum, N. G.; Read, B. E.; Williams, G. *Anelastic and Dielectric Effects in Polymeric Solids*; Dover Publications, 1967.
(149) Bergman, R.; Alvarez, F.; Alegría, A.; Colmenero, J. Dielectric Relaxation in PMMA Revisited. *J. Non-Cryst. Solids* **1998**, *235–237*, 580–583.
(150) Mpoukouvalas, K.; Floudas, G.; Williams, G. Origin of the α, β, (Bα), and "Slow" Dielectric Processes in Poly(Ethyl Methacrylate). *Macromolecules* **2009**, *42* (13), 4690–4700.
(151) Beiner, M. Relaxation in Poly(Alkyl Methacrylate)s: Crossover Region and Nanophase Separation. *Macromol. Rapid Commun.* **2001**, *22* (12), 869–895.
(152) Teixeira, S. S.; Dias, C. J.; Dionisio, M.; Costa, L. C. New Method to Analyze Dielectric Relaxation Processes: A Study on Polymethacrylate Series. *Polym. Int.* **2013**, *62* (12), 1744–1749.
(153) Onsager, L. Electric Moments of Molecules in Liquids. *J. Am. Chem. Soc.* **1936**, *58* (8), 1486–1493.
(154) Kirkwood, J. G. The Dielectric Polarization of Polar Liquids. *J. Chem. Phys.* **1939**, *7* (10), 911–919.
(155) Kirkwood, J. G. The Influence of Hindered Molecular Rotation on the Dielectric Polarisation of Polar Liquids. *Trans. Faraday Soc.* **1946**, *42* (0), A007-A012.
(156) Frohlich, H. *Theory of Dielectrics: Dielectric Constant and Dielectric Loss*, 2 edition.; Oxford University Press: Oxford, 1987.
(157) Rellick, G. S.; Runt, J. A Dielectric Study of Poly(Ethylene-Co-Vinyl Acetate)–poly(Vinyl Chloride) Blends. II. Loss Curve Broadening and Correlation Parameters. *J. Polym. Sci. Part B Polym. Phys.* **1986**, *24* (2), 313–324.

(158) Yang, X.; Loos, J.; Veenstra, S. C.; Verhees, W. J. H.; Wienk, M. M.; Kroon, J. M.; Michels, M. A. J.; Janssen, R. A. J. Nanoscale Morphology of High-Performance Polymer Solar Cells. *Nano Lett.* **2005**, *5* (4), 579–583.
(159) Noh, Y.-Y.; Zhao, N.; Caironi, M.; Sirringhaus, H. Downscaling of Self-Aligned, All-Printed Polymer Thin-Film Transistors. *Nat. Nanotechnol.* **2007**, *2* (12), 784–789.
(160) Cho, W. K.; Kong, B.; Choi, I. S. Highly Efficient Non-Biofouling Coating of Zwitterionic Polymers: Poly((3-(Methacryloylamino)Propyl)-Dimethyl(3-Sulfopropyl)Ammonium Hydroxide). *Langmuir* **2007**, *23* (10), 5678–5682.
(161) Ideal Glass Transitions in Thin Films: An Energy Landscape Perspective. *J. Chem. Phys.* **2003**, *119* (4), 1897–1900.
(162) Lang, R. J.; Merling, W. L.; Simmons, D. S. Combined Dependence of Nanoconfined Tg on Interfacial Energy and Softness of Confinement. *ACS Macro Lett.* **2014**, *3* (8), 758–762.
(163) Hanakata, P. Z.; Douglas, J. F.; Starr, F. W. Interfacial Mobility Scale Determines the Scale of Collective Motion and Relaxation Rate in Polymer Films. *Nat. Commun.* **2014**, *5*, 4163.
(164) Lipson, J. E. G.; Milner, S. T. Percolation Model of Interfacial Effects in Polymeric Glasses. *Eur. Phys. J. B* **2009**, *72* (1), 133.
(165) Priestley, R. D.; Mundra, M. K.; Barnett, N. J.; Broadbelt, L. J.; Torkelson, J. M. Effects of Nanoscale Confinement and Interfaces on the Glass Transition Temperatures of a Series of Poly (n-Methacrylate) Films. *Aust. J. Chem.* **2007**, *60* (10), 765–771.
(166) van Zanten, J. H.; Wallace, W. E.; Wu, W. Effect of Strongly Favorable Substrate Interactions on the Thermal Properties of Ultrathin Polymer Films. *Phys. Rev. E* **1996**, *53* (3), R2053–R2056.
(167) Sharp, J. S.; Forrest, J. A. Dielectric and Ellipsometric Studies of the Dynamics in Thin Films of Isotactic Poly(Methylmethacrylate) with One Free Surface. *Phys. Rev. E Stat. Nonlin. Soft Matter Phys.* **2003**, *67* (3 Pt 1), 031805.
(168) Schönhals, A.; Goering, H.; Schick, C. Segmental and Chain Dynamics of Polymers: From the Bulk to the Confined State. *J. Non-Cryst. Solids* **2002**, *305* (1–3), 140–149.
(169) Napolitano, S.; Capponi, S.; Vanroy, B. Glassy Dynamics of Soft Matter under 1D Confinement: How Irreversible Adsorption Affects Molecular Packing, Mobility Gradients and Orientational Polarization in Thin Films. *Eur. Phys. J. E* **2013**, *36* (6), 1–37.
(170) Serghei, A.; Kremer, F. Metastable States of Glassy Dynamics, Possibly Mimicking Confinement-Effects in Thin Polymer Films. *Macromol. Chem. Phys.* **2008**, *209* (8), 810–817.
(171) Havriliak, S.; Negami, S. A Complex Plane Representation of Dielectric and Mechanical Relaxation Processes in Some Polymers. *Polymer* **1967**, *8*, 161–210.
(172) Li, H.; Zhang, Y. M.; Xue, M. Z.; Liu, Y. G. Amphiphilic Block Copolymers of Polyvinyl Alcohol and Polystyrene and Their Surface Properties. *Polym. J.* **2005**, *37* (11), 841–846.
(173) Casalini, R.; Zhu, L.; Baer, E.; Roland, C. M. Segmental Dynamics and the Correlation Length in Nanoconfined PMMA. *Polymer* **2016**, *88*, 133–136.
(174) Wang, J.; McKenna, G. B. A Novel Temperature-Step Method to Determine the Glass Transition Temperature of Ultrathin Polymer Films by Liquid Dewetting. *J. Polym. Sci. Part B Polym. Phys.* **2013**, *51* (18), 1343–1349.

(175) Zhang, C.; Guo, Y.; Priestley, R. D. Glass Transition Temperature of Polymer Nanoparticles under Soft and Hard Confinement. *Macromolecules* **2011**, *44* (10), 4001–4006.
(176) Roth, C. B.; McNerny, K. L.; Jager, W. F.; Torkelson, J. M. Eliminating the Enhanced Mobility at the Free Surface of Polystyrene: Fluorescence Studies of the Glass Transition Temperature in Thin Bilayer Films of Immiscible Polymers. *Macromolecules* **2007**, *40* (7), 2568–2574.
(177) Communication: Experimentally Determined Profile of Local Glass Transition Temperature across a Glassy-Rubbery Polymer Interface with a Tg Difference of 80 K. *J. Chem. Phys.* **2015**, *143* (11), 111101.
(178) Guo, Y.; Zhang, C.; Lai, C.; Priestley, R. D.; D'Acunzi, M.; Fytas, G. Structural Relaxation of Polymer Nanospheres under Soft and Hard Confinement: Isobaric versus Isochoric Conditions. *ACS Nano* **2011**, *5* (7), 5365–5373.
(179) Rauscher, P. M.; Pye, J. E.; Baglay, R. R.; Roth, C. B. Effect of Adjacent Rubbery Layers on the Physical Aging of Glassy Polymers. *Macromolecules* **2013**, *46* (24), 9806–9817.
(180) Simmons, D. S. An Emerging Unified View of Dynamic Interphases in Polymers. *Macromol. Chem. Phys.* **2016**, *217* (2), 137–148.
(181) Fakhraai, Z.; Forrest, J. A. Measuring the Surface Dynamics of Glassy Polymers. *Science* **2008**, *319* (5863), 600–604.
(182) Richert, R. Dynamics of Nanoconfined Supercooled Liquids. *Annu. Rev. Phys. Chem.* **2011**, *62* (1), 65–84.
(183) Casalini, R.; Prevosto, D.; Labardi, M.; Roland, C. M. Effect of Interface Interaction on the Segmental Dynamics of Poly(Vinyl Acetate) Investigated by Local Dielectric Spectroscopy. *ACS Macro Lett.* **2015**, *4* (9), 1022–1026.
(184) McDonald, D. L. Neutron Diffraction Study of the Debye–Waller Factor for Aluminum. *Acta Crystallogr.* **1967**, *23* (2), 185–191.
(185) Sanz, A.; Ruppel, M.; Douglas, J. F.; Cabral, J. T. Plasticization Effect of C 60 on the Fast Dynamics of Polystyrene and Related Polymers: An Incoherent Neutron Scattering Study. *J. Phys. Condens. Matter* **2008**, *20* (10), 104209.
(186) Chung, P. C.; Glynos, E.; Green, P. F. The Elastic Mechanical Response of Supported Thin Polymer Films. *Langmuir* **2014**, *30* (50), 15200–15205.
(187) Torres, J. M.; Stafford, C. M.; Vogt, B. D. Elastic Modulus of Amorphous Polymer Thin Films: Relationship to the Glass Transition Temperature. *ACS Nano* **2009**, *3* (9), 2677–2685.
(188) Chung, P. C.; Green, P. F. The Elastic Mechanical Response of Nanoscale Thin Films of Miscible Polymer/Polymer Blends. *Macromolecules* **2015**, *48* (12), 3991–3996.
(189) Geng, K.; Yang, F.; Druffel, T.; Grulke, E. A. Nanoindentation Behavior of Ultrathin Polymeric Films. *Polymer* **2005**, *46* (25), 11768–11772.
(190) Soles, C. L.; Douglas, J. F.; Wu, W.; Dimeo, R. M. Incoherent Neutron Scattering as a Probe of the Dynamics in Molecularly Thin Polymer Films. *Macromolecules* **2003**, *36* (2), 373–379.
(191) Jackson, C. L.; McKenna, G. B. The Glass Transition of Organic Liquids Confined to Small Pores. *J. Non-Cryst. Solids* **1991**, *131*, 221–224.
(192) Dong, B. X.; Huang, B.; Tan, A.; Green, P. F. Nanoscale Orientation Effects on Carrier Transport in a Low-Band-Gap Polymer. *J. Phys. Chem. C* **2014**, *118* (31), 17490–17498.

(193) Yang, H.; Glynos, E.; Huang, B.; Green, P. F. Out-of-Plane Carrier Transport in Conjugated Polymer Thin Films: Role of Morphology. *J. Phys. Chem. C* **2013**, *117* (19), 9590–9597.
(194) Ferroelectric Thin Films: Review of Materials, Properties, and Applications. *J. Appl. Phys.* **2006**, *100* (5), 051606.
(195) Baschnagel, J.; Varnik, F. Computer Simulations of Supercooled Polymer Melts in the Bulk and in Confined Geometry. *J. Phys. Condens. Matter* **2005**, *17* (32), R851.
(196) Fryer, D. S.; Peters, R. D.; Kim, E. J.; Tomaszewski, J. E.; de Pablo, J. J.; Nealey, P. F.; White, C. C.; Wu, W. Dependence of the Glass Transition Temperature of Polymer Films on Interfacial Energy and Thickness. *Macromolecules* **2001**, *34* (16), 5627–5634.
(197) Ellison, C. J.; Kim, S. D.; Hall, D. B.; Torkelson, J. M. Confinement and Processing Effects on Glass Transition Temperature and Physical Aging in Ultrathin Polymer Films: Novel Fluorescence Measurements. *Eur. Phys. J. E* **2002**, *8* (2), 155–166.
(198) Paeng, K.; Richert, R.; Ediger, M. D. Molecular Mobility in Supported Thin Films of Polystyrene, Poly(Methyl Methacrylate), and Poly(2-Vinyl Pyridine) Probed by Dye Reorientation. *Soft Matter* **2011**, *8* (3), 819–826.
(199) Svanberg, C. Glass Transition Relaxations in Thin Suspended Polymer Films. *Macromolecules* **2007**, *40* (2), 312–315.
(200) Fukao, K.; Uno, S.; Miyamoto, Y.; Hoshino, A.; Miyaji, H. Dynamics of $\ensuremath{\alpha}$ and $\ensuremath{\beta}$ Processes in Thin Polymer Films: Poly(Vinyl Acetate) and Poly(Methyl Methacrylate). *Phys. Rev. E* **2001**, *64* (5), 051807.
(201) Evans, C. M. Modulus, Confinement, and Temperature Effects on Surface Capillary Wave Dynamics in Bilayer Polymer Films Near the Glass Transition. *Phys. Rev. Lett.* **2012**, *109* (3).
(202) Paeng, K.; Swallen, S. F.; Ediger, M. D. Direct Measurement of Molecular Motion in Freestanding Polystyrene Thin Films. *J. Am. Chem. Soc.* **2011**, *133* (22), 8444–8447.
(203) Casalini, R.; Labardi, M.; Roland, C. M. Dynamics of Poly(Vinyl Methyl Ketone) Thin Films Studied by Local Dielectric Spectroscopy. *J. Chem. Phys.* **2017**, *146* (20), 203315.
(204) Serghei, A.; Huth, H.; Schick, C.; Kremer, F. Glassy Dynamics in Thin Polymer Layers Having a Free Upper Interface. *Macromolecules* **2008**, *41* (10), 3636–3639.
(205) Sharma, R. P.; Green, P. F. Role of "Hard" and "Soft" Confinement on Polymer Dynamics at the Nanoscale. *ACS Macro Lett.* **2017**, 908–914.
(206) Sharma, R. P.; Green, P. F. Component Dynamics in Polymer/Polymer Blends: Role of Spatial Compositional Heterogeneity. *Macromolecules* **2017**, *50* (17), 6617–6630.
(207) Steiner, U.; Klein, J.; Eiser, E.; Budkowski, A.; Fetters, L. J. Complete Wetting from Polymer Mixtures. *Science* **1992**, *258* (5085), 1126–1129.
(208) Steiner, U.; Klein, J. Growth of Wetting Layers from Liquid Mixtures. *Phys. Rev. Lett.* **1996**, *77* (12), 2526–2529.
(209) Thomas, K. R.; Clarke, N.; Poetes, R.; Morariu, M.; Steiner, U. Wetting Induced Instabilities in Miscible Polymer Blends. *Soft Matter* **2010**, *6* (15), 3517–3523.
(210) Bhatia, Q. S.; Pan, D. H.; Koberstein, J. T. Preferential Surface Adsorption in Miscible Blends of Polystyrene and Poly(Vinyl Methyl Ether). *Macromolecules* **1988**, *21* (7), 2166–2175.
(211) Frieberg, B.; Kim, J.; Narayanan, S.; Green, P. F. Surface Layer Dynamics in Miscible Polymer Blends. *ACS Macro Lett.* **2013**, *2* (5), 388–392.

(212) Ogawa, H.; Kanaya, T.; Nishida, K.; Matsuba, G. Phase Separation and Dewetting in Polystyrene/Poly(Vinyl Methyl Ether) Blend Thin Films in a Wide Thickness Range. *Polymer* **2008**, *49* (1), 254–262.
(213) Ogawa, H.; Kanaya, T.; Nshida, K.; Matsuba, G. Composition Fluctuations before Dewetting in Polystyrene/Poly(Vinyl Methyl Ether) Blend Thin Films. *Polymer* **2008**, *49* (10), 2553–2559.
(214) Madkour, S.; Szymoniak, P.; Schick, C.; Schönhals, A. Unexpected Behavior of Ultra-Thin Films of Blends of Polystyrene/Poly(Vinyl Methyl Ether) Studied by Specific Heat Spectroscopy. *J. Chem. Phys.* **2017**, *146* (20), 203321.
(215) Madkour, S.; Szymoniak, P.; Heidari, M.; von Klitzing, R.; Schönhals, A. Unveiling the Dynamics of Self-Assembled Layers of Thin Films of Poly(Vinyl Methyl Ether) (PVME) by Nanosized Relaxation Spectroscopy. *ACS Appl. Mater. Interfaces* **2017**, *9* (8), 7535–7546.
(216) Madkour, S.; Szymoniak, P.; Radnik, J.; Schönhals, A. Unraveling the Dynamics of Nanoscopically Confined PVME in Thin Films of a Miscible PVME/PS Blend. *ACS Appl. Mater. Interfaces* **2017**, *9* (42), 37289–37299.
(217) Ermi, B. D.; Karim, A.; Douglas, J. F. Formation and Dissolution of Phase-Separated Structures in Ultrathin Blend Films. *J. Polym. Sci. Part B Polym. Phys.* **1998**, *36* (1), 191–200.
(218) Yin, H.; Madkour, S.; Schönhals, A. Unambiguous Evidence for a Highly Mobile Surface Layer in Ultrathin Polymer Films by Specific Heat Spectroscopy on Blends. *Macromolecules* **2015**, *48* (14), 4936–4941.
(219) Tammer, M.; Monkman, A. P. Measurement of the Anisotropic Refractive Indices of Spin Cast Thin Poly(2-Methoxy-5-(2'-Ethyl-Hexyloxy)-p-Phenyl-Enevinylene) (MEH-PPV) Films. *Adv. Mater.* **2002**, *14* (3), 210–212.
(220) Gurau, M. C.; Delongchamp, D. M.; Vogel, B. M.; Lin, E. K.; Fischer, D. a; Sambasivan, S.; Richter, L. J. Measuring Molecular Order in Poly(3-Alkylthiophene) Thin Films with Polarizing Spectroscopies. *Langmuir ACS J. Surf. Colloids* **2007**, *23* (2), 834–842.
(221) Serghei, A. Challenges in Glassy Dynamics of Polymers. *Macromol. Chem. Phys.* **2008**, *209* (14), 1415–1423.
(222) Serghei, A.; Tress, M.; Kremer, F. The Glass Transition of Thin Polymer Films in Relation to the Interfacial Dynamics. *J. Chem. Phys.* **2009**, *131* (15), 154904.
(223) Newman, C. R.; Frisbie, C. D.; da Silva Filho, D. A.; Brédas, J.-L.; Ewbank, P. C.; Mann, K. R. Introduction to Organic Thin Film Transistors and Design of N-Channel Organic Semiconductors. *Chem. Mater.* **2004**, *16* (23), 4436–4451.
(224) Riedel, C.; Sweeney, R.; Israeloff, N. E.; Arinero, R.; Schwartz, G. A.; Alegria, A.; Tordjeman, P.; Colmenero, J. Imaging Dielectric Relaxation in Nanostructured Polymers by Frequency Modulation Electrostatic Force Microscopy. *Appl. Phys. Lett.* **2010**, *96* (21).
(225) Labardi, M.; Prevosto, D.; Nguyen, K. H.; Capaccioli, S.; Lucchesi, M.; Rolla, P. Local Dielectric Spectroscopy of Nanocomposite Materials Interfaces. *J. Vac. Sci. Technol. B* **2010**, *28* (3), C4D11-C4D17.
(226) Corrales, T. P.; Laroze, D.; Zardalidis, G.; Floudas, G.; Butt, H.-J.; Kappl, M. Dynamic Heterogeneity and Phase Separation Kinetics in Miscible Poly(Vinyl Acetate)/Poly(Ethylene Oxide) Blends by Local Dielectric Spectroscopy. *Macromolecules* **2013**, *46* (18), 7458–7464.

(227) Nguyen, H. K.; Prevosto, D.; Labardi, M.; Capaccioli, S.; Lucchesi, M.; Rolla, P. Effect of Confinement on Structural Relaxation in Ultrathin Polymer Films Investigated by Local Dielectric Spectroscopy. *Macromolecules* **2011**, *44* (16), 6588–6593.
(228) Nguyen, H. K.; Labardi, M.; Capaccioli, S.; Lucchesi, M.; Rolla, P.; Prevosto, D. Interfacial and Annealing Effects on Primary α-Relaxation of Ultrathin Polymer Films Investigated at Nanoscale. *Macromolecules* **2012**, *45* (4), 2138–2144.
(229) Papadimitrakopoulos, F.; Wisniecki, P.; Bhagwagar, D. E. Mechanically Attrited Silicon for High Refractive Index Nanocomposites. *Chem. Mater.* **1997**, *9* (12), 2928–2933.
(230) Colvin, V. L.; Schlamp, M. C.; Alivisatos, A. P. Light-Emitting Diodes Made from Cadmium Selenide Nanocrystals and a Semiconducting Polymer. *Nature* **1994**, *370* (6488), 354–357.
(231) Shiojiri, S.; Hirai, T.; Komasawa, I.; Komasawa, I. Immobilization of Semiconductor Nanoparticles Formed in Reverse Micelles into Polyurea via in Situ Polymerization of Diisocyanates. *Chem. Commun.* **1998**, No. 14, 1439–1440.
(232) Tang, C.; Hackenberg, K.; Fu, Q.; Ajayan, P. M.; Ardebili, H. High Ion Conducting Polymer Nanocomposite Electrolytes Using Hybrid Nanofillers. *Nano Lett.* **2012**, *12* (3), 1152–1156.
(233) Kelzenberg, M. D.; Boettcher, S. W.; Petykiewicz, J. A.; Turner-Evans, D. B.; Putnam, M. C.; Warren, E. L.; Spurgeon, J. M.; Briggs, R. M.; Lewis, N. S.; Atwater, H. A. Enhanced Absorption and Carrier Collection in Si Wire Arrays for Photovoltaic Applications. *Nat. Mater.* **2010**, *9* (4), 368–368.
(234) Tjong, S. C. Structural and Mechanical Properties of Polymer Nanocomposites. *Mater. Sci. Eng. R Rep.* **2006**, *53* (3–4), 73–197.
(235) Kim, J.; Yang, H.; Green, P. F. Tailoring the Refractive Indices of Thin Film Polymer Metallic Nanoparticle Nanocomposites. *Langmuir* **2012**, *28* (25), 9735–9741.
(236) Money, B. K.; Hariharan, K.; Swenson, J. Glass Transition and Relaxation Processes of Nanocomposite Polymer Electrolytes. *J. Phys. Chem. B* **2012**, *116* (26), 7762–7770.
(237) Meng, D.; Kumar, S. K.; Lane, J. M. D.; Grest, G. S. Effective Interactions between Grafted Nanoparticles in a Polymer Matrix. *Soft Matter* **2012**, *8* (18), 5002–5010.
(238) Ganesan, V.; Ellison, C. J.; Pryamitsyn, V. Mean-Field Models of Structure and Dispersion of Polymer-Nanoparticle Mixtures. *Soft Matter* **2010**, *6* (17), 4010–4025.
(239) Kumar, S. K.; Jouault, N.; Benicewicz, B.; Neely, T. Nanocomposites with Polymer Grafted Nanoparticles. *Macromolecules* **2013**, *46* (9), 3199–3214.
(240) Srivastava, S.; Agarwal, P.; Archer, L. A. Tethered Nanoparticle–Polymer Composites: Phase Stability and Curvature. *Langmuir* **2012**, *28* (15), 6276–6281.
(241) F. Green, P. The Structure of Chain End-Grafted Nanoparticle / Homopolymer Nanocomposites. *Soft Matter* **2011**, *7* (18), 7914–7926.
(242) Akcora, P.; Liu, H.; Kumar, S. K.; Moll, J.; Li, Y.; Benicewicz, B. C.; Schadler, L. S.; Acehan, D.; Panagiotopoulos, A. Z.; Pryamitsyn, V.; et al. Anisotropic Self-Assembly of Spherical Polymer-Grafted Nanoparticles. *Nat. Mater.* **2009**, *8* (4), 354–359.
(243) Borukhov, I.; Leibler, L. Enthalpic Stabilization of Brush-Coated Particles in a Polymer Melt. *Macromolecules* **2002**, *35* (13), 5171–5182.
(244) Chen, X. C.; Green, P. F. Structure of Thin Film Polymer/Nanoparticle Systems: Polystyrene (PS) Coated-Au Nanoparticle/Tetramethyl Bisphenol-A Polycarbonate Mixtures (TMPC). *Soft Matter* **2011**, *7* (3), 1192–1198.

(245) Frischknecht, A. L.; Hore, M. J. A.; Ford, J.; Composto, R. J. Dispersion of Polymer-Grafted Nanorods in Homopolymer Films: Theory and Experiment. *Macromolecules* **2013**, *46* (7), 2856–2869.
(246) Meli, L.; Arceo, A.; Green, P. F. Control of the Entropic Interactions and Phase Behavior of Athermal Nanoparticle/Homopolymer Thin Film Mixtures. *Soft Matter* **2009**, *5* (3), 533–537.
(247) Maxwell, J. C. *A Treatise on Electricity and Magnetism*; Clarendon Press, 1873.
(248) Wagner, K. W. Erklärung der dielektrischen Nachwirkungsvorgänge auf Grund Maxwellscher Vorstellungen. *Arch. Für Elektrotechnik* **1914**, *2* (9), 371–387.
(249) Sinha, S. K.; Jiang, Z.; Lurio, L. B. X-Ray Photon Correlation Spectroscopy Studies of Surfaces and Thin Films. *Adv. Mater.* **2014**, *26* (46), 7764–7785.
(250) Hu, X.; Jiang, Z.; Narayanan, S.; Jiao, X.; Sandy, A. R.; Sinha, S. K.; Lurio, L. B.; Lal, J. Observation of a Low-Viscosity Interface between Immiscible Polymer Layers. *Phys. Rev. E* **2006**, *74* (1), 010602.
(251) Evans, C. M.; Deng, H.; Jager, W. F.; Torkelson, J. M. Fragility Is a Key Parameter in Determining the Magnitude of Tg-Confinement Effects in Polymer Films. *Macromolecules* **2013**, *46* (15), 6091–6103.
(252) Riggleman, R. A.; Yoshimoto, K.; Douglas, J. F.; de Pablo, J. J. Influence of Confinement on the Fragility of Antiplasticized and Pure Polymer Films. *Phys. Rev. Lett.* **2006**, *97* (4), 045502.
(253) Betzabe Gonzalez-Campos, J.; Garcia-Carvajal, Z. Y.; Prokhorov, E.; Luna-Barcenas, J. G.; Mendoza-Duarte, M. E.; Lara-Romero, J.; del Rio, R. E.; Sanchez, I. C. Revisiting the Thermal Relaxations of Poly(Vinyl Alcohol). *J. Appl. Polym. Sci.* **2012**, *125* (5), 4082–4090.
(254) Urakawa, O.; Fuse, Y.; Hori, H.; Tran-Cong, Q.; Yano, O. A Dielectric Study on the Local Dynamics of Miscible Polymer Blends: Poly(2-Chlorostyrene)/Poly(Vinyl Methyl Ether). *Polymer* **2001**, *42* (2), 765–773.
(255) Tretinnikov, O. N.; Zagorskaya, S. A. Determination of the Degree of Crystallinity of Poly(Vinyl Alcohol) by FTIR Spectroscopy. *J. Appl. Spectrosc.* **2012**, *79* (4), 521–526.
(256) Hassan, C. M.; Peppas, N. A. Structure and Applications of Poly(Vinyl Alcohol) Hydrogels Produced by Conventional Crosslinking or by Freezing/Thawing Methods. In *Biopolymers · PVA Hydrogels, Anionic Polymerisation Nanocomposites*; Advances in Polymer Science; Springer Berlin Heidelberg, 2000; pp 37–65.